S-nitrosylation in Neuropathic pain and Autophagy

Dissertation

for attaining the PhD degree

of Natural Sciences

submitted to the Faculty of Biochemistry, Chemistry and Pharmacy

of the Johann Wolfgang Goethe University

in Frankfurt am Main

by

Reynir Scheving

from Reykjavík, Iceland

Frankfurt am Main (2013)

(D30)

accepted by the Faculty of Biochemistry, Chemistry and Pharmacy (14) of the

Johann Wolfgang Goethe University as a dissertation.

Dean: Prof. Dr. Thomas Prisner

Expert assessor: Prof. Dr. Jochen Klein
Prof. Dr. Irmgard Tegeder

Date of the disputation:

This thesis is dedicated to the loving memory of my father Sveinn G. Scheving (27.aug.1933 – 05.jun.2009) who taught me the value of an education.

"*The important thing is not to stop questioning. Curiosity has its own reason for existing*."

- Albert Einstein

Table of Contents

List of Figures

List of Tables

1. Introduction

1.1 Neuropathic pain

Nociceptive pain is a basic function of the nervous system that functions as an important defense mechanism that protects tissue from immediate injury and helps survival of the individual. This is evident in congenital SCN9A channelopathy that results in a complete inability to sense pain (Cox et al. 2006). The inability to sense pain predisposes the individual to injuries and mutilations early in life and has a dramatic effect on life expectancy (Manfredi et al. 1981).

Neuropathic pain, on the other hand, is a maladaptive form of chronic pain caused by a primary injury or lesions in the central or peripheral nervous systems. Cutting and crushing injuries are common causes of neuropathic pain, for example after limb amputations or during a slipped disk injury respectively. Some diseases like multiple sclerosis, HIV/AIDS and diabetes can result in neural degeneration and disrupt the processing of pain signals causing pain. Also neurotoxic chemicals and drugs such as those used in cancer chemotherapy (e.g. Cisplatin, Oxaliplatin, and Vincristine) can cause pain by damaging neurons. (Boyce-Rustay and Jarvis 2009, Farquhar-Smith 2011, Manas et al. 2011, Nickel et al. 2012, Windebank and Grisold 2008). The main characteristics of neuropathic pain establish themselves in the unpleasant and abnormal sensations such as an increased response to painful stimuli (hyperalgesia) and painful response to benign stimulation (allodynia).

About 7-8 % of the population suffers from chronic neuropathic pain according to epidemiological studies. The effects of pain on people's quality of life can be quite dramatic. The extended symptoms of chronic pain include for example decrease in mobility, inability to work, and depression. This is exacerbated by the difficulty in treating neuropathic pain properly (Manas et al. 2011, Bouhassira et al. 2008, Torrance et al. 2006).

Since there is currently no proven way to prevent or cure neuropathic pain, treatment for chronic neuropathic pain often requires a multifaceted approach of drugs, surgery, rehabilitation and psychological treatment. Several classes of drugs (see Table 1) are sometimes effective in treating neuropathic pain, however complete relief is very rare. Antidepressants and anticonvulsants are most commonly used. NICE guidelines recommend using amitriptyline, a tricyclic antidepressant, or pregabalin, an anticonvulsant, as first line treatment, if no contraindications or comorbities prevent its use. Switching between amitriptyline and pregabalin or combining them is then considered second-line treatment. (NICE 2010)

Table 1 Drugs used for the treatment of Neuropathic Pain (Beers and Berkow 2012)

Class	Drugs	Comments
Anticonvulsants	Carbamazepine, Gabapentin, Phenytoin, Pregabalin, Valproate	Gabapentin is the most widely used, while pregabalin is a common second choice
Antidepressants	Amitriptyline, Duloxetine, Desipramine	
Central α_2-adrenergic agonists	Clonidine, Tizanidine	
Corticosteroids	Dexamethasone, Prednisone	Used only for pain with an inflammatory component
NMDA-receptor antagonists	Memantine, Dextromethorphan	
Oral Na channel blockers	Mexiletine	Used only for neuropathic pain
Opioids	Butorphanol, Codeine, Hydromorphone, Levorphanol, Meperidine, Methadone, Morphine, Nalbuphine, Oxycodone, Oxymorphone, Pentazocine	Should only be considered as third-line treatment
Topical	Capsaicin, EMLA®, Lidocaine	
Other	Baclofen, Pamidronate	

Opioid analgesics sometimes provide some relief but are less effective than for nociceptive pain, and have many and sometimes severe side effects and may lead to abuse and addiction. Opioids should only be considered as third-line treatment according to the clinical guidelines of the United Kingdom´s National Institute for Health and Clinical Excellence (NICE) (i.e. after amitriptyline and pregabalin treatment has failed) (NICE 2010). In the end, the goals of the treatment are to reduce the pain as much as possible, delicately balancing the side effects versus pain relief and helping patients deal with any residual pain.

Given the problems with treating neuropathic pain and the consequences to people's quality of life, as well as the high prevalence of the condition it is important to conduct research on this problem, in particular novel pathways that could lead to pain relief without the damaging side effects of current treatments.

1.2 Models for neuropathic pain

Animal models are very important for research into the biological mechanism and potential therapies of neuropathic pain. A plethora of models have been reported in the literature. Jaggi et al describe about 40 models in detail in their exhaustive review (Jaggi, Jain and Singh 2011). The

models have many different characteristics and advantages and have made a great contribution to the understanding of pain mechanisms. The models are variously induced by physical injury to peripheral nerves, disease models such as diabetes-induced neuropathy, or by drugs such as anti-cancer agents like vincristine or anti HIV drugs like the nucleoside reverse transcriptase inhibitor zalcitabine.

1.2.1 SNI model

The model applied in this work is the SNI model developed by Decosterd et al (Decosterd and Woolf 2000). In this model two of the terminal branches of the sciatic nerve, the tibial and common peroneal nerves, are ligated leaving the sural nerve intact (see Figure 1). Cutting these two branches produces a neuropathic pain like sensation in the paw of the mouse. Two variants of this model have been developed where the ligation of different nerve combinations are used, in one variant the common peroneal nerve and sural nerve are ligated leaving the tibial nerve intact, and in the other the tibial nerve is ligated leaving the sural and common peroneal nerves intact. (Decosterd and Woolf 2000, Bourquin et al. 2006)

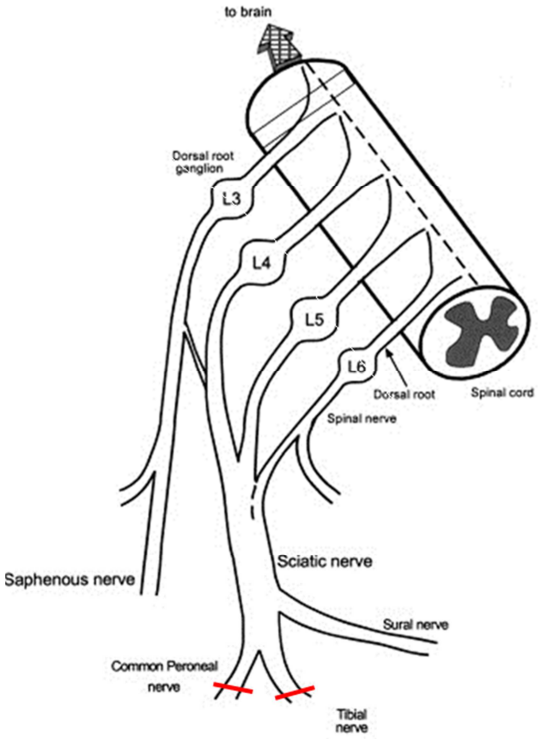

Figure 1 Schematic overview of the SNI
Adapted from Decosterd et al 2000. Two of the terminal branches of the sciatic nerve, the tibial and common peroneal nerves, are ligated leaving the sural nerve intact branches producing a neuropathic pain like sensation in the paw of the mouse

Mechanical and thermal hyperalgesia occur within 24 hours of the injury showing the greatest effect after about one week post injury.

The SNI is relatively simple to perform compared to many other models for neuropathic pain. After anesthesia the skin of the left hind leg of the mouse is shaved and a cut made directly through the biceps femoris muscle. The three terminal branches of the sciatic nerve, the tibial, common peroneal and sural nerves, now being visible, the tibial and common peroneal nerves are ligated with 5-0 silk followed by an axotomy of 2 mm distal nerve. Care must be taken not to touch or stretch the sural nerve as this could interfere with the sensitization. (Decosterd and Woolf 2000)

The SNI operation produces consistent, robust, and substantial changes in thermal and mechanical sensitivity that closely mimic clinical neuropathic pain and therefore is very useful as an experimental model.

1.3 Role of Nitric oxide in pain

Nitric Oxide (NO) has emerged as an important pro-nociceptive signaling molecule (Schmidtko, Tegeder and Geisslinger 2009) which, however, may also reduce hyperexcitability (Jin et al. 2011). It is likely that the effects of NO release depend on the cellular redox status and the amount and site of its production by nitric oxide synthases (NOS).

Reduction or inhibition of neuropathic and inflammatory pain has been achieved with a variety of ways that influence nitric oxides effects or production, such as:

- Chemical inhibition of NOS (Meller et al. 1990, Minami et al. 1995, Aley, McCarter and Levine 1998, Schmidtko et al. 2008, Schmidtko et al. 2003).
- Inhibitors of the NOS-coenzyme tetrahydrobiopterin (Tegeder et al. 2006, Miyamoto et al. 2009).
- Deletion of neuronal NOS (Boettger et al. 2007).
- Deletion of inducible NOS (Guhring et al. 2000).

However, the intrathecal injection of NO donors has been shown to both increase and decrease sensitivity to nociceptive stimuli (Schmidtko et al. 2009, Tegeder et al. 2002).

NO is known to partly exert its effect in pain via reduction of cGMP production and attenuation of protein kinase G activation (Schmidtko et al. 2008, Schmidtko et al. 2003). However, NO is a multifaceted molecule and in addition to the activation of soluble guanylylcyclase (sGC) it may also modulate enzyme function or protein interactions and transport at various levels by direct protein S-nitrosylation (SNO) of critical cysteine residues (Matsushita et al. 2003, Whalen et al. 2007, Hara et al. 2005, Jaffrey et al. 2001, Yoshida et al. 2006, Nott et al. 2008, Uehara et al. 2006, Tian et al. 2008, Gu et al. 2002).

1.4 S-Nitrosylation (SNO)

Protein S-Nitrosylation is a post translational covalent addition of nitric oxide to the thiol group of cysteine. This reaction is an electrophilic attack of nitrosonium (NO^+) equivalent on the sulfur, followed by deprotoation. Reactions involving nitroxyl (NO^-) equivalents or NO radicals have also been demonstrated. It was assumed that the reaction happened according to the reaction:

$2\ NO + O_2 \rightarrow 2\ NO_2$

$NO_2 + NO \rightarrow N_2O_3 = {}^{+}ON\ldots NO_3^{-}$

${}^{+}ON\ldots NO_3^{-} + RSH \rightarrow RSNO + HNO_2$

Where O_2 acts as an electron acceptor and RSH is the substance to be nitrosylated. Under physiological conditions where the concentration of NO is in the nano-molar and oxygen in the micro-molar ranges the first reaction proceeds rather slowly and is therefore the rate limiting reaction. However it has also been shown that specific proteins can catalyze SNO synthesis. For example ceruloplasmin, a plasma protein involved in iron metabolism and an antioxidant, was shown to generate low molecular RSNO, in particular S-nitrosoglutathione (GSNO). Type I copper servers as the electron acceptor and NO+ is transferred to the thiol of glutathione. (Inoue et al. 1999) Hemoglobin can also serve to catalyze SNO formation (Gow and Stamler 1998). SNOs are also formed by nitric oxide synthase (NOS), either directly through NO-formation or through the coproduction of NO and superoxide in the presence of glutathione (Schmidt et al. 1996). Thus under physiological conditions S-nitroso-proteins are not produced by a direct reaction between NO and a thiol group but requires oxygen, transition metals or other relevant electron acceptors (Lindermayr, Sell and Durner 2009). Alterations in the subcellular environment (e.g. changes in pH, hypoxia, or other disease related changes) can affect the occurrence and reversibility of S-nitrosylation.

1.4.1 Detection and analysis of SNO

Detection of SNO modifications of proteins in tissues has proven difficult to achieve (Torta et al. 2008). Due to low *in vivo* levels and instability of the S-NO bond, detection of SNO directly from complex mixtures by mass spectrometry (MS) is very inefficient. Detection of modifications in synthetic or purified recombinant proteins was achieved by electrospray ionization-mass spectrometry (Mirza, Chait and Lander 1995, Hao and Gross 2006, Lee et al. 2007). Although application of this approach is limited, it has the advantage to require little sample manipulation and therefore may better represent the *in vivo* situation, by avoiding loss of nitrosylation modifications.

The simplest methods to detect nitrosylation of proteins are chemoluminescent or colorimetric techniques, such as diaminofluorescein fluorometry (Itoh et al. 2000) or the Saville-Griess assay (Saville 1958), respectively. These methods can quantify the total content of SNO in samples but do not allow identification of the modified proteins.

The most commonly applied approach to detect and identify SNO modifications is the biotin-switch technique (BST) developed by Jaffrey et al. (Jaffrey et al. 2001). In this method, the SNO modification is first selectively reduced by ascorbate and replaced with a biotin-label. The biotin-tag can then be

exploited in many ways such as: affinity pull down of labeled protein (Jaffrey et al. 2001, Dall'Agnol et al. 2006), identification by anti-biotin antibodies (Jaffrey et al. 2001), or direct identification of SNO labeling sites by mass spectrometry (Hao et al. 2006, Whalen et al. 2007). The biotin-switch is highly specific for SNO modifications. However, the method is technically challenging and laborious. Other drawbacks are that acetone precipitation steps can cause loss of sample, and that there is a risk of false positives due to endogenous biotinylation and photocatalysed biotinylation of blocked thiols.

The biotin switch with an avidin affinity pulldown step does not discriminate between multiple SNO sites on the same protein. This can be a substantial problem as one study found up to 45% of SNO proteins to have more than one SNO site (Doulias et al. 2010). To account for this it was part of my project to develop an Elisa based detection method. For this approach the nitrosylation sites were labeled with biotin followed by sandwich ELSIA purification with target specific antibodies and detection of biotinylation with an anti-biotin infrared-labeled (700) fluorescent antibody. The use of an anti-biotin antibody allows for more than one SNO site per protein to be detected similar to the fluorescent labeling. The method however, does not account for lack of antibody specificity (Scheving et al. 2012).

Further BST-based methodological developments utilize other switch labels of nitrosylation sites. His-Tag peptide label has the advantage of binding irreversibly to the modified cysteine and identification of the modified site by MS is facilitated by the generation of a diagnostic peptide (Camerini et al. 2007).

Two-dimensional difference gel electrophoresis (2-D DIGE) can be applied if the SNO modifications in the samples are labeled with fluorescent dyes (Kettenhofen et al. 2008, Chouchani et al. 2010). When two samples (e.g. control vs. disease) are labeled with Cy3 and Cy5 and separated in one 2-D gel, relevant *in vivo* nitrosylation for each condition can be filtered and identified by MS. The difference approach also reduces false positive results since they are identically detected in both samples and can be excluded from further studies. The main drawbacks of this method are high costs and technical challenge. Moreover, this technique tends to identify mainly abundant proteins.

A recent development of using mass spectrometry to detect and identify SNO-modifications is the SNO-Site Identification (SNOSID). The SNOSID method utilizes the Biotin-switch method to label SNO-modifications followed by trypsin digestion and affinity purification resulting in enrichment of peptides that contain the NO target cysteine (Hao et al. 2006). Purified peptides are then eluted and analyzed by mass spectrometry. This potentially allows a high throughput identification of SNO modifications, though it requires a high amount of sample and sample preparation steps can cause sample loss.

The ICAT (isotope-coded affinity tags) method utilizes labeling reagents consisting of a reactive group, an isotopically coded linker, and an affinity isolation tag. After labeling the samples with two different isotopes, the samples are combined and subjected to protease digestion, affinity pull-down, and analysis by mass spectrometry. This allows the relative quantification of each analyzed protein between the samples, although as with the other methods the sample handling can cause loss of sample and mostly abundant proteins can be identified (Gygi et al. 1999).

Ischiropoulos et al. developed a method where phenylmercury-biotin compounds are used to react directly with the S-NO group followed by purification upon capture and subsequent release from agarose beads. The proteins or peptides are then sequenced by MS. This method avoids the use of ascorbate for the reduction and thus is less likely to falsely identify disulfide bridges or other oxidative modification instead of S-nitrosylation (Doulias et al. 2010).

Using stable isotope labeling by amino acids in cell culture (SILAC) (Ong et al. 2002, Gygi et al. 1999, Zhu et al. 2002) it is theoretically possible to simultaneously detect nitrosylated proteins and non nitrosylated proteins and calculate the level of nitrosylation as a ratio of expressed proteins. This approach could be useful to circumvent many of the disadvantages the currently available methods have. SILAC utilizes metabolic incorporation of a given “heavy” form of amino acids into the proteins where the amino acids have been incorporated with stable isotopic nuclei (e.g. deuterium, 13C, 15N). Thus, after growing the target organism (i.e. cells or animals) in “heavy” labeled culture media or with heavy diet the “heavy” protein can be extracted. When mixed with extracted proteins from any experimental setting with the same or like organism and analyzed by mass spectrometry the ratio of heavy and light proteins in each sample can be determined and compared between experimental groups.

By labeling cysteine residues in the standard with iodoacetamide (IAM) and N-ethyl-maleimide (NEM) (in a 1:1 ratio) a standard for the detection of SNO modified cysteine can be established. When the samples are first dark labeled with either of these cysteine reactive agents, and then after precipitation and ascorbate reduction of SNO sites the remaining cysteine are labeled with the respective other cysteine reactive agent, and finally mixed with the SILAC standard, the ratio of SNO labeled proteins versus the heavy cysteine labeled proteins can be assayed by mass spectrometry due to the mass difference of the proteins peptides. The non-nitrosylated portion (i.e. dark labeled) of the same protein is then in a similar manner compared with the heavy standard and the ratio of nitrosylated and non-nitrosylated protein can be calculated from the two resulting ratios.

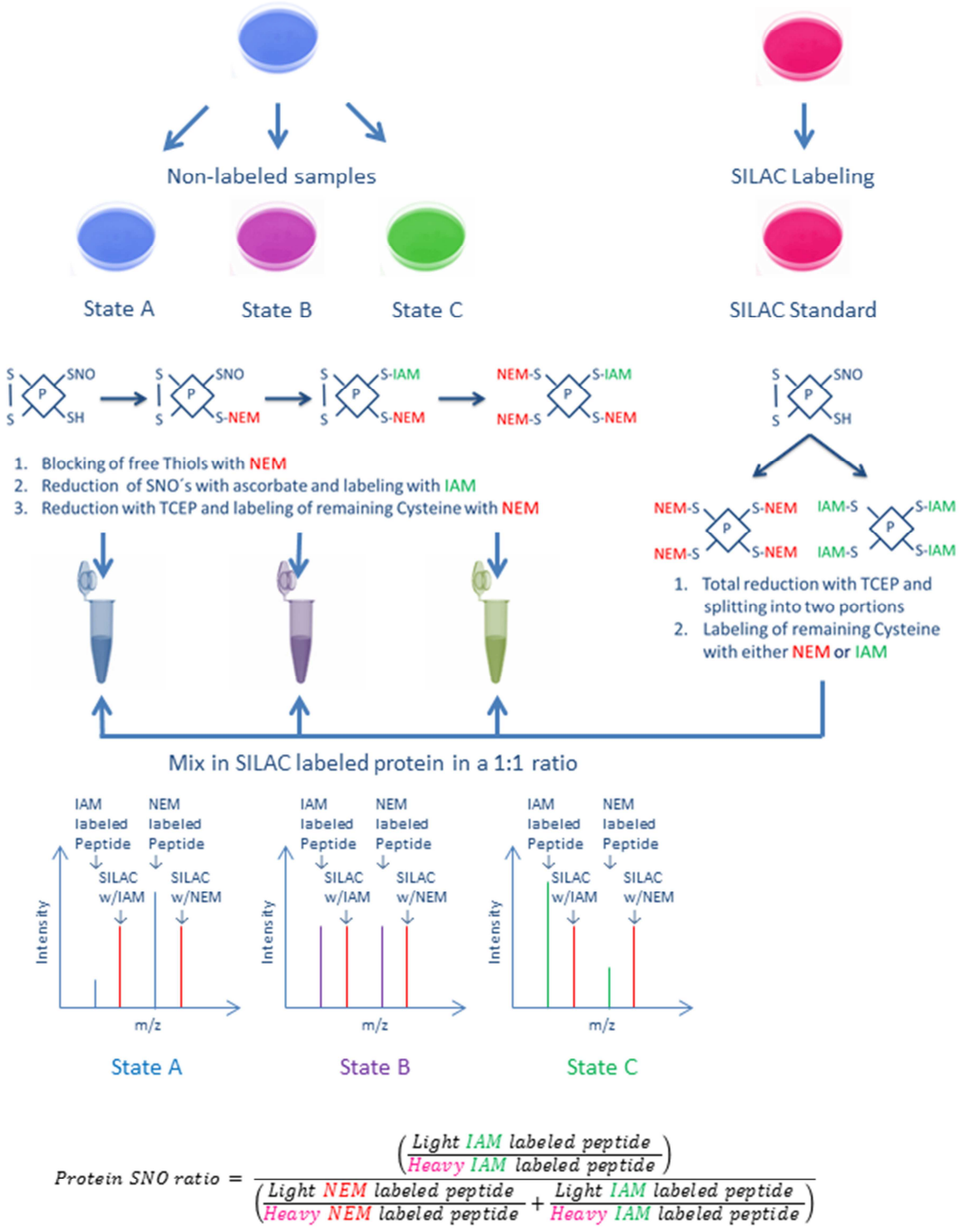

$$Protein\ SNO\ ratio = \frac{\left(\frac{Light\ IAM\ labeled\ peptide}{Heavy\ IAM\ labeled\ peptide}\right)}{\left(\frac{Light\ NEM\ labeled\ peptide}{Heavy\ NEM\ labeled\ peptide} + \frac{Light\ IAM\ labeled\ peptide}{Heavy\ IAM\ labeled\ peptide}\right)}$$

Figure 2 Schematic overview of the SNO-SILAC approach

The main advantage of this approach is the simultaneous identification of both changes in protein expression and the level of nitrosylation. Other prominent advantages are the increased spectrum of proteins as this approach is not as limited by the poor resolution of hydrophobic proteins in DIGE, and the direct identification of the SNO site as well as a more confident identification of the SNO proteins. This approach also allows determination of the level of modifications of different SNO sites within the same protein.

Once the sites of S-Nitrosylation have been determined it is possible to elucidate the effects of the nitrosylation by using point mutations of the respective cysteine. For example, by introducing a C694S point mutation into NADPH oxidase 5 (Nox5) Qian et al were able to show a dramatically lowered Nox5 activity, NO sensitivity, and biotin labeling of Nox5. Other cysteine point mutations in Nox5 did not show these effects, suggesting that endogenously produced NO can directly S-Nitrosylate and inhibit the activity of Nox5 (Qian et al. 2012). Another example can be found from Tang et al. They showed how S-Nitrosylation of the Apo2L/Trail Receptor DR4 induced by the NO donor nitrosocobolamine promotes cell death. A point mutation in DR4 of cysteine 336 to alanine desensitized cells against cell death induced by nitrosocobolamine and reduced biotin labeling of DR4. The C336A mutant also displayed a reduced caspase-8 enzymatic activity following nitrosocobolamine compared with other mutants, highlighting the importance of S-Nitrosylation on the protein's activity.(Tang et al. 2006)

Thus there are many methods available for the detection of protein S-nitrosylation (see Table 2), though none of them is alone sufficient to provide conclusive evidence for S-nitrosylation. This requires the use of multiple methods to triangulate and confirm that the proteins are truly S-nitrosylated. To then address the functional consequences of SNO of a single protein point mutations of the respective cysteine are required and functional assays must be developed and applied in unison.

Table 2 Summary of methods for the detection and identification of S-Nitrosylation

Method	Quantification (method)	Protein ID	Site ID	Purification	Labeling	Reduction
Direct MS	X	√	√	X	X	X
Organomercuric	X	√	√	Biotin-Avidin	Biotin	X
SNOSID	X	√	√	Biotin-Avidin	Biotin	Ascorbate
ICAT	√ (MS)	√	√	Biotin-Avidin	Biotin	Ascorbate
Biotin switch	√ (Immuno-detection)	√	X	Biotin-Avidin	Biotin	Ascorbate
SNO-DIGE	√ (Fluroscent labeling)	√	X	X	CyDye	Ascorbate
SNO-LISA	√ (Immuno-detection)	√	X	Immuno-absorbent	Biotin	Ascorbate
Diamino fluorescein	√ (total)	X	X	X	X	X
Saville assay	√ (total)	X	X	X	X	X
SNO-SILAC	√ (MS)	√	√	X	Thiol reactive agent	Ascorbate

1.4.2 S-Nitrosylation in pain

Presently not many studies have addressed the implications of SNO in pain. Lu et al. published in 2011 that rapid S-nitrosylation of actin by NO donors was implicated in inhibitory action on inhibitory synaptic transmission in the spinal dorsal horn (Lu et al. 2011). However a variety of proteins that are known to be involved in pain processing, and neuronal or glial adaptions to ongoing nociceptive stimulation or injury have been shown to be targets of S-nitrosylation (see Figure 3). Specifically S-nitrosylation affects the functions of:

- glutamate receptors (Lipton et al. 1993, Kim et al. 1999)
- receptor trafficking (Huang et al. 2005, Selvakumar, Huganir and Snyder 2009)
- transcription factors (Choi et al. 2000, Reynaert et al. 2004, Li et al. 2007, Tsang et al. 2009)
- pro-inflammatory enzymes (Gu et al. 2002)
- heat-shock proteins (Martinez-Ruiz et al. 2005)
- proteases (Mannick et al. 2001),
- cytoskeletal (Lu et al. 2009) and synaptosomal (Palmer et al. 2008) proteins,
- Ion channels (Evans and Bielefeldt 2000, Yoshida et al. 2006, Jian et al. 2007, Asada, Kurokawa and Furukawa 2009).

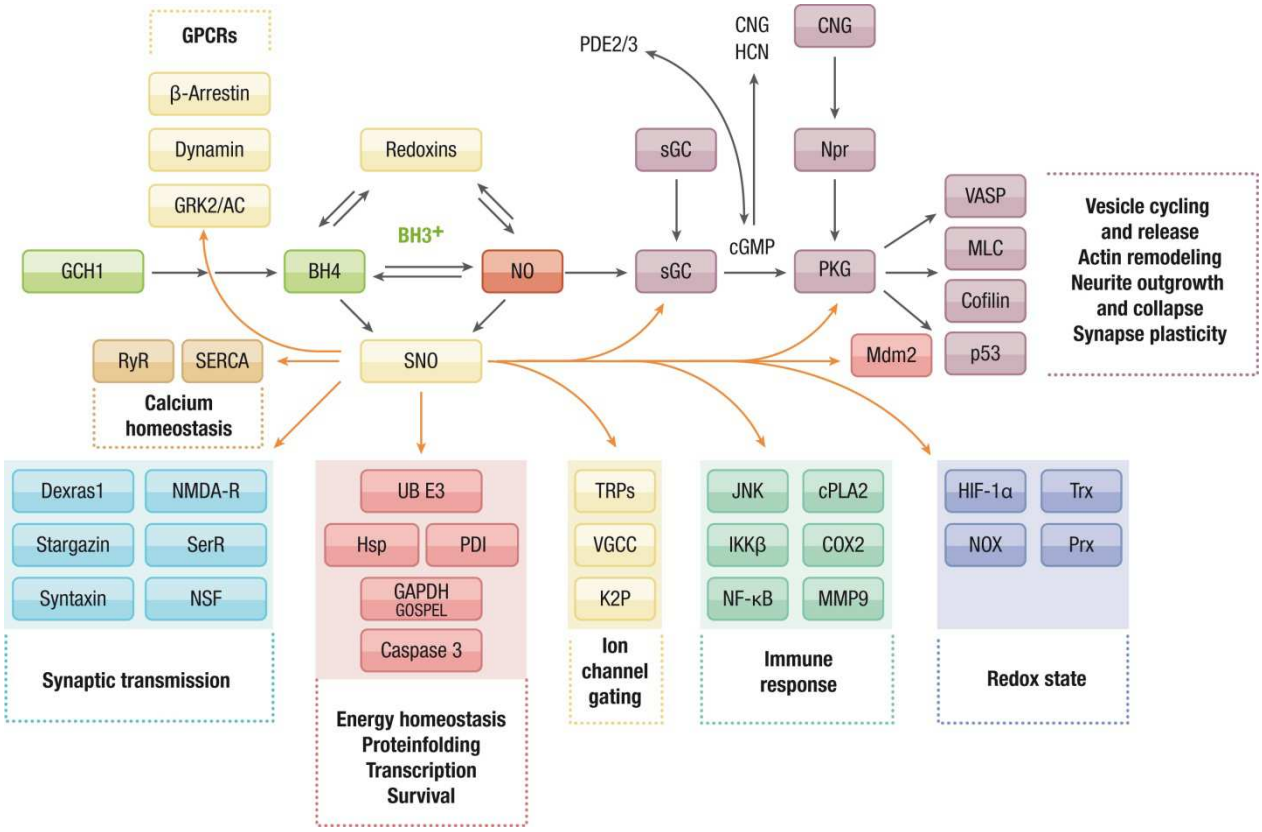

Figure 3 Nitric oxide signaling pathways.
NOS activity depends on the availability of its enzyme cofactor, tetrahydrobiopterin (BH4), which is produced in a multistep synthesis cascade initiated by the GTP cyclohydrolase 1 (GCH1). NO activates sGC, which produces cGMP, leading to activation of PKG, phosphodiesterases (PDE2 and PDE3), CNGs, and HCNs. In neurons, activation of PKG regulates neurite outgrowth and collapse and neurotransmitter release. In addition to this classic NO/sGC/PKG signaling pathway, NO modifies nociceptor sensitivity and synaptic functions by direct S-nitrosylation of glutamate receptors, scaffolding and motor proteins, ion channels, kinases, proteases, and redoxins. AC, adenylyl cyclase; Hsp, heat-shock protein; JNK, c-Jun N-terminal kinase; K2P, two-pore potassium channel; Mdm2, murine double minute 2; MLC, myosin light chain; NOX, NADPH oxidase; Npr, natriuretic peptide receptor; Prx, peroxiredoxin; SERCA, sarco/endoplasmic reticulum Ca2-ATPase; SerR, serine racemase; UB E3, ubiquitin 3 ligase; VASP, vasodilator-stimulated phosphoprotein.

Although this may seem like quite diverse targets there are three main schemes that emerge from this on closer inspection. The three major schemes that potentially modulate pain by SNO are:

1) Ion channels
2) Membrane fusion and fission
3) Proteasome or protease-mediated protein degradation

Thus NO mediated S-nitrosylation may serve to propagate the nociceptive signals similarly to the regulation by phosphorylation and de-phosphorylation, and might have just as much impact on the nociceptive response and adaption to long lasting injuries such as axonal injury (Tegeder et al. 2011).

1.4.2.1 Ion channels and membrane fusion and fission proteins

Although the methods currently available for the identification of S-Nitrosylation are not very effective for membrane proteins several important candidates in terms of neuropathic pain have been identified as S-Nitrosylated (see Table 3). However, most targets have only been identified in cell culture using NO-donors such as NONOate or CysNO, as a result the impact of S-Nitrosylation of most of these proteins *in vivo* remains to be elucidated.

The best studied example of SNO affecting ion channel gating is the N-Methyl-D-aspartic acid (NMDA) glutamate type receptor. Direct S-nitrosylation of the NR2A subunit at cysteine 399 results in a change of its channel gating properties that curtail the excessive calcium influx in neurons and in protects from excitotoxic insults (Lipton et al. 1993, Kim et al. 1999, Choi et al. 2000). Glutamate is one of the most important primary excitatory neurotransmitters and pharmacological experiments have shown that blocking the NMDA receptor reduces nociception and prevents nerve injury-evoked death of nociceptive neurons in the dorsal horn (Scholz et al. 2005, Laughlin, Kitto and Wilcox 1999). This suggests that glutamate excitotoxicity and NMDA receptor hyperexcitability are involved in neuronal death and development of neuropathic pain, and that S-nitrosylation may have a protective role.

The NMDA receptor has also been shown to be indirectly controlled by S-nitrosylation of several proteins interacting with the receptor. Overstimulation of the NMDA receptor and permanent SNO of Dexras1 may cause iron overload and neurotoxicity (Jaffrey, Fang and Snyder 2002, Cheah et al. 2006). NMDA receptor activation enhances the SNO of astroglial serine racemase (ASR) through activation of nNOS that releases NO into the postsynaptic neuron. SNO of ASR in turn increases the release of D-serine, a co-agonist of glutamate and leads to the development of long-term potentiation (Mustafa et al. 2007, Chiang et al. 2007). Proteomic screening has additionally detected SNO in the excitatory amino acid transporter 2 and glutamine synthase (Goerg et al. 2007, Butterfield et al. 2006).

Table 3 S-Nitrosylation of ion channels and membrane proteins

Target protein	SNO Site	Effect of SNO on target function	Presumed consequence in nociception	Source
Cyclic nucleotide-gated channels	Cys460	Activation	Increase of nociceptive neuron sensitivity	(Broillet 2000)
Glutamate receptor 6 (GluR6)	N.D.	Modulation of nNOS and GluR6 coupling and subsequent activation of c-Jun N-terminal kinase signaling.	Increase of nociceptive neuron sensitivity	(Yu et al. 2008)
KCNQ1 potassium channel	Cys445	Modulation of channel function	Increase of nociceptive neuron sensitivity	(Asada et al. 2009)
Potassium channel hKv1.5	N.D.	Blocks hKv1.5 channels by SNO and by a cyclic GMP-dependent mechanism	Increase of nociceptive neuron sensitivity	(Nunez et al. 2006)
Ryanodine receptor (RyR1)	Cys3635	Reduction of RyR1 open channel probability and Sarcoplasmic reticulum Ca2+ leak	Modulation of ESPCs in lamina II nociceptive neurons in spinal cord	(Sun et al. 2001, Salanova et al. 2008, Bellinger et al. 2009, Aracena-Parks et al. 2006)
Ryanodine receptor 2 (RyR2)	N.D.	Sarcoplasmic reticulum diastolic calcium leak and arrhythmogenesis	Modulation of ESPCs in lamina II nociceptive neurons in spinal cord	(Gonzalez et al. 2007)
Transient receptor potential protein 5 (TRPC5)	Cys553 and Cys558	Nitrosylation of native TRPC5 upon G protein-coupled ATP receptor stimulation elicits entry of Ca2+ into endothelial cells.	Increase of nociceptive neuron sensitivity	(Yoshida et al. 2006)
Voltage gated calcium channels	N.D.	Increase of calcium influx	Increase of nociceptive neuron sensitivity	(Jian et al. 2007)
N-ethylmaleimide sensitive factor (NSF)	Cys11, 21, 334, 568, 582	Inhibition of SNARE complex disassembly, reduction of synaptic vesicle exocytosis, increase of membrane insertion of AMPA-R GluR2	Decrease of nociceptive neuron sensitivity to noxious stimuli, decrease of LTP at nociceptive synapses.	(Huang et al. 2005, Matsushita et al. 2003)
NMDA-R Subunit NR2A	Cys399	Reduction of calcium influx	Prevention of glutamate excitotoxicity and hyperexcitability	(Lipton et al. 1993, Choi et al. 2000)
NMDA-R Subunit NR1	Cys744, 798	Reduction of calcium influx	Prevention of glutamate excitotoxicity and hyperexcitability	(Takahashi et al. 2007)
Stargazin	Cys302	Increase of AMPA-R membrane insertion	Increase of nociceptive neuron sensitivity.	(Selvakumar et al. 2009),
Syntaxin 1	Cys145	Regulation of synaptic vesicle exocytosis	Prevention of excess glutamate or neuropeptide release.	(Palmer et al. 2008)
TRPC5	Cys553, 558	Increase of channel gating for calcium entry	Increase of nociceptive neuron sensitivity.	(Yoshida et al. 2006)

The ATPase N-ethylmaleimide-sensitive factor (NSF) is a crucial protein for membrane trafficking in many cells, including neurons, and functions as a soluble NSF attachment protein receptor (SNARE) chaperone that binds to SNARE complexes and uses the energy of ATP hydrolysis to disassemble the complex, thus facilitating SNARE recycling. Upon S-nitrosylation of NSF, vesicle exocytosis was reduced because SNO-NSF lost the ability to disassemble the SNARE complex, despite maintaining its ATPase activity. Nitric oxide also inhibited the dissociation of NSF from the synaptic vesicle protein syntaxin which itself is modified by S-nitrosylation and is involved in the regulation of neurotransmitter release (Palmer et al. 2008, Huang et al. 2005, Sollner and Sequeira 2003, Matsushita et al. 2003). Syntaxin 1a-deficient mice developed enhanced allodynia after peripheral nerve injury and dorsal horn excitatory postsynaptic currents were enhanced in both frequency and amplitude in these mice (Takasusuki et al. 2007).

Thus direct S-nitrosylation of one crucial ATPase may modify nociceptive signal transduction at multiple sites with variable outcome, depending on the stimulus and the site of NO release and being mediated mainly by adaptation of membrane fusion and fission and receptor compartmentalization.

1.4.2.2 Proteasome or protease-mediated protein degradation

Disruption in protein folding and degradation are the hallmark of many neurodegenerative disorders such as Multiple Sclerosis and Alzheimer´s disease. Recent evidence suggests that the disruption of these processes can be caused by redox reactions triggered by excessive levels of NO. S-nitrosylation-mediated targeting of protein degradation pathways including autophagy and proteasomal degradation may constitute a general mechanism by which nitric oxide interferes with the removal of misfolded proteins and the stability of transcription factors and hence long-term adaptations to neuronal stress. S-nitrosylation may also be important for the quality control of mitochondria. Under neuronal stress, including that caused by axonal injury, there is an up-regulation of heat-shock proteins such as the 27-kDa heat-shock protein (Lewis et al. 1999, Benn et al. 2002) and protein disulfide isomerase (PDI) (Walker et al. 2010). This adaption helps the neuron survive the injury by facilitating protein maturation and transport of unfolded secretory proteins. Uehara et al. have shown that the S-nitrosylation of PDI, as well as various chaperones, is linked with protein misfolding and neuronal death (Uehara et al. 2006). S-nitrosylation of PDI compromises its catalytic chaperone and thiol-disulfide oxidoreductase function, leading to accumulation of misfolded proteins and, eventually, cell death. Thus, excessive NO levels may interfere with an adaptive response to protect neurons.

In addition S-nitrosylation may affect protein stability by modulation of ubiquitination and proteasomal degradation, S-nitrosylation has been found to regulate the activity of hypoxia-inducible factor (Li et al. 2007), tumor suppressor p53, iron response proteins, glyceraldehyde-3-phosphate dehydrogenase (GAPDH), and IκB/NF-κB by regulating the degradation of the respective S-nitrosylated protein, a regulatory partner, or the ubiquitin E3 ligase. Thus, although the mechanism and localization of S-nitrosylation may differ and depend on the close association of NOS and the respective targeted protein, S-nitrosylation ultimately affects the ability of the neuron to dispose of protein waste which may impact on neuron survival and hence, development and maintenance of chronic pain (DiAntonio and Hicke 2004, Bingol and Schuman 2005, Sutton and Schuman 2006).

Table 4 S-Nitrosylation in proteasome or protease-mediated protein degradation

Target protein	SNO Site	Effect of SNO on target function	Presumed consequence of SNO in nociception	Source
β-arrestin 2	Cys410.	Promotion of GPCR endocytosis and recycling	Function of cannabinoid and opioid receptors and tolerance.	(Ozawa et al. 2008)
GAPDH	N.D.	Increase of binding to and signaling of Siah	Increase of glutamate excitotoxicity	(Hara et al. 2005, Mohr, Stamler and Brune 1996)
GOSPEL	Cys47	Facilitation of GAPDH-GOSPEL binding, and neuroprotection by GOSPEL	Decrease of glutamate excitotoxicity	(Sen et al. 2009)
NF-κB p50	Cys62	Inhibition of DNA binding capacity	Anti-inflammatory	(Kelleher et al. 2007)
NF-κB p65	N.D.	Inhibition of DNA binding capacity	Anti-inflammatory	(Kelleher et al. 2007)
Hypoxia-inducible factor 1 (HIF-1)	Cys533	Stabilization and increase of transcriptional activity	Increase of nociceptive neuron sensitivity and pro-inflammatory	(Li et al. 2007)
Protein-disulphide isomerase (PDI)	N.D.	Inhibition of catalytic activity, accumulation of polyubiquitinted proteins and activation of the unfolded protein response	Increase of ER stress	(Uehara et al. 2006, Walker et al. 2010)

1.4.2.3 Autophagy

Rodriguez-Muela et al. recently published a study showing that autophagy and protein degradation can promote survival of retinal ganglion cells after optic nerve axatomy in mice (Rodriguez-Muela et al. 2012). Neuronal death after axonal injury is believed to be crucial in the development of neuropathic pain, and thus any process that interferes or enhances the odds of a neuron recovering from injury is likely to attenuate chronic pain. Sarkar et al. were able to show that through inhibition of the SNO substrates JNK1 and IKKβ, NO impaired autophagy. This was supported by the fact that

overexpression of nNOS, iNOS, or eNOS impaired the formation of autophagosomes. Sarkar et al. also showed that inhibition of NOS enhanced the clearance of autophagic substrates and reduced neurodegeneration in models of Huntington´s disease, leading to the conclusion that nitrosative-stress mediated protein aggregation in neurodegenerative diseases may be in part due to inhibition of autophagy (Sarkar et al. 2011).

In light of the increased NO content of neurons after injury and the fact that the cGMP/PKG pathway does not fully explain the effects of NO in pain it may be hypothesized that the pro-nociceptive effects of NO are also mediated through the direct S-Nitrosylation of proteins. The main mechanisms of S-Nitrosylation in adaption to pain signaling are most likely found in ion-channels, receptors, mitochondrial quality control, as well as proteins involved in protein recycling. It is thus interesting to study the S-nitrosoproteome of the neuropathic pain model to figure out which proteins are important targets of SNO.

1.5 Context and problem statement

With increasing evidence of the pro-nociceptive role of NO in pain, and that the cGMP and PKG pathway do not entirely explain NO´s effect, it is important to elucidate the functional role of SNO in this context. The limited number of studies into the effects of SNO in pain and autophagy leave much room for investigation and contemplation. To address this lack of information I set out to investigate the SNO-proteome of the spinal cord after induction of neuropathic pain by SNI treatment. It is thus the aim of this study is to identify potential targets of S-Nitrosylation and de-nitrosylation in neuropathic pain in the mouse spinal cord. However, limits to this investigation are noted from the start, mainly as the methods used are expensive and time consuming and all underrepresent membrane proteins thus making the exploration of the full membrane SNO-proteome impossible. With respect to the animal model, I limit the study to the role of S-Nitrosylations in neuropathic pain induced by the SNI model. Although an investigation into the role of other types of chronic pain, such as inflammatory pain, would be interesting other types of pain models are nevertheless not covered. The study is also limited to S-Nitrosylations and does not investigate any of the other various oxidative modifications of cysteine thiols such as disulfide bridges, sulfoxidation, or glutathionylation. The study is also limited to the spinal cord of the mouse, although certainly the tissue from the dorsal root ganglia, brain sensory cortex, and the thalamus would be interesting as well they are not investigated, in part due to the small amounts of tissue recoverable from these parts.

Emerging from the initial screening as one of the most interesting schemes of potential targets for SNO for us, as well as recently being related to pain and pain recovery, a secondary aim of this study is to investigate the potential role of NO and SNO in proteasomal degradation and autophagy. Here I have limited the scope to autophagy induced by rapamycin (macro autophagy) in a cell culture of neuroblastoma cells (SHSY-5Y) overexpressing nNOS or wild type.

2. Methods and materials

2.1 Materials

Chemical	Abbreviation	Manufacturer
3-[(3-cholamidopropyl) dimethylammonio]-1-propanesulfonate	Chaps	Sigma-Aldrich, Seelze
Acetic acid 100%		Merck KGaA, Darmstadt
Acetone		Sigma
Acetonitrile		Sigma-Aldrich, Seelze
Ascorbate		Sigma-Aldrich, Seelze
Biotin-HPDP		Thermo Scientific
Bovine serum albumin	BSA	Carl Roth GmbH & Co, Karlsruhe
Bradford-Reagent		Sigma-Aldrich, Seelze
Calcium chloride	CaCl2	Merck KGaA, Darmstadt
Calcium chloride		Sigma-Aldrich, Seelze
Chloroform		Merck KGaA, Darmstadt
Complete mini protease inhibitor		Roche
CuSO4		Sigma-Aldrich, Seelze
Cysteine		Sigma-Aldrich, Seelze
Dimethylsulfoxid	DMSO	Sigma-Aldrich, Seelze
Dithiothreitol	DTT	AppliChem GmbH, Darmstadt
Ethanol 70%		Carl Roth GmbH & Co, Karlsruhe
Ethanol absolute		Sigma-Aldrich, Seelze
Ethylenacetat		Carl Roth GmbH & Co, Karlsruhe
Ethylenediaminetetraacetic acid	EDTA	Sigma-Aldrich, Seelze
Glycerol		Carl Roth GmbH & Co, Karlsruhe
Glycin		Carl Roth GmbH & Co, Karlsruhe
High Capacity Streptavidin Agarose Resin		Pierce
Hydrochloric acid	HCl	Sigma-Aldrich, Seelze
Iodoacetamide	IAM	Sigma-Aldrich, Seelze
IPG-Buffer		GE Healthcare
Isoflurane		Abbott GmbH und Co KG, Wiesbaden
Isopropanol 100%		Carl Roth GmbH & Co, Karlsruhe
Magnesiumchlorid	$MgCl_2$	Merck KGaA, Darmstadt
Methanol 100%		Sigma-Aldrich, Seelze
MyOne Streptavidin Dynabeads		Invitrogen
N-Ethylmaleimide	NEM	Fluka
Neucuproine		Sigma-Aldrich, Seelze
Nicotinamide adenine dinucleotide	NAD	Sigma-Aldrich, Seelze
Nicotinamide adenine dinucleotide phosphate	NADPH	Sigma-Aldrich, Seelze
Nω-Nitro-L-arginine methyl ester hydrochloride	L-NAME	Sigma-Aldrich, Seelze
Odyssey Blocking Puffer		Li-COR Odyssey, Bad Homburg
PageRuler™ Prestained Protein Ladder		Fermentas

Pefabloc		Roche Diagnostics, Mannheim
PonceauS		Carl Roth GmbH & Co, Karlsruhe
Potassium chloride	KCl	Merck KGaA, Darmstadt
Precision Plus Protein Dual Color		BioRad Laboratories, California
Protease inhibitor cocktail		Sigma-Aldrich, Seelze
Rapamycin		Sigma-Aldrich, Seelze
Rotiphorese® Gel 30		Carl Roth GmbH & Co, Karlsruhe
Saccharose		Carl Roth GmbH & Co, Karlsruhe
Sodium acetate		Carl Roth GmbH & Co, Karlsruhe
Sodium chloride	NaCl	Sigma-Aldrich, Seelze
Sodium citrate		Carl Roth GmbH & Co, Karlsruhe
Sodium dihydrogen phosphate		Sigma-Aldrich, Seelze
Sodium dodecyl sulfate	SDS	Serva Electrophoresis GmbH, Heidelberg
Sodium hydrogen phosphate		Sigma-Aldrich, Seelze
Sodium hydroxide pellets		Sigma-Aldrich, Seelze
TEMED		Carl Roth GmbH & Co, Karlsruhe
Tetrahydrobiopterin	BH4	Sigma-Aldrich, Seelze
Thiourea		Sigma-Aldrich, Seelze
Tris Base		AppliChem GmbH, Darmstadt
tris(hydroxymethyl)aminomethane	Tris	Sigma-Aldrich, Seelze
TritonX-100		Merck KGaA, Darmstadt
Tween20		Sigma-Aldrich, Seelze
Urea		Serva
β–Mercaptoethanol	βME	Merck KGaA, Darmstadt

Cell culture chemicals	**Abbreviation**	**Manufacturer**
RPMI 1640		Gibco, Paisley, Scotland
Fetal calf serum	FCS	Gibco, Paisley, Scotland
Trypsin		Gibco, Paisley, Scotland
Penicillin G		Gibco, Paisley, Scotland
Streptomycin		Gibco, Paisley, Scotland
L-Gluatamie		Gibco, Paisley, Scotland
SILAC™ Protein ID & Quantitation Media Kit Lysine (DMEM-Flex)		Invitrogen, Karlsruhe
SILAC™ Stable Isotopic [13C6]-L-Arginine		Invitrogen, Karlsruhe

Kits	**Manufacturer**
Cy3 and Cy5 minimal labeling kit	GE Healthcare
Lowry assay kit	BioRad Laboratories, California

2.2 General solutions and buffers

Phosphate buffered saline (PBS):	1.7 M	NaCl
	34 mM	Potassium Chloride
	111 mM	Disodium hydrogen phosphate
	18.4 mM	Potassium dihydrogen phosphate
		pH adjusted to 7.4
Tris buffered saline (TBS)	50 mM	Tris
	150 mM	NaCl
		Adjust pH to 7.6
PBS-T:	0.1%	Tween 20 diluted in PBS
SDS Running buffer	25 mM	Tris-Base
	0.2 M	Glycin
	0.1 %	SDS
Laemmli buffer (4x)	0.2 M	Tris-HCl-buffer (0.5 M, pH 6.8)
	10 %	SDS
	40 %	Glycerol
	0.004 %	Bromphenolblue
	20 %	ß-Mercaptoethanol
Western blot blocking buffer	50 %	Odyssey Blocking Puffer
	50 %	PBS
Antibody incubation buffer	50 %	Odyssey Blocking Puffer
	50 %	PBS-T
Transfer buffer	48 mM	Tris-Base
	39 mM	Glycin
	20 %	Methanol
	0.0037 %	SDS
Ponceau-staining solution	3 %	Trichloroacetic acid
	0.1 %	Ponceau S

2.3 Western blot

2.3.1.1 Western gels (recipe for 2 mini-gels)

	Separation gel (10%)	**Separation gel (12%)**	**Stacking gel**
Water	4.16 ml	3.44 ml	2.40 ml
Tris buffer (1.5 M pH 8,8)	2.46 ml	2.46 ml	1.00 ml
Acrylamide (Rotiphorse Gel 30)	3.28 ml	3.94 ml	0.50 ml
SDS	98.40 µl	98.40 µl	40 µl
APS (10%)	49.20 µl	49.20 µl	40 µl
Temed	4.92 µl	4.92 µl	4 µl

Separation of protein mixtures and subsequent identification with target specific antibodies was performed using SDS-polyacrylamide gel electrophoresis (SDS-PAGE) and western blotting (Burnette 1981). For the SDS-PAGE a vertical Mini-Protean® 3 electrophoresis system (Bio-Rad, Munich) using 1 mm thick gels that consisted of a separation gel (10 % or 12 % polyacrylamide, about 5.5 cm tall) and a stacking gel (3.75 % polyacrylamide, about 1.5 cm tall). Approximately 30 µg of protein was used per sample mixed with Laemmli buffer in a 4:1 ratio and heated to 95°C for 5 minutes before being loaded in to the wells of the stacking gel. Each gel also contained in a single well five µl of protein weight marker (Precision Plus Protein®, Biorad, Munich). The electrophoretic process was generally performed in two separate steps. First, the protein solutions were transferred into the stacking gels using a voltage of 80 V and after entry into the separating gel the current is increased to 120 V until adequate separation of the proteins was achieved as evident by the separation of the molecular weight standard.

After electrophoretic separation, the proteins were transferred to a Nitrocellulose membrane (0.2 micron protan, Whatman, Dassel). The gels are placed on top of the blotting paper and briefly equilibrated with the Transfer buffer, and then transferred using a Trans-Blot Semi-Dry Transfer Cell (Bio-Rad, Munich) under 100 V for 60 minutes. The success of the transfer was confirmed by staining the blot with Ponceau solution and after washing away the Ponceau stain with PBS the unspecific binding sites of the membrane were blocked using a blocking solution, for 2 hours at room temperature or overnight at 4°C.

2.3.1.2 Target detection with primary antibodies

For the detection of specific proteins the blots were incubated with primary antibodies according to Table 5.

Table 5 Antibodies used and their dilution

Protein	Gene	Dilution	Condition	Species	Producer	Product ID
Protein disulfide-isomerase	pdi	1:200	2 h, RT	Rabbit	Cell Signaling	C81H6
Glutathione synthetase	gss	1:200	1.5 h, RT	Rabbit	abcam	ab91591
Aconitate hydratase 2	aco2	1:200	2 h, RT	Rabbit	abcam	ab83528
Peroxiredoxin-6	prdx6	1:1000	2 h, RT	Mouse	abcam	ab16947
Tubulin-α	tuba	1:2000	2 h, RT	Mouse	Upstate	05-829
Tubulin-β	tubb	1:2000	2 h, RT	Mouse	Promega	G7121
GAPDH	gapdh	1:2000	2 h, RT	Mouse	Ambion	AM 4300

After incubation, the membranes were washed with PBS-T 3 times for 5 – 10 minutes each time, followed by incubation with secondary antibody accordingly to the host species of the primary antibody. Secondary antibodies against the target antibodies were used according to Table 6.

Table 6 Secondary antibodies used and their dilution

Species	Dilution	Condition	Species	Producer	Product ID
α-Rabbit 680	1:1000	1 h, RT	Goat	LI-COR	926-68071
α-Rabbit 800	1:1000	1 h, RT	Goat	LI-COR	926-32211
α-Mouse 800	1:1000	1 h, RT	Goat	LI-COR	926-32210
α-Goat 680	1:1000	1 h, RT	Goat	LI-COR	926-68074
α-Sheep 800	1:1000	1 h, RT	Rabbit	Rockland	713-430-002

After incubation with the secondary antibody, the membranes were washed again using the same procedure and scanned using Odyssey infrared scanner (Licor, Lincoln) and quantified using the Odyssey 2.1 software.

2.4 Animals and treatments

In this work C57BL/6 mice were used. At the time of operation, they were six to eight weeks old and were housed under a 12-h light/dark cycle with lights on at 7 a.m. and off at 7 p.m. with food and water *ad libitum*. The experiments adhered to the guidelines of the Committee for Research and Ethical Issues of the International Association for the Study of Pain (IASP), were approved by the local Ethics Committee for Animal Research (Darmstadt, Germany) and adhered to the guidelines of GV-SOLAS for animal welfare in science.

2.4.1 Nerve injury model

Surgery was carried out under 1.5–2 % isoflurane anesthesia. For the spared nerve injury (SNI), two of the three peripheral branches of the sciatic nerve, the common peroneal and the tibial nerves, were ligated with silk (6–0) and distally transected, leaving the sural nerve intact (Decosterd and Woolf 2000). In sham control experiments, the sciatic nerve was exposed but not cut. For the animals treated with Nω-Nitro-L-arginine methyl ester hydrochloride (L-NAME) 30 mg/kg were injected intra peritoneal one hour before the SNI surgery and then again 30 minutes before sacrificing.

Mice were sacrificed twenty-four hours or seven days after surgery with isoflurane or $CO_{2,}$ plus exsanguination. The L4-L6 lumbar spinal cord, ipsi-lateral to the SNI injury was excised, frozen in liquid nitrogen and stored at -80°C.

2.4.2 Behavioral assessments of nociception

The sensitivity to mechanical and heat stimulation of the paws ipsi and contralateral to the sciatic nerve injury was measured at baseline before surgery, 24h after SNI before drug injection, and at 1h, and 4h after intraperitoneal injection of 30 mg/kg of L-NAME or vehicle (PBS).

After adaptation of the animals to the experimental environment, the latency for paw withdrawal was measured using a Dynamic Plantar Aesthesiometer (Ugo Basile, Italy) which assesses the sensitivity to pointy mechanical stimulation. The blunt pin-like steel rod was pushed against the plantar paw with ascending force (0-5 gram over a 10-second period, 0.2 g/sec) and then maintained at 5 gram until the paw was withdrawn. The paw withdrawal latency was calculated as the mean of three consecutive trials at ≥ 30 s intervals.

The sensitivity to painful heat stimuli was assessed by means of the Hargreaves test, which employs a radiant heat source placed underneath the respective hind paw. The withdrawal latency to the heat stimulus was recorded automatically upon paw withdrawal that turns off the heat beam. Three tests were averaged for each testing session. An observer blinded for the treatment assessed behavior.

For statistical analysis data were submitted to analysis of variance for repeated measurements (rmANOVA) and subsequent t-tests employing a correction of alpha according to Bonferroni. Eight mice were treated per group, P was set to 0.05.

2.5 Bradford assay

Protein concentrations determined with the Bradford assay (Marion M 1976) used Bradford reagent (Sigma). A protein standard curve using standards ranging from 0-5 µg/µl was prepared using a dilution series of a BSA solution. Two hundred microliters of Bradford reagent (Sigma) with 10 µl of 1:10 diluted protein solution or standard were mixed. After two minutes, the absorption at 595 nm was measured using Spectra Fluor Plus ® instrument and XFluor ® software (Tecan, Crailsheim).

2.6 Lowry assay

Protein concentrations determined with the Lowry assay (Lowry et al. 1951) used the DC Protein Assay (Bio-Rad, Munich). A protein standard curve using standards ranging from 0.0 – 2 µg/µl was prepared using a dilution series of a BSA solution. Five microliters of protein sample are incubated with 25 µl of Reagent A, followed by 200 µl of Reagent B and incubated at room temperature for about 15 minutes and then the absorption at 690 nm was measured using Spectra Fluor Plus® instrument and XFluor® software (Tecan, Crailsheim).

2.7 2D-SNO-DIGE

2.7.1 Buffers and solutions

Tissue washing buffer	25 mM	NEM in PBS
DIGE buffer (for maleimide labeling)	7 M	Urea
	2 M	Thiourea
	2 % (65 mM)	CHAPS
	30 mM	Tris
	ad 50 ml	Water
	pH adjusted to 7.5 - 8.0 and degased.	
Tissue homogenization buffer for SNO-DIGE	1 tablet	Complete Protease inhibitor
	1 M	NEM
	ad 10 ml	DIGE buffer
Ascorbate Stock	200 mM	Sodium ascorbate
	1 ml	DIGE buffer
Copper stock	1 mM	Copper sulphate x 5 H_2O
	1000 µl	DIGE buffer
10x Reduction stock AC	10 mM	Ascorbate
	0.01 mM	Copper sulphate x 5 H_2O
	1000 µl	DIGE buffer
100x Reduction stock AC	100 mM	Ascorbate
	0.1 mM	Copper sulphate x 5 H_2O
	1000 µl	DIGE buffer
DIGE rehydration buffer	8 M	Urea
	2 % (65 mM)	Chaps
	a.d. 50 ml	Water
	20 mM	DTT (add directly before use)
	0.5 %	IPG buffer (add directly before use)
Equilibration buffer	50 mM	Tris-HCl pH 8,8
	6 M	Urea
	30%	Glycerol
	2 %	SDS
	-	Bromophenol blue
	ad 500 ml	Water
Equilibration buffer with DTT	10 mg/ml	DTT added directly before use
Equilibration buffer with Iodoacetamide	40 mg/ml	IAM added directly before use

SDS running Buffer (10X)	250 mM	TRIS
	2 M	Glycin
	1 %	SDS
	ad 1000 ml	Water
2D-Gels	252 ml	AB-mix (acrylamide -bisacrylamide; 49,5% T, 3% C)
	100 ml	10X SDS Gel buffer Tris-Cl pH 8.8
	500 µl	TEMED
	ad 1000ml	Water (degas and precool)
	4 ml	10% APS
Agarose Sealing buffer	500 mg	Agarose
	20 mg	Bromphenolblue
	ad 100 ml	1x SDS Running buffer

2.7.2 Tissue homogenization

Tissue from the mouse was weighed and then briefly washed with ice-cold washing buffer (PBS with 25 mM NEM). Then 200 µl of tissue homogenization buffer for SNO-DIGE was added to the sample for every 5 mg of tissue weight and the tissue homogenized using a potter under argon and low-light conditions. After homogenization the tissue was incubated at room temperature for 5 minutes and then centrifuged (20.000 x g, 20 minutes, 4°C). The resulting supernatant was then precipitated in ice-cold acetone and placed at -20°C for at least one hour, the pellet was discarded. After incubation at -20°C the sample was centrifuged again (20.000 x g, 20 minutes, 4°C) and the supernatant discarded. The pellet was then dried under argon for about 45 minutes until the pellet was dry.

After drying the pellet was dissolved in 200 µl DIGE buffer for maleimide labeling for every 5 mg of original tissue and the concentration of protein measured using the Bradford assay.

2.7.3 Labeling

Pooled Standard

Five µg from each sample was pipetted into a tube and brought to a final volume of 90 µl with DIGE buffer. Ten µl of 10X Reduction stock AC was added and then 20 µl of Cy3 dye. The standard was mixed by pipetting, followed by a short spin on a centrifuge. The standard was then incubated for 1 hour at room temperature in the dark. After incubation, the reaction was quenched with 20µl of 2 mM cysteine and further incubated for 30 minutes at room temperature in the dark. After quenching the standard was frozen at -20°C overnight. After removal from freezer and thawing, 140 µl of 2X Rehydration buffer (with 2.8 mg DTT and 5 µl Pharmalyte per 1 ml) was added and mixed by pipetting.

2.7.3.1 Samples

Five µg of sample were pipetted to separate tubes and brought to a final volume of 9 µl with DIGE buffer. One µl of 10X Reduction stock AC was added and then 2 µl of Cy5 dye. The samples were mixed by pipetting, followed by a short spin on a centrifuge. The samples were then incubated for 1 hour at room temperature in the dark. After incubation the reaction was quenched with 2µl of 2 mM cysteine and incubated for 30 minutes at room temperature in the dark. After quenching the samples were frozen at -20°C overnight. After removal from freezer and thawing, 14 µl of 2X Rehydration buffer (with 2.8 mg DTT and 5 µl Pharmalyte per 1 ml) were added to each sample and mixed by pipetting. To each sample 28 µl of the pooled standard was added and mixed by pipetting, followed by brief centrifugation.

2.7.3.2 Preparative gel sample

Fifty µg from each sample was pipetted into a tube and brought to a final volume of 250 µl with DIGE buffer. Ten µl of 100X Reduction stock AC was added and then 20 µl of Cy3 preparative dye. The standard was mixed by pipetting, followed by a short spin on a centrifuge. The sample was then incubated for 1 hour at room temperature in the dark. After incubation, the reaction was quenched with 20µl of 20 mM cysteine and incubated for 30 minutes at room temperature in the dark. After quenching 270 µl of 2X Rehydration buffer (with 5.6 mg DTT and 5.5µl Pharmalytes (IPG buffer)) was added to the sample and mixed by pipetting, and then centrifuged briefly. 100 µl were removed from the sample and stored at -20°C overnight. The rest of the preparative sample (450µl) was placed in a rehydration tray with an IEF strip (24cm, 3-10 linear) and allowed to rehydrate the strip overnight.

2.7.4 2D Electrophoresis

IEF Strips (24 cm, pH 3-10 Linear) are placed on the IEF device manifold and covered with Immobiline DryStrip Cover Fluid (GE Healthcare) and the samples loaded using active rehydration at the start of the IEF.

The IEF Program used was as follows:

Current per strip	75 µA
Temperature	20°C
Step 1	step and hold 150V, 3 hours
Step 2	step and hold 300V, 3 hours
Step 3	gradient to 1000V, 10 hours
Step 4	gradient to 8000V, 3 hours
Step 5	step and hold 8000V, 5 hours

After the IEF run is complete, the cover fluid was poured off and the IEF strips briefly washed with water to wash away any residual cover fluid. The strips were then incubated with Equilibration

buffer containing DTT for 15 minutes followed by incubation with Equilibration buffer containing IAM for 15 minutes.

For the second dimension, the gel strips were placed on top of 12.5% SDS gels and sealed with a 0.5 % agarose gel. Before sealing a weight marker was added to the gels anode side (-) side by putting a small amount (10 µl) of the weight marker (PageRuler™ Prestained Protein Ladder, Fermentas) on a small piece of porous paper and placing it on the anode side after the IEF strip has been loaded. The gels were then run at 15W/gel for about 6.5 hours.

2.7.5 Scanning

The gels were scanned using a Typhoon using the following settings:

Fluorescence:	Cy3, Cy5.
PMT:	600V
Press sample:	Yes
Focus:	+3 mm.
Pixel size:	100 µm.
DIGE File naming format:	Cy3 Standard.

2.7.6 Analysis and Spot picking

The 2D SNO-DIGE analysis was composed of 10 analytical gels from 10 mice, 5 from each group of control and SNI-treated. The pooled standard was used to normalize the spots. Two gels were used as preparative gels for spot picking and MS analysis, with either 400 µg or 100 µg of protein.

For the 2D SNO-DIGE with L-NAME treated animals, samples from three animals of each group (naïve, SNI and SNI+L-NAME) were used comprising a DIGE analysis of nine analytical gels and one preparative gel. To assess the impact of anesthesia, skin incision, and exposure of the sciatic nerve, sham-operated mice were compared with naïve mice. For the sham control experiment, four mice were used in each group (naïve vs. sham).

Gels were scanned using a Typhoon™ 9400 Imager (GE Healthcare). Cy3 fluorescent images, at a resolution of 100 µm, were scanned with a 532 nm laser and a 580 nm emission filter and Cy5 fluorescent images with a 633 nm laser and a 670 nm emission filter. Analysis of the gel images was performed with the DeCyder™ software version 6.0 (GE Healthcare) according to the manufacturer's recommendations. The estimated number of spots was set at 2500 per gel and the spots were first matched automatically using the batch function, then checked and manually corrected as needed. Matched spots were compared across groups according to the standardized abundance and considered significantly modified if the average ratio between treated and untreated mice was < -1.2 or > 1.2, and $P < 0.05$ (students t-test). Protein spots showing significant changes between treated

and untreated mice were picked from the gel using an Ettan™ Spot Picker supplied with 2.0 mm picker head and placed in perforated 96 well plates (Thermo Scientific).

2.7.7 Mass spectrometry peptide and protein sequencing

The in gel digestion with trypsin and peptide extraction were done essentially as described by Collins et al. (Collins et al. 2004). Trypsinized peptides were dissolved in 5 % acetonitrile supplied with 0.5 % formic acid in water and separated on a 75 µm ID emitter tip (NewObjectives) filled with 3 µm C18 Hypersil GOLD reversed phase silica (Thermo Scientific) placed in front of an Orbitrap (Thermo Scientific) mass spectrometer. Nano-HPLC runs (60 min for in-gel digests and 90 min for SNO-SID samples) with an increasing acetonitrile gradient from 5 % to 50 % containing 0.1 % formic acid were performed using Agilent 1200 Nano-HPLC equipment with a flow of 200 nl/min. Eluted peptides were submitted online to ESI-MS/MS analysis. The MS data was acquired by a survey scan in a mass range of 400 to 1600 m/z followed by CID fragmentation of up to five precursor ions using Data Dependent Acquisition (exclusion time 3 min, rejection of singly charged precursor ions). Peak lists were generated by Xtract_MSn (Thermo Scientific) and searched using Mascot Server (version 2.2) against a database containing 16,327 species specific (*Mus musculus*) protein sequences downloaded from www.uniprot.org. The Mascot search settings were as follows: maximum missed cleavages 1, precursor mass tolerance 10 ppm, fragment ion tolerance 0.8 Da and optional modifications allowed on methionine (oxidation) and cysteine (modification by NEM and carbamidomethylation by iodoacetamide). Only peptides with individual ion scores indicating identity ($p < 0.05$) were considered significant.

2.7.8 Protein Identification

As the protein sequencing commonly reveals more than protein in each picked gel spot the selection of prime candidate for each spot was done by identifying the molecular mass and calculating the theoretical isoelectric point value of the proteins and matching them to the position of the gel as well as using indirect quantitative values of quantitation based on the number of sequenced peptides, coverage and emPAI values.

2.8 Identification of SNO sites (SNOSID)

Trypsin digestion buffer	50 mM	Tris
	1 mM	$CaCl_2$
	ad 10 ml	Water
		pH adjusted to 7.8
Washing buffer	5 mM	NH_4HCO_3
	10 %	Acetonitrile (MS Grade)
	ad 10 ml	Water (MS Grade) pH adjusted to 8.0

Ten µg of protein from samples prepared for the SNO-DIGE were reduced with 1 mM ascorbate and 10 µM $CuSO_4$ in trypsin digestion buffer and labeled with 200 nM Biotin-HPDP (Thermo Scientific). After one hour incubation, 500 ng of MS grade trypsin (Promega) and 10 % acetonitrile (Geyer) were added and the solution incubated at 37 °C for 16 hours. The trypsinization was stopped with 0.5 mM phenylmethanesulfonylfluoride and the biotinylated peptides were purified with MyOne Streptavidin Dynabeads (Invitrogen) by incubation for one hour. After washing with MS buffer (5 mM NH_4HCO_3, 10 % acetonitrile, pH 8) the peptides were eluted with 5 mM DTT in washing buffer and incubated with 20 mM iodoacetamide for 30 minutes at room temperature (Derakhshan, Wille and Gross 2007). Protein sequencing of resulting peptides was performed the same as for identification of in-gel trypsinized peptides after picking from DIGE gels (see page 28).

2.9 Prediction of SNO sites

For the prediction of SNO sites I used the GPS-SNO 1.0 (Group-based Prediction System) algorithm (Xue et al. 2010). Protein sequences from Uniprot were used based on the protein identification from Mass spectrometry sequencing. Threshold was set at Medium and the sequences run using the Batch version.

2.10 Biotin switch and immunodetection

2.10.1 Buffers

Washing buffer	25 mM	NEM in TBS
Homogenization buffer	2%	SDS
	25 mM	NEM
	100 µM	neocuproine
	1 tablet / 10 ml	Complete® mini protease inhibitor
	ad 10 ml	TBS
ELISA coating buffer	100 mM	$NaHCO_3$
	33 mM	Na_2CO_3
	ad 50 ml	Water
		pH adjusted to 9.5

2.10.2 Tissue homogenization

Tissue for the Biotin-Switch-Technique (BST) and SNO-ELISA was briefly washed with 1 ml of Washing buffer, then homogenized in 200 µl of Homogenization buffer and incubated at room temperature for 5 minutes, centrifuged (16.000 x g, 4°C for 20 minutes) and the supernatant precipitated in ice-cold acetone overnight at -20°C and subsequently centrifuged (16.000 x g, 4°C, 20 minutes). Proteins were dried, dissolved in 400 µl TBS containing 1 % SDS and the protein concentrations determined with a Lowry assay kit (Bio-Rad, Munich).

2.10.3 Biotin switch

Fifty µg of protein were reduced with 1 mM ascorbate and 10 µM $CuSO_4$ in TBS and labeled with 200 nM biotin-HPDP (Thermo Scientific). After one-hour incubation, the solution was precipitated in ice-cold acetone overnight at -80°C. After overnight precipitation, the samples were centrifuged (16.000 x g, 4°C, 20 minutes) and the supernatant acetone was removed. The remaining pellet was allowed to dry for 30 minutes and then dissolved in 50 µl TBS and incubated with 50 µl of High Capacity Streptavidin Agarose Resin (Pierce) beads for 20 minutes. After washing, bound proteins were eluted from the beads with 50 µl SDS buffer containing 5 % mercaptoethanol. The solution was then concentrated with a vacuum rotator (Eppendorf) and the proteins analyzed by western blotting (see page 20).

2.10.4 Biotin switch ELISA (SNO-ELISA)

In addition to the Biotin-Switch with Western Blot detection I developed a novel ELISA based approach to identify the nitrosylation of the target proteins. Nitrosylation sites were labeled with biotin with the biotin switch (above) followed by sandwich ELSIA detection. For this, primary antibodies directed against candidate proteins were coated to the surface of a 96-well plate overnight at 4°C in ELISA coating buffer. Antibodies were directed against protein disulfide-isomerase (*pdi*, 1:500, Cell Signaling, C81H6), glutathione synthetase (*gss*, 1:500, abcam, ab91591), aconitate hydratase 2 (*aco2*, 1:500, abcam, ab83528), peroxiredoxin-6 (*prdx6*, 1:1000, abcam, ab16947), tubulin-beta (*tubb*, 1:500, Promega, G7121), and GAPDH (*gapdh*, 1:500, Ambion, AM 4300). After washing, 1% BSA in PBS was used to block the plate. Subsequently, 20 µg of the SNO-site biotinylated proteins in blocking buffer were loaded per well and incubated overnight at 4°C. After washing, anti-biotin 700 (1:500, manufacturer, Rockland, 600-130-098) was added to the plate and incubated for 2 hours at room temperature. After washing, the plate was then analyzed for the infrared fluorescence on an Odyssey Scanning system to determine the extent of protein biotinylation, and thus indirectly S-nitrosylation.

2.11 Cell culture

Human Neuroblastoma cells (SHSY-4Y) were grown using RPMI 1640 medium supplemented with heat-inactivated 10% fetal bovine serum, 1 % Penicillin / streptomycin, and 2 mM glutamine at 37°C in 5% CO_2 atmosphere at 37°C in a humidified tissue culture incubator.

2.11.1 SILAC cell culture

Human Neuroblastoma cells (SHSY-4Y) were grown using SILAC™ Protein ID & Quantitation Media Kit Lysine (DMEM-Flex) and SILAC™ Stable Isotopic [13C6]-L-Arginine with heat-inactivated 10% fetal bovine serum, 1 % Penicillin / streptomycin, and 2 mM glutamine at 37°C in 5% CO_2 atmosphere at

37°C in a humidified tissue culture incubator. Cells were grown for a minimum of 5 cell cycles before harvesting.

2.11.2 Neuronal NOS-Overexpression

To produce a stable cell line of nNOS over expressing SHSY-5Y neuroblastoma a lentiviral construct was generated using a vector purchased from GeneCopoeia, product ID Mm04153, for mouse Nitric oxide synthase 1.

Lentiviral particles were produced by transient co-transfection of HEK293T cells seeded in 6 cm dishes with 10 µg of vector DNA (Mm04153), together with three helper plasmids (5 µg of pMDL/RRE, 3 µg of RSV-Rev, and pMD2G-VSVG). The calcium phosphate precipitation method was used for transfection according to standard techniques. Cell supernatant containing lentivirus particles was harvested at 48 hours after transfection, and passed through a 0.45 µm filter, and concentrated by centrifugation for 90 min at 40,000 rpm at 4°C. The virus pellet was suspended in 25 µl cold 0.1M PBS and the titer was assessed by GFP expression analysis in transduced tumor cells. Viral titers were 2–3 x 10^7 transduction units/ml.

For transduction, 5 x 10^5 SHSY-5Y cells were seeded in 10 cm dishes and transduced with the respective lentivirus particles at 10 MOI in complete medium. After 3 days the efficiency of virus infection was determined by flow cytometry on the basis of eGFP expression. To exclude the non-infected cells, GFP-positive cells were isolated by the FACSAria Cell sorter (Becton Dickinson, Germany).

2.11.3 Cell stimulation

To induce autophagy in NOS-overexpressing and wild-type SHSY-5Y, 1x10^6 cells were seeded in 75 cm^2 culture flasks and grown to c.a. 60% confluence in RPMI medium supplemented with GlutaMAX™. The cells were then stimulated with 1 µM rapamycin added to RPMI culture medium supplemented with GlutaMAX™. Thirty microliters of a 1 mM stock solution of rapamycin dissolved in ethanol was used. Ethanol in the same amount was added to the untreated cells (vehicle). NOS over-expressing cells were supplemented with 10 µM NAD, 40 µM NADPH, and 100 µM tetrahydrobiopterin for NO production by NOS. Each cell type and stimulation was performed and analyzed in triplicate.

After 6 hour stimulation the cells were washed with PBS and then scraped using standard cell scraper, collected in a 15 ml tube and centrifuged at 1200 rpm for 3 minutes. After centrifugation cells were suspended in PBS and transferred to a 1.5 ml tube, followed by centrifugation and removal of PBS.

2.11.4 Saville-Griess assay

40 mM $NaNO_2$	2.76 mg	$NaNO_2$
	1 ml	Water
40 µM $NaNO_2$	10 µl	40 mM $NaNO_2$
	10 ml	Water
2 N HCl (2 M)	21 ml	37% HCl
	79 ml	Water
0.5% (w/v) ammonium sulfamate	500 mg	ammonium sulfamate
	100 ml	Water
Hg/SN solution	400 mg	$HgCl_2$
	5 g	Sulfanilamide
	20 ml	2 N HCl
	ad 100 ml	Water
Hg/SN/NEDD solution	20 mg	(N-1-(naphthyl)ethylenediamine dihydrochloride)
	10 ml	Hg/SN solution

NO content of protein was determined with the Saville-Griess assay (Saville 1958) adapted for use with microtiter plates. A NO standard curve was prepared with serial dilutions of freshly prepared 40 µM $NaNO_2$. One hundred micrograms of protein were added to a well and diluted to 100 µl. To each well of samples 30 µl of 0.5% ammonium sulfamate (ASM; Aldrich) in water were added followed by 30 µl of 2 N HCl to all wells and incubated for 1 to 2 minutes. After incubation 40 µl of Hg/SN/NEDD solution was added to all wells and incubated for 10 min at room temperature. After incubation, the absorption at 595 nm was measured using Spectra Fluor Plus ® instrument and XFluor ® software (Tecan, Crailsheim).

2.12 SNO-SILAC

2.12.1 Solutions and reagents

SDT-lysis buffer	4 % (w/v)	SDS
	100 mM	Tris/HCl
	150 mM	NaCl
	1 tablet	Protease inhibitors per 10 ml
UA buffer	8 M	Urea
	100 mM	Tris/HCl
		pH adjusted to 8.5
UB buffer	8 M	Urea
	100 mM	Tris/HCl
		pH adjusted to 8.0

ASC / IAM solution	8 M	Urea
	100 mM	Tris/HCl, pH adjusted to 8.5
	1 mM	Ascorbate
	50 mM	Iodoacetamide in UA
	1 µM	CuSO4

2.12.2 Preparation of SILAC Standards

Cell pellet of cells grown in SILAC medium was homogenized in SDT-Lysis buffer containing 10 mM TCEP for 30 minutes and then split in two parts. One part was incubated with 40 mM IAM and the other 40 mM NEM. After centrifugation (16.000 g, 20 min, RT) the solutions were precipitated in ice-cold acetone overnight at -20°C and then solubilized in SDT-Lysis buffer and protein concentration measured with GE NanoVue Spectrophotometer.

2.12.3 Preparation of cells

Cell pellets were homogenized in SDT-Lysis buffer containing 25 mM NEM and incubated for 5 minutes at room temperature. After centrifugation (16.000 g, 20 min, RT) the solutions were precipitated in ice-cold acetone overnight at -20°C and then solubilized in SDT-Lysis buffer and protein concentration measured with a GE NanoVue Spectrophotometer.

2.12.4 Sample processing

Twenty microgram of protein sample are added to a FASP column and diluted with 200 µl UA buffer; then centrifuged at 14.000 x g for 40 minutes, RT. Then 200 µl UA buffer are added and centrifugation repeated. The S-Nitrosylations in the sample are then reduced with 200 µl of ASC / IAM solution (1 mM Ascorbate, 50mM IAM, 1 µM $CuSO_4$) and incubated for 45 minutes followed by addition 20 µg of SILAC standard and centrifugation (14.000 x g for 40 minutes, RT). Samples were washed with with 200 µl UA buffer; then centrifuged at 14.000 x g for 40 minutes, RT. TCEP 10 mM was added to the sample after dilution with UA buffer and incubated for 30 minutes followed by addition of 40 mM NEM and incubation for 30 minutes. Samples were finally washed twice with 100 µl of UB buffer and centrifuged (14.000 x g for 30 minutes, RT) after each washing. Filtrate was discarded after each centrifugation step as the proteins (> 10 kDa) remain in the FASP filter unit.

2.12.5 Sample lysis and desalting

ABC buffer	5 mM	NH_4HCO_3
	1 mM	$CaCl_2$
	ad 10 ml	Water (MS Grade)
		pH adjusted to 8.0

2 X Acidification buffer	5 mM	NH_4HCO_3
	6 %	Acetonitrile
	0.1 %	TFA (CF_3COOH)
	ad 10 ml	Water (MS Grade)
		pH adjusted to 8.0

After dilution with UB buffer, endoproteinase Lys-C was added in a 1:50 ratio (800 ng) and mixed by shaking for 1 min. Then the samples in the filters were incubated overnight in a wet chamber at room temperature. After overnight incubation 150 µl of ABC buffer containing 400 ng Trypsin (1:100 ratio to protein) were added to the samples and they mixed by shaking for 1 min, followed by incubation at RT for 4 hours. The FASP filters are then centrifuged (14.000 g, 40 minutes, RT) and the filtrate collected. After addition of 50 µl 0.5 M NaCl in water, the filter is centrifuged again centrifuged (14.000 g, 20 minutes, RT) and the filtrate pooled with the previous filtrate followed by acidification with 2 X Acidification buffer in a 1:1 ratio.

Samples are then desalted on SPE columns. MILI-SPE Extraction disk cartridge (C18-SD) is primed with 1 ml of CH_3OH and centrifuged (1,500 x g for 1 min), followed by washing with 0.5 ml of 0.1% CF_3COOH, 70% CH_3CN in water and centrifuged, and then 0.5 ml of 0.1% CF_3COOH in water and centrifuged. Samples were then loaded onto the column and centrifuged at 150 x g for 3 min. Samples are washed with 0.5 ml of 0.1% CF_3COOH in water and centrifuge at 150 x g for 3 min. SPE cartridge is then transferred to a new tube and 0.5 ml of 70% CH_3CN in water added to the cartridge and centrifuged at 150 x g for 3 min. The resulting elute containing desalted peptides is then concentrated in a vacuum centrifuge and solubilized in ABC buffer before injection and analysis in mass spectrometer.

2.13 Western blot for autophagy targets

Western blot was performed as described on page 20 above and incubated with primary antibodies according to Table 7 and appropriate secondary antibodies according to Table 6.

Table 7 Primary antibodies for autophagy targets

Target	Gene	Dilution	Conditions	Species	Producer	Product ID
Ubiquitin	ubb	1:1000	1 d, 4°C	Mouse	Santa-Cruz	SC-3936
β-Actin	b-actin	1:1000	1 h, RT	Rabbit	Sigma	N/A
LC-3β	map1lC3b	1:750	2 d, 4°C	Rabbit	Cell Signaling	2775S
p62 (SQSTM1)	sqstm1	1:200	1 d, 4°C	Sheep	Abcam	ab 31545
Neuronal-NOS	nos1	1:1000	1 d, 4°C	Rabbit	Santa-Cruz	SC-648
HSC70	hspa8	1:1000	1 d, 4°C	Goat	Santa-Cruz	SC-1059

3. Results

3.1 Effects of L-NAME on pain behavior

It is fundamental to this study that we see an effect on pain sensation should we inhibit the production of nitric oxide in the central nervous system. In fact this can readily be demonstrated. At 24 hours after an SNI operation, the nerve injury induced hyperalgesia resulted in a paw withdrawal latency of 2 and 1.5 seconds in response to mechanical and thermal stimulation, respectively. By the peritoneal injection of L-NAME, an unspecific inhibitor of NOS, the withdrawal latencies returned back to baseline demonstrating the complete reversal of hyperalgesia. (See Figure 4)

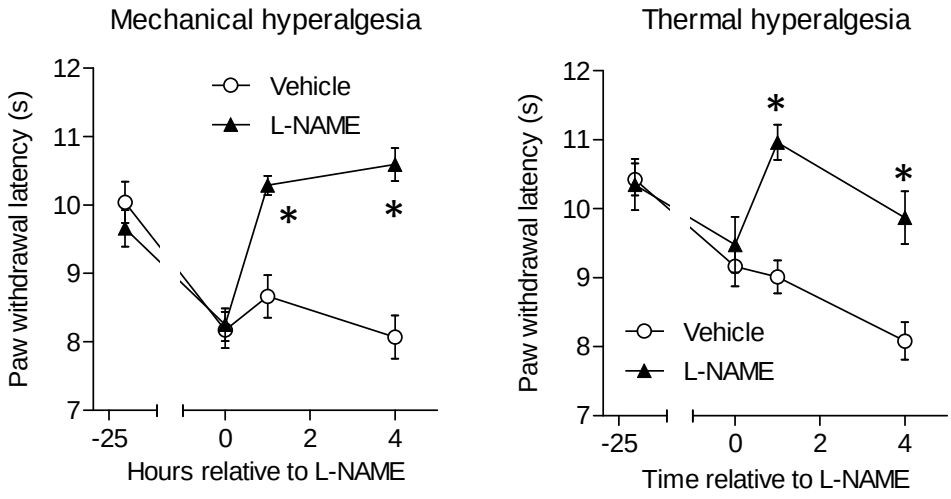

Figure 4 Effects of L-NAME on pain behaviour
Paw withdrawal latencies upon mechanical (left) and heat (right) stimulation of the ipsilateral hind paw at baseline and after SNI, before and after injection of L-NAME or vehicle (n = 8 per group). The asterisks indicate time points which differed significantly between groups (ANOVA for repeated measurements, $P < 0.05$).

Thus preventing the production of nitric oxide in the central and peripheral nervous systems reverses the hyperalgesia. This may be in part mediated through inhibition of cGMP signaling and potentially in part by S-nitrosylation.

3.2 2D SNO-DIGE analysis of protein S-nitrosylation in the spinal cord after SNI

3.2.1 Effects of SNI operation

To explore the potential direct targets of NO that result in S-nitrosylation, I employed the 2D SNO-DIGE using tissue from spinal cord parts L4-L6 twenty four hours after SNI operation. An analysis of spinal cord tissue from SNI treated mice vs. Naïve revealed 57 significantly regulated spots. Spots were considered significantly regulated if the relative change +/- 20% and students T-test $p < 0.05$. Out of these 57 spots 31 showed an increase in SNO and 26 spots a decrease in SNO. The 57 spots were identified to contain 53 unique proteins, with four of them (*aco2, atp5h, dpysl2,* and *serpinb1a*) appearing each in two spots that showed consistent SNO regulation. Based on information from the Uniprot website the proteins were categorized according to their main known function. The functional categorization (see Figure 6) showed that 11 proteins are involved in ATP production and mitochondrial function (classifications: energy metabolism and glucose metabolism), 8 contribute to protein metabolism or folding and 9 regulate neuronal signaling. The functional classifications of the identified proteins suggest that mitochondria, ER and pre- and postsynaptic densities are major intracellular sites where S-nitrosylation occurs.

The most profound changes in nitrosylation levels were found in glutathione S-transferase Mu 1 (*gstm1*, Ratio SNI vs. Naive: 2.78), malate dehydrogenase, mitochondrial (*mdh2*, 1.76), and protein RUFY3 (*rufy3*, 1.74) in terms of up-nitrosylation. Neurofilament medium polypeptide (*nefm*, -4.25), ATP synthase subunit d, mitochondrial (*atp5h*, -3.19), peroxiredoxin-6 (*prdx6*, -3.05), and aconitate hydratase, mitochondrial (*aco2*, -2.43) showed the strongest decrease in S-nitrosylation. Five of these seven proteins (i.e. *aco2, mdh2, prdx6, gstm1,* and *atp5h*) are involved in redox regulation or energy metabolism. See Table 8. A complete list of identified proteins in the SNO-DIGE after SNI is shown in Table 9.

Table 8 Proteins with most profound changes in SNO levels in spinal cord 24 hours after SNI

Spot no.	Gene Name	Name	Ratio	T-test	SNOSID Site	Functional classification
53	*gstm1*	Glutathione S-transferase Mu 1	+2.78	0.002		Redox regulation
44	*mdh2*	Malate dehydrogenase, mitochondrial	+1.76	0.010	89, 93, 212, 275, 285	Energy metabolism
20	*rufy3*	Protein RUFY3	+1.74	0.016		Signaling
33	*psmc5*	26S protease regulatory subunit 8	-2.01	0.012		Protein metabolism
52	*prdx6*	Peroxiredoxin-6	-3.05	0.021	47	Redox regulation
57	*atp5h*	ATP synthase subunit d, mitochondrial	-3.19	0.023	101	Energy metabolism
1	*nefm*	Neurofilament medium polypeptide	-4.25	0.050		Cytoskeleton

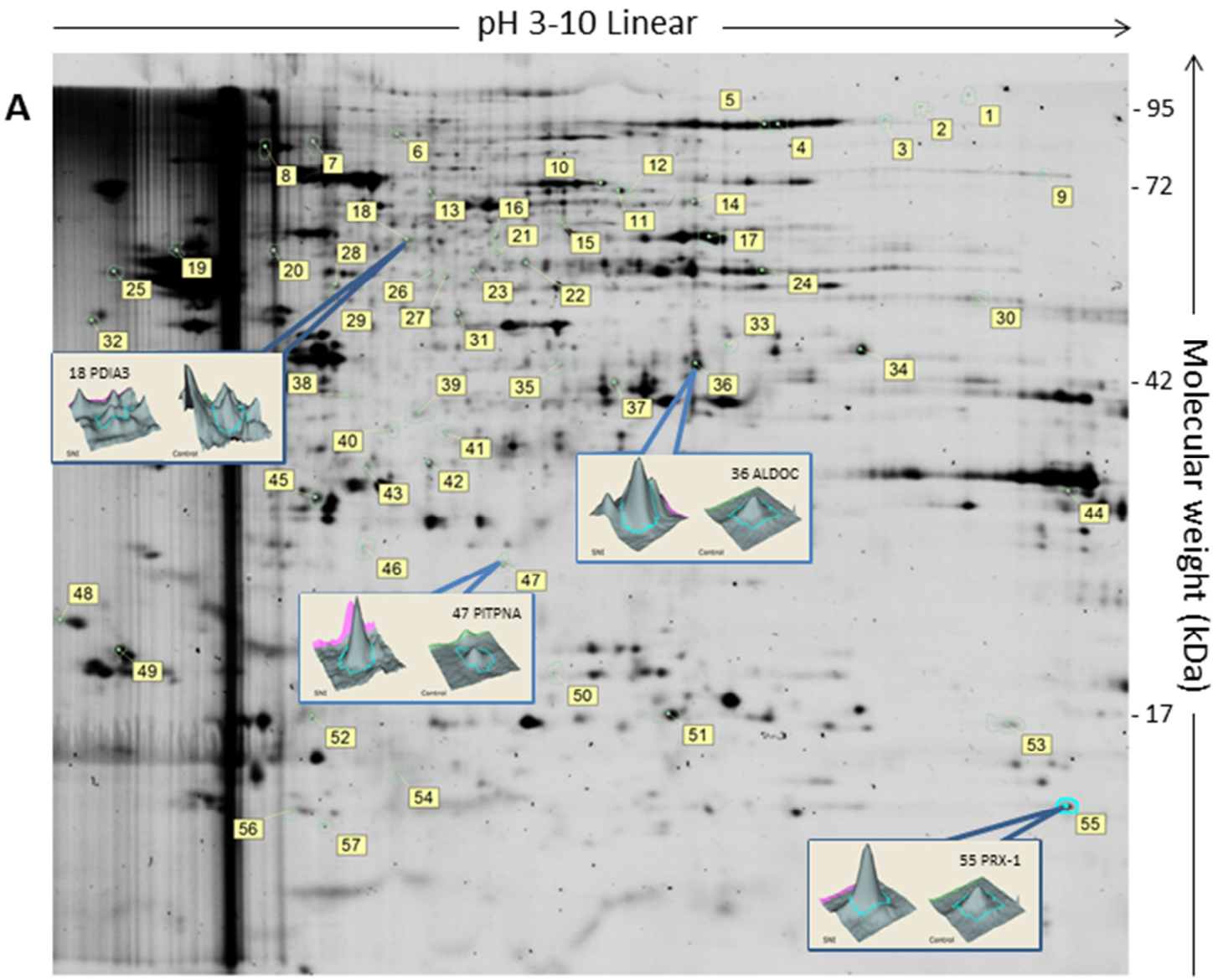
A
pH 3-10 Linear
Molecular weight (kDa)
95
72
42
17
18 PDIA3
36 ALDOC
47 PITPNA
55 PRX-1
SNI
Control

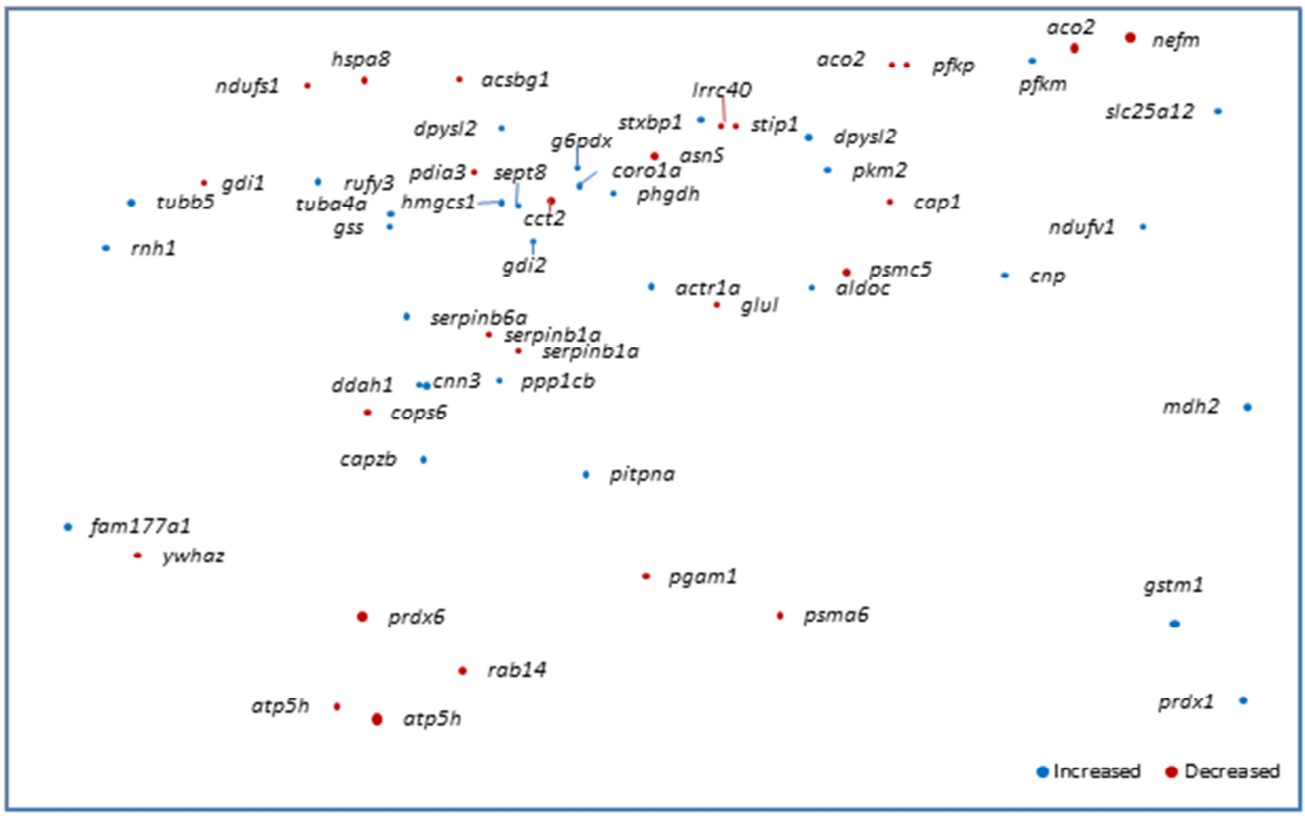
B
hspa8
ndufs1
acsbg1
lrrc40
aco2
pfkp
aco2
nefm
pfkm
slc25a12
dpysl2
stxbp1
stip1
dpysl2
g6pdx
asn5
gdi1
rufy3
pdia3
sept8
coro1a
pkm2
tubb5
tuba4a
hmgcs1
phgdh
cap1
gss
cct2
ndufv1
rnh1
gdi2
psmc5
cnp
actr1a
aldoc
glul
serpinb6a
serpinb1a
serpinb1a
ddah1
cnn3
ppp1cb
mdh2
cops6
capzb
pitpna
fam177a1
ywhaz
pgam1
gstm1
prdx6
psma6
rab14
atp5h
atp5h
prdx1
Increased
Decreased

Figure 5 Representative 2D SNO DIGE gel and spot analysis of the spinal cord after SNI
Representative gel from the analysis of S-nitrosylated proteins in SNI treated vs. naïve mice. Four examples of the peak images from the DeCyder analysis are shown for spots 18 (protein disulfide-isomerase A3 (Pdia3), SNO Ratio -1.29, p: 0.0440), 36 (fructose-bisphosphate aldolase C (Aldoc), Ratio 1.55, p: 0.024), 47 (phosphatidylinositol transfer protein alpha isoform (Pitpna), Ratio 1.58, p: 0.044), and 55 (peroxiredoxin-1 (Prdx1), Ratio 1.65, p: 0.026). The numbers indicate the spots picked for and identified by ESI-MS/MS. SNO regulation of these spots is shown in Table 1. In the spot map (bottom) proteins with increased S-nitrosylation are shown in blue, those with a decrease in red. The size of the spots correlates with the extent of SNO-increase or decrease. The spots are labeled with the gene names of the identified proteins.

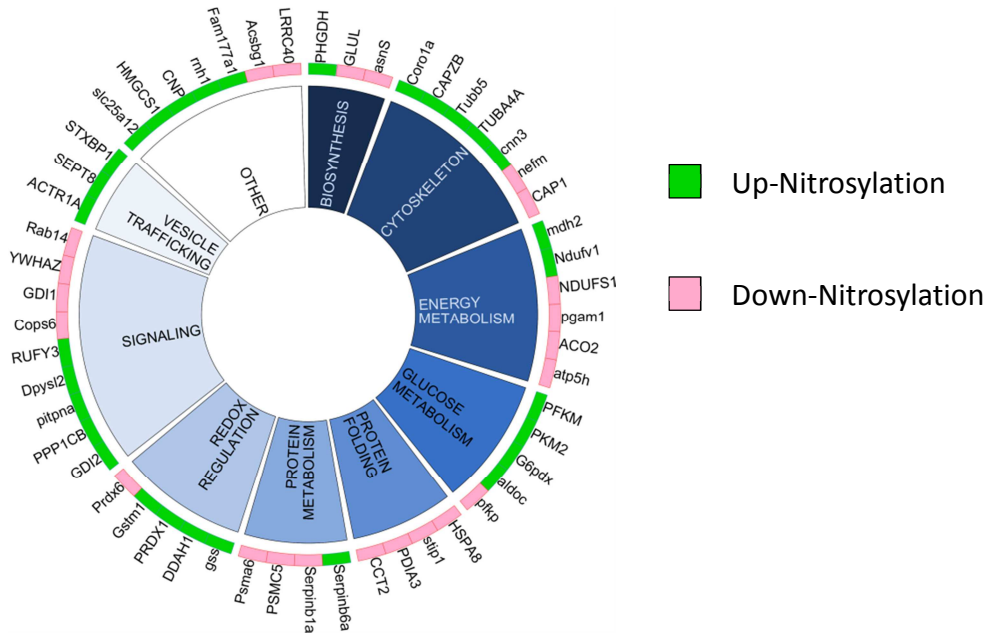

Figure 6 Functional categorization of S-Nitrosylated proteins after SNI
Categories of proteins with significant increases and decreases of S-nitrosylation in the spinal cord after sciatic nerve injury as assessed with the 2D SNO-DIGE. Categorization was based on UniProt general annotations. The outer circle shows the number of up- and down-nitrosylated proteins per category.

3.2.2 Effects of L-NAME treatment

In light of the well documented, and previously demonstrated, anti-nociceptive effects of NOS inhibitors mice were treated with the NOS inhibitor L-NAME prior to SNI operation and compared the SNO proteins between the three groups, i.e. naïve vs. SNI vs. SNI + L-NAME (N = 3). In parallel, the effects of L-NAME on nociceptive behavior were assessed. In this experiment 54 unique proteins were identified from 69 spots which showed increases or decreases of S-nitrosylation after SNI. A complete list of identified proteins is shown in Appendix IV.

Eight proteins showed an increase in S-nitrosylation ($p < 0.05$) after SNI. Out of these eight proteins, six showed a decrease of SNO modifications in the L-NAME+SNI treated group as compared to SNI while two remained unchanged (Figure 7 a). Effects of L-NAME were strongest for actin related protein 3 (*actr3*) which is part of the Arp2/3 complex and involved in actin branching. L-NAME treatment prior to SNI also significantly reduced the constitutive S-nitrosylation of several proteins including several mitochondrial proteins, heat shock cognate 71 kDa (*hspa8*), dynamin-1 (Dnm1) and glyceraldehyde-3-phosphate dehydrogenase (GAPDH, Figure 7 b) whose nitrosylation and denitrosylation has been reported to change its function in the context of NO-mediated

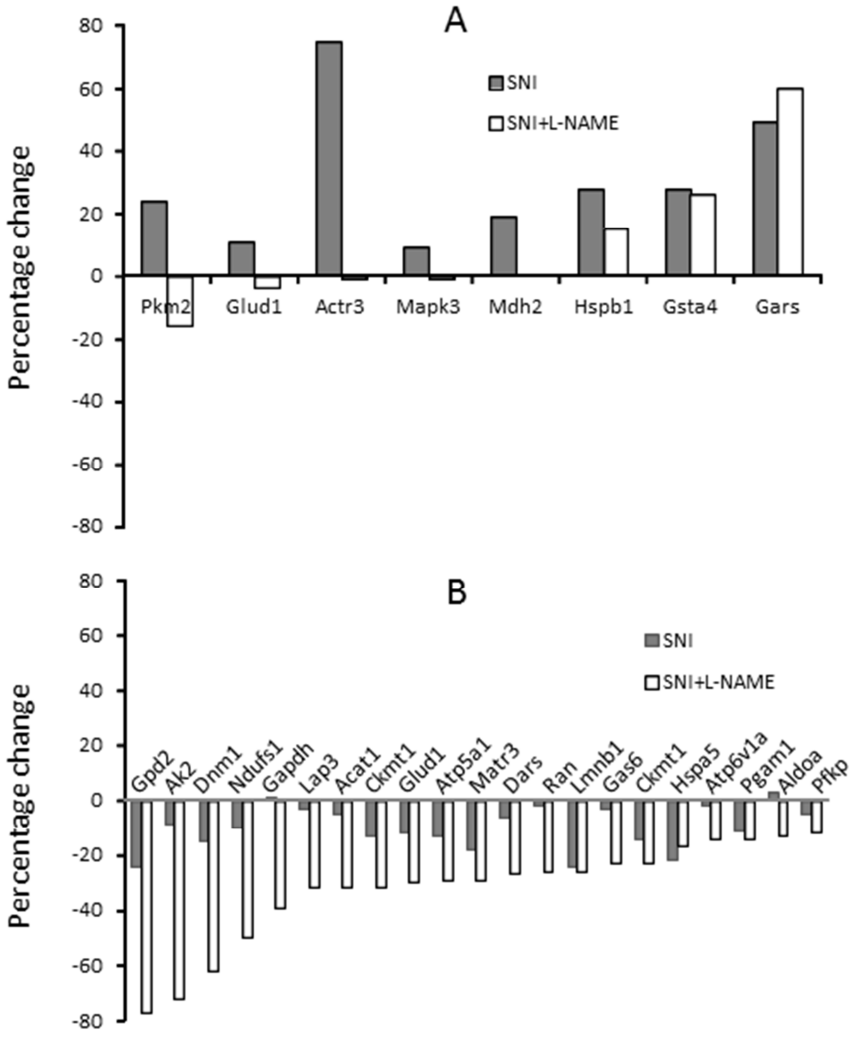

neurotoxicity.

Figure 7 S-Nitrosylation after SNI and L-NAME treatment
Fig A shows all proteins which were significantly up-nitrosylated after nerve injury. Fig. B shows all proteins which were significantly denitrosylated by L-NAME as compared to the naïve animals.

Table 9 Protein modification by S-nitrosylation after Spared Nerve Injury of the sciatic nerve in the mouse spinal cord

Spot no.	UniProt ID	Gene Name	Name	Ratio	T-test	Mass	*pI*	Pept.	Seq. Cov.	SNOSID Site	Predicted SNO site	Functional meaning of SNO sites	Functional description	Functional classification
1	NFM_MOUSE	*nefm*	Neurofilament medium polypeptide	-4.25	0.0500	95916	4.44	57	24%		None	None	Involved in the maintenance of neuronal caliber.	Cytoskeleton
2	ACON_MOUSE	*aco2*	Aconitate hydratase, mitochondrial	-2.43	0.0210	85464	8.02	7	12%	126, 448, 451	410	Metal binding 448, 451 Iron-sulfur (4Fe-4S)	Catalyzes the isomerization of citrate to isocitrate via cis-aconitate	Energy metabolism
3	K6PF_MOUSE	*pfkm*	6-phosphofructokinase, muscle type	1.58	0.0205	85269	8.08	63	47%		631	None known	Catalytic activity: ATP + D-fructose 6-phosphate = ADP + D-fructose 1,6-bisphosphate.	Glucose metabolism
4	K6PP_MOUSE	*pfkp*	6-phosphofructokinase type C	-1.20	0.0440	85455	7.12	6	8%		80, 111, 342, 410, 722	None known	(see above)	Glucose metabolism
5	ACON_MOUSE	*aco2*	Aconitate hydratase, mitochondrial	-1.32	0.0110	85464	8.02	163	62%	126, 448, 451	410	Metal binding 448, 451 Iron-sulfur (4Fe-4S)	Catalyzes the isomerization of citrate to isocitrate via cis-aconitate	Energy metabolism
6	ACBG1_MOUSE	*acsbg1*	Long-chain-fatty-acid--CoA ligase ACSBG1	-1.25	0.0370	80426	5.74	52	47%		10, 500	None	Mediates activation of long-chain fatty acids for both synthesis of cellular lipids, and degradation via beta-oxidation.	Lipid metabolism
7	HSP7C_MOUSE	*hspa8*	Heat shock cognate 71 kDa protein	-1.61	0.0050	70871	5.17	6	10%		574, 603	Modified residue 601 N6-acetyllysine	Chaperone.	Protein folding
8	NDUS1_MOUSE	*ndufs1*	NADH-ubiquinone oxidoreductase 75 kDa subunit, mitochondrial	-1.27	0.0025	79749	5.41	134	59%		75, 92, 564, 710, 727	Metal binding 75, 92 Iron-sulfur 1 (2Fe-2S),	Core subunit of the mitochondrial membrane respiratory chain NADH dehydrogenase (Complex I).	Energy metabolism
9	CMC1_MOUSE	*slc25a12*	Calcium-binding mitochondrial carrier protein Aralar1	1.28	0.0215	74570	8.41	82	66%		85, 375, 563	Domain 40 – 85 EF-hand 1	Calcium-dependent mitochondrial aspartate and glutamate carrier.	Aminoacid Transport
10	STXB1_MOUSE	*stxbp1*	Syntaxin-binding protein 1	1.53	0.0070	67569	6.96	54	42%		45, 110, 366	None known	May regulate synaptic vesicle docking and fusion, Essential for neurotransmission and binds syntaxin, a component of the synaptic vesicle fusion machinery.	Vesicle trafficking
11	LRC40_MOUSE	*lrrc40*	Leucine-rich repeat-containing protein 40	-1.44	0.0280	68076	6.45	29	53%		227, 329, 438, 469	None known	#N/A	Unknown
12	STIP1_MOUSE	*stip1*	Stress-induced-phosphoprotein 1	-1.26	0.0340	62582	6.39	6	10%	26	26, 403, 461	None known	Mediates the association of the molecular chaperones HSC70 and HSP90.	Protein folding
13	DPYL2_MOUSE	*dpysl2*	Dihydropyrimidinase-related protein 2	1.30	0.0366	62278	6.34	80	65%	248, 504	248, 439	Modified residue 431, 499, 509 Phosphotyrosine,	Necessary for signaling by class 3 semaphorins and cytoskeletal remodeling. Plays a role in axon guidance, neuronal growth cone collapse and cell migration.	Signaling
14	DPYL2_MOUSE	*dpysl2*	Dihydropyrimidinase-related protein 2	1.59	0.0260	62278	6.34	12	52%	248, 504	248, 439	Modified residue 431, 499, 509 Phosphotyrosine,	(see above)	Signaling

Spot no.	UniProt ID	Gene Name	Name	Ratio	T-test	Mass	*pI*	Pept.	Seq. Cov.	SNOSID Site	Predicted SNO site	Functional meaning of SNO sites	Functional description	Functional classification
15	ASNS_MOUSE	*asns*	Asparagine synthetase [glutamine-hydrolyzing]	-1.54	0.0290	64283	6.13	31	39%		2	Active site 2 For GATase activity	Catalytic activity: ATP + L-aspartate + L-glutamine + H2O = AMP + diphosphate + L-asparagine + L-glutamate.	Biosynthesis
16	G6PD1_MOUSE	*g6pdx*	Glucose-6-phosphate 1-dehydrogenase X	1.51	0.0300	59263	6.05	18	38%		13, 269, 294	Active site 263 Proton acceptor	Catalytic activity: D-glucose 6-phosphate + NADP+ = 6-phospho-D-glucono-1,5-lactone + NADPH.	Glucose metabolism
17	KPYM_MOUSE	*pkm2*	Pyruvate kinase isozymes M1/M2	1.37	0.0428	57845	7.52	165	84%	49, 152	326, 358, 423, 474	Modified residues 45, 148 Phosphothreonine, Binding site 328 Substrate	Glycolytic enzyme that catalyzes the transfer of a phosphoryl group from phosphoenolpyruvate (PEP) to ADP, generating ATP. Stimulates POU5F1-mediated transcriptional activation.	Glucose metabolism
18	PDIA3_MOUSE	*pdia3*	Protein disulfide-isomerase A3	-1.29	0.0440	56678	5.79	39	56%		5, 60, 406, 409	Signal peptide 1 – 24, Active sites 60, 406, 409 Nucleophile, Disulfide bonds 57 ↔ 60, 406 ↔ 409 Redox-active.	Catalytic activity: Catalyzes the rearrangement of -S-S- bonds in proteins.	Protein folding
19	GDIA_MOUSE	*gdi1*	Rab GDP dissociation inhibitor alpha	-1.26	0.0230	50522	4.7	58	75%	202, 317	317, 335	Modified residue 333 Phosphotyr., Modified residue 339 Phosphotyr.	Regulates the GDP/GTP exchange reaction of most Rab proteins by inhibiting the dissociation of GDP and binding of GTP to them.	Signaling
20	RUFY3_MOUSE	*rufy3*	Protein RUFY3	1.74	0.0160	53007	5.16	30	43%		29	None known	Implicated in the formation of a single axon by developing neurons.	Signaling
21	COR1A_MOUSE	*coro1a*	Coronin-1A	1.36	0.0103	50989	6.04	54	51%		24, 332	None known	May be a crucial component of the cytoskeleton of highly motile cells.	Cytoskeleton
22	SERA_MOUSE	*phgdh*	D-3-phosphoglycerate dehydrogenase	1.37	0.0070	56586	6.51	52	41%		48, 111, 254, 295, 369	Active site 265, Active site 283 Proton donor, Binding site 260 NAD	Catalytic activity: 3-phospho-D-glycerate + NAD+ = 3-phosphonooxypyruvate + NADH. Catalytic activity: 2-hydroxyglutarate + NAD+ = 2-oxoglutarate + NADH.	Biosynthesis
23	TCPB_MOUSE	*cct2*	T-complex protein 1 subunit beta	-1.28	0.0250	57477	5.97	61	32%		346, 371, 395, 412	None known	Molecular chaperone; assists folding of proteins upon ATP hydrolysis.	Protein folding
24	CAP1_MOUSE	*cap1*	Adenylyl cyclase-associated protein 1	-1.29	0.0080	51575	7.23	15	31%		92, 355	Modified residue 80 N6-acetyllysine	Directly regulates filament dynamics and implicated in a number of complex developmental and morphological processes, including mRNA localization and the establishment of cell polarity	Cytoskeleton
25	TBB5_MOUSE	*tubb5*	Tubulin beta-5 chain	1.61	0.0400	49671	4.52	4	12%	12, 354	12, 303, 354	None known	Major constituent of microtubules.	Cytoskeleton
26	HMCS1_MOUSE	*hmgcs1*	Hydroxymethylglutaryl-CoA synthase, cytoplasmic	1.46	0.0115	57569	5.55	44	48%		417	None known	Condenses acetyl-CoA with acetoacetyl-CoA to form HMG-CoA, a substrate for HMG-CoA reductase	Lipid Biosynthesis

Spot no.	UniProt ID	Gene Name	Name	Ratio	T-test	Mass	*pI*	Pept.	Seq. Cov.	SNOSID Site	Predicted SNO site	Functional meaning of SNO sites	Functional description	Functional classification
27	SEPT8_MOUSE	*sept8*	Septin-8	1.33	0.0335	49812	5.88	74	65%		400	Coiled coil 320 – 412	Filament-forming cytoskeletal GTPase. May play a role in cytokinesis. May play a role in platelet secretion.	Vesicle trafficking
28	TBA4A_MOUSE	*tuba4a*	Tubulin alpha-4A chain	1.31	0.0180	49924	4.7	28	52%	54, 347	4, 295, 347, 376	None known	Major constituent of microtubules.	Cytoskeleton
29	GSHB_MOUSE	*gss*	Glutathione synthetase	1.32	0.0447	52247	5.54	21	45%		422	Binding site 425 ATP	Catalytic activity: ATP + gamma-L-glutamyl-L-cysteine + glycine = ADP + phosphate + glutathione.	Redox regulation
30	NDUV1_MOUSE	*ndufv1*	NADH dehydrogenase [ubiquinone] flavoprotein 1, mitochondrial	1.23	0.0030	50834	7.99	1	2%	187	None	None known	Core subunit of the mitochondrial membrane respiratory chain NADH dehydrogenase (Complex I)	Energy metabolism
31	GDIB_MOUSE	*gdi2*	Rab GDP dissociation inhibitor beta	1.43	0.0392	50537	6.12	76	78%		317, 335	None known	Regulates the GDP/GTP exchange reaction of most Rab proteins by inhibiting the dissociation of GDP and binding of GTP to them.	Signaling
32	RINI_MOUSE	*rnh1*	Ribonuclease inhibitor	1.27	0.0170	49816	4.39	41	60%		80, 90, 194, 204, 404, 422	None known	Inhibitor of pancreatic RNase and angiogenin. May also function in the modulation of cellular activities	RNA metabolism
33	PRS8_MOUSE	*psmc5*	26S protease regulatory subunit 8	-2.01	0.0120	45626	7.29	44	69%		None	None	Involved in the ATP-dependent degradation of ubiquitinated proteins.	Protein metabolism
34	CN37_MOUSE	*cnp*	2',3'-cyclic-nucleotide 3'-phosphodiesterase	1.48	0.0346	47123	9.08	10	15%	111	417	Modified residue 110 Phosphotyrosine	Catalytic activity: Nucleoside 2',3'-cyclic phosphate + H2O = nucleoside 2'-phosphate.	Myelin metabolism
35	ACTZ_MOUSE	*actr1a*	Alpha-centractin	1.65	0.0274	42614	6.62	95	71%		222	None known	Component of a multi-subunit complex involved in microtubule based vesicle motility. It is associated with the centrosome.	Trafficking
36	ALDOC_MOUSE	*aldoc*	Fructose-bisphosphate aldolase C	1.55	0.0240	39395	7.14	23	58%	178	None	Active site 188 Proton acceptor	Catalytic activity: D-fructose 1,6-bisphosphate = glycerone phosphate + D-glyceraldehyde 3-phosphate.	Glucose metabolism
37	GLNA_MOUSE	*glul*	Glutamine synthetase	-1.34	0.0240	42120	7.09	12	25%	99, 346, 359	269, 359	None known	Essential for proliferation of fetal skin fibroblasts. Catalyzes the production of glutamine and 4-aminobutanoate.	Biosynthesis
38	SPB6_MOUSE	*serpinb6a*	Serpin B6	1.57	0.0140	42599	5.35	20	41%		None	None	Inhibitor of cathepsin G, kallikrein-8 and thrombin. May be involved in the regulation of serine proteinases present in the brain or extravasated from the blood.	Protein metabolism
39	ILEUA_MOUSE	*serpinb1a*	Leukocyte elastase inhibitor A	-1.28	0.0375	42575	6.13	33	59%		None	None	Regulates the activity of the neutrophil proteases and thus, forms complexes with chymotrypsin, elastase, cathepsin G and proteinase-3.	Protein metabolism

Spot no.	UniProt ID	Gene Name	Name	Ratio	T-test	Mass	*pI*	Pept.	Seq. Cov.	SNOSID Site	Predicted SNO site	Functional meaning of SNO sites	Functional description	Functional classification
40	DDAH1_MOUSE	*ddah1*	N(G),N(G)-dimethylarginine dimethylaminohydrolase 1	1.31	0.0061	31381	5.84	25	48%		222	None known	Hydrolyzes N(G),N(G)-dimethyl-L-arginine (ADMA) and N(G)-monomethyl-L-arginine (MMA) which act as inhibitors of NOS. Has therefore a role in nitric oxide generation.	Redox Regulation
41	ILEUA_MOUSE	*serpinb1a*	Leukocyte elastase inhibitor A	-1.34	0.0187	42575	6.13	5	13%		None	None	Regulates the activity of the neutrophil proteases and thus, forms complexes with chymotrypsin, elastase, cathepsin G and proteinase-3.	Protein metabolism
42	PP1B_MOUSE	*ppp1cb*	Serine/threonine-protein phosphatase PP1-beta catalytic subunit	1.25	0.0273	37187	6.07	26	42%		104	None known	Protein phosphatase (PP1) is essential for cell division, it participates in the regulation of glycogen metabolism, muscle contractility and protein synthesis. Involved in regulation of ionic conductances and long-term synaptic plasticity.	Signaling
43	CNN3_MOUSE	*cnn3*	Calponin-3	1.36	0.0270	36429	5.29	20	42%		None	None	Implicated in the regulation and modulation of smooth muscle contraction. It is capable of binding to actin, calmodulin, troponin C and tropomyosin. The interaction of calponin with actin inhibits the actomyosin Mg-ATPase activity.	Cytoskeleton
44	MDHM_MOUSE	*mdh2*	Malate dehydrogenase, mitochondrial	1.76	0.0096	35611	8.91	39	69%	89, 93, 212, 275, 285	132	Nucleotide binding 140 – 142 NAD,	Catalytic activity: (S)-malate + NAD+ = oxaloacetate + NADH.	Energy metabolism
45	CSN6_MOUSE	*cops6*	COP9 signalosome complex subunit 6	-1.32	0.0243	35880	5.56	27	44%		None	None	Component of the COP9 signalosome complex (CSN), a complex involved in various cellular and developmental processes.	Signaling
46	CAPZB_MOUSE	*capzb*	F-actin-capping protein subunit beta	1.72	0.0257	31345	5.44	2	7%		8	Modified residue 2 N-acetylserine	Binds in a Ca^{2+}-independent manner to the fast growing ends of actin filaments (barbed end) thereby blocking the exchange of subunits at these ends.	Cytoskeleton
47	PIPNA_MOUSE	*pitpna*	Phosphatidylinositol transfer protein alpha isoform	1.58	0.0435	31893	6.33	9	16%		None	None	Catalyzes transfer of PtdIns and phosphatidylcholine between membranes.	Signaling
48	F177A_MOUSE	*fam177a1*	Protein FAM177A1	1.59	0.0390	23578	4.22	12	39%		None	None	N/A	Unknown
49	1433Z_MOUSE	*ywhaz*	14-3-3 protein zeta/delta	-1.32	0.0410	27771	4.42	12	44%	94	25, 94	None known	Adapter protein implicated in the regulation of a large spectrum of both general and specialized signaling	Signaling

Spot no.	UniProt ID	Gene Name	Name	Ratio	T-test	Mass	*pI*	Pept.	Seq. Cov.	SNOSID Site	Predicted SNO site	Functional meaning of SNO sites	Functional description	Functional classification
													pathway.	
50	PGAM1_MOUSE	*pgam1*	Phosphoglycerate mutase 1	-1.51	0.0072	28832	7.22	23	53%	153	55	Site 62 Interaction with carboxyl group of phosphoglycerates	Interconversion of 3- and 2-phosphoglycerate with 2,3-bisphosphoglycerate as the primer of the reaction.	Energy metabolism
51	PSA6_MOUSE	*psma6*	Proteasome subunit alpha type-6	-1.64	0.0100	27372	6.35	1	5%		47, 201	None known	The proteasome has an ATP-dependent proteolytic activity.	Protein metabolism
52	PRDX6_MOUSE	*prdx6*	Peroxiredoxin-6	-3.05	0.0210	24871	5.58	2	15%	47	47	Active site 47 Cysteine sulfenic acid (-SOH) intermediate Disulfide bond 47 Interchain; in linked form	Involved in redox regulation of the cell. Can reduce H(2)O(2) and short chain organic, fatty acid, and phospholipid hydroperoxides.	Redox regulation
53	GSTM1_MOUSE	*gstm1*	Glutathione S-transferase Mu 1	2.78	0.0020	25970	7.89	52	72%		None	None	Conjugation of reduced glutathione to a wide number of exogenous and endogenous hydrophobic electrophiles.	Redox regulation
54	RAB14_MOUSE	*rab14*	Ras-related protein Rab-14	-2.02	0.0040	23897	5.79	1	7%		None	None	May be involved in vesicular trafficking and neurotransmitter release.	Signaling
55	PRDX1_MOUSE	*prdx1*	Peroxiredoxin-1	1.65	0.0260	22162	8.31	45	63%	173	52, 173	Active site 52 Cysteine sulfenic acid (-SOH) intermediate, Disulfide bond 52-173 Interchain	Involved in redox regulation of the cell. Reduces peroxides with reducing equivalents provided through the thioredoxin system but not from glutaredoxin.	Redox Regulation
56	ATP5H_MOUSE	*atp5h*	ATP synthase subunit d, mitochondrial	-1.72	0.0440	18749	5.38	8	43%	101	None	None	Produces ATP from ADP in the presence of a proton gradient across the membrane generated by the respiratory chain.	Energy metabolism
57	ATP5H_MOUSE	*atp5h*	ATP synthase subunit d, mitochondrial	-3.19	0.0230	18749	5.38	18	69%	101	None	None	(see above)	Energy metabolism

S-nitrosylation in the dorsal horn of the L4/5 mouse spinal cord was assessed by 2D SNO-DIGE analysis and subsequent identification by electrospray ionization mass spectrometry (ESI-MS/MS). SNO Upregulation is shown in blue, SNO down regulation in red. Triplicate 2D gels of naïve and SNI-treated mice were analyzed and statistically compared by t-tests, P was set at 0.05. Identification of the modified cysteines was done with the SNO site identification method (SNOSID). SNO site predictions were obtained with the SNO-GPS software (Xue et al. 2010). Abbreviations: pI, isoelectric point; Pept, Peptides identified; Seq. Cov. Peptide sequence coverage.

3.2.3 Effects of Sham operation

To control for the effects of the surgery the SNO-DIGE proteome of Sham operated mice was compared to that of Naïve mice. For the sham control mice the sciatic nerve was exposed but not cut.

In this experiment the SNO-DIGE revealed 18 regulated spots. Out of these, 3 spots showed an increase and 15 spots a decrease in S-nitrosylation. The 18 spots contained 15 unique proteins, with 12 of them down-nitrosylated and 3 up-nitrosylated in the Sham treated mice (namely *etfa, car2* and *qdpr*). Three of the proteins with a reduction of S-nitrosylation were represented each in 2 spots (*uqcrc1, mdh1,* and *pgam1*) with consistent SNO regulation. Only one protein, phosphoglycerate mutase 1 (*Pgam1*), showed a similar reduction of S-nitrosylation in sham and SNI-treated mice. Two further matching proteins, glutamate decarboxylase, (*glna*) and aldolase 3 (*aldoc*), showed an increase of S-nitrosylation after SNI but a decrease after sham surgery. A complete list of identified proteins is shown in Appendix V.

3.3 SNO-site identification (SNOSID)

From the SNO-DIGE information it is not possible to identify which cysteine is nitrosylated in each protein. In order to directly identify which cysteines are SNO-modified as well as to compare different techniques SNO modifications with SNOSID technique were also screened. The SNOSID employs the biotin switch technique on trypsinized proteins, followed by avidin purification of the biotin labeled peptides and sequencing by mass spectrometry. In naïve mice SNOSID identified 203 S-nitrosylated peptides (Figure 8 a) from 131 unique proteins (Figure 8 b). After SNI 161 SNO-peptides were identified from 101 unique proteins. These numbers were reduced in the mice pretreated with L-NAME before SNI. In this group only 92 SNO-peptides from 37 proteins were identified. The complete list of SNOSID results is shown in Appendix VI. Considering only proteins which were significantly up- or denitrosylated after SNI in the 2D SNO-DIGE experiments, SNOSID revealed SNO-modified cysteines in 17 out of the 53 regulated SNO-proteins in the first experiment including naïve versus SNI treated mice and 14 out of 54 proteins matched this criterion in the second experiment, which compared naïve versus SNI versus SNI + L-NAME treated mice. Six proteins were found in all three experiments, namely aconitate hydratase (mitochondrial), fructose-bisphosphate aldolase C, pyruvate kinase isozymes M1/M2, malate dehydrogenase (mitochondrial), NADH dehydrogenase [ubiquinone] flavoprotein 1 (mitochondrial), and phosphoglycerate mutase 1. The latter was also found in the sham experiment to be denitrosylated.

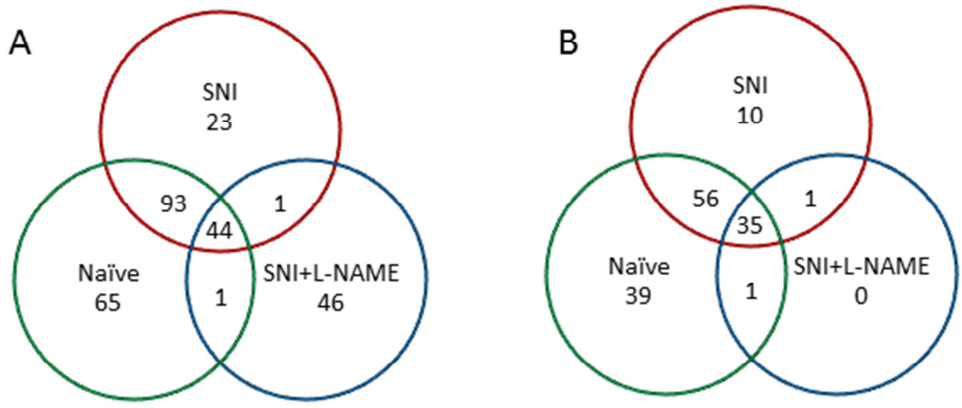

Figure 8 S-nitrosylated peptides and proteins identified by SNOSID
Venn diagrams of S-nitrosylated peptides and respective proteins identified by SNOSID Fig. A shows the number of peptides which had one or more S-nitrosylated cysteines. Fig. B shows the corresponding number of individual proteins. The comparison of the treatment groups show that S-nitrosylation sites were substantially reduced by L-NAME.

3.4 Confirmation of S-Nitrosylation of selected targets

3.4.1 Biotin-switch Western Blot analysis of selected proteins

To confirm the S-nitrosylation of the top hits of potential targets identified by the SNO-DIGE and SNOSID I employed the biotin switch technique (BST). For BST, SNO sites were labeled with biotin, followed by avidin pull-down and immunoblot analysis with target specific antibodies. The selected targets were protein disulfide isomerase (PDI), glutathione S-synthetase (GSS), peroxiredoxin-6 (Prdx6), mitochondrial aconitase 2 (Aco2), β–tubulin (Tubb), and α-tubulin (Tuba). The BST confirmed SNO-modifications in the selected proteins, but comparisons between naïve and SNI-treated mice did not reveal significant changes between naïve and SNI-treated mice (see Figure 9).

3.4.2 Biotin switch ELISA

In addition to the Biotin-Switch with Western Blot detection a novel ELISA based approach was developed to identify the nitrosylation of the target proteins. Nitrosylation sites were labeled with biotin as described above followed by sandwich ELSIA detection as described above. Antibodies were directed against protein disulfide-isomerase (*pdi*, 1:500, Cell Signaling, C81H6), glutathione synthetase (*gss*, 1:500, abcam, ab91591), aconitate hydratase 2 (*aco2*, 1:500, abcam, ab83528), peroxiredoxin-6 (*prdx6*,

1:1000, abcam, ab16947), tubulin-beta (*tubb*, 1:500, Promega, G7121), and GAPDH (*gapdh*, 1:500, Ambion, AM 4300).

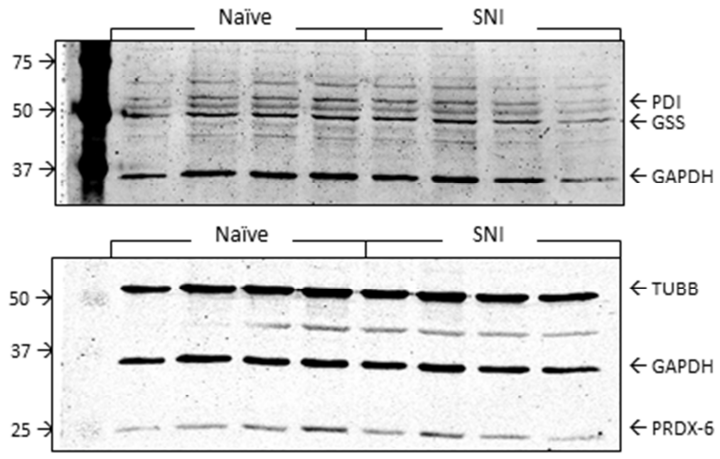

Figure 9 Biotin switch analysis
Biotin switch analysis of selected proteins which were found to be significantly SNO-modified in the spinal cord after sciatic nerve injury in 2D SNO DIGE experiments. SNO-modified proteins were identified by biotin labeling, avidin purification and subsequent immunoblot analysis with specific antibodies. GAPDH was used a loading control.

3.4.3 Time dependent S-nitrosylation

To assess whether S-nitrosylation after SNI was a short lasting early event or a longer lasting adaptive mechanisms the S-nitrosylation of candidate target proteins (GSS, PDI, GAPDH, TUBB, PRX-6, ACO2) 1 and 7 days after SNI using the ELISA was assessed as described above. For PDI, GSS and Prdx6 alterations of S-nitrosylation which were apparent at 1 day after SNI had normalized at 7 days. Instead for ACO2, S-nitrosylation was significantly increased at 7 days after SNI, but was almost normal at 1 day suggesting that ACO2 S-nitrosylation was a chronic modification (Figure 10).

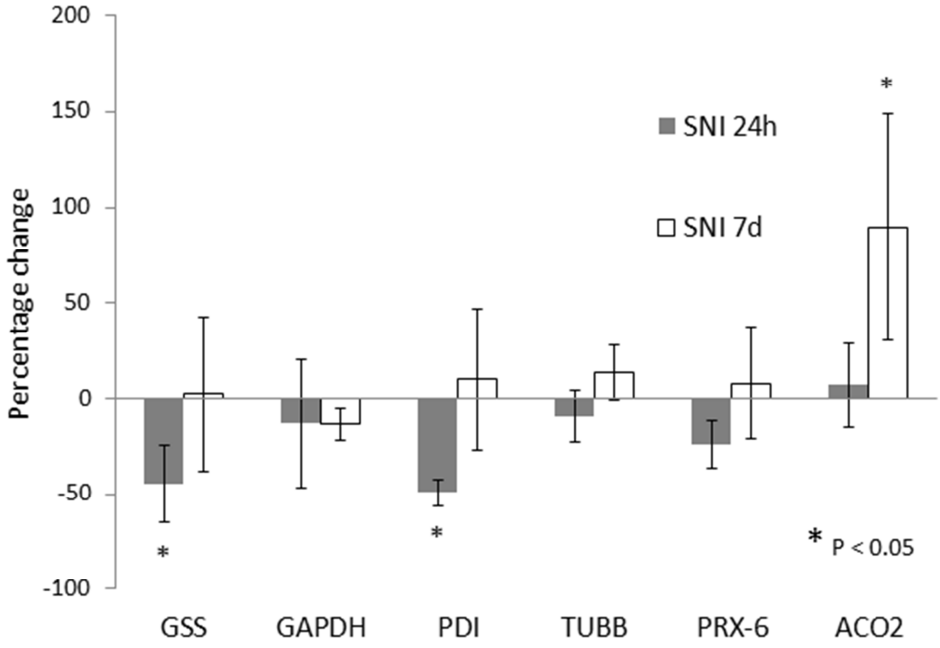

Figure 10 Time dependent S-nitrosylation
Percentage change of protein S-nitrosylation of candidate proteins in the spinal cord 1 and 7 days after sciatic nerve injury. Time courses of protein S-nitrosylation of glutathione synthetase, GSS; protein disulfide isomerase, PDI; glycerinaldehyde-3-phosphate-dehydrogenase, GAPDH; beta tubulin, TUBB; peroxiredoxin-6, PRX-6 and mitochondrial aconitase 2, ACO2 as assessed by a biotin switch ELISA in triplicate of n = 4 mice per group. The asterisks indicate significant difference versus naïve control mice, $P < 0.05$.

3.5 Method establishment

3.5.1 Specificity of ascorbate reduction and CyDye labeling

To test if reduction with ascorbate was selective for S-nitrosylation the protein homogenate of NIH3T3 mouse fibroblast, that do no express nitric oxide synthase and thus produce very little nitric oxide, was reduced with ascorbate or TCEP. TCEP is a strong reduction agent, reducing all cysteine oxidative modifications to free SH, while ascorbate is selective only for the relatively weak SNO bond.

The protein homogenate was subsequently labeled with Cy3 and Cy5 maleimide dyes and run according to the standard 2D PAGE protocol of the 2D SNO-DIGE, and scanned using the Typhoon and analyzed using the Decyder software.

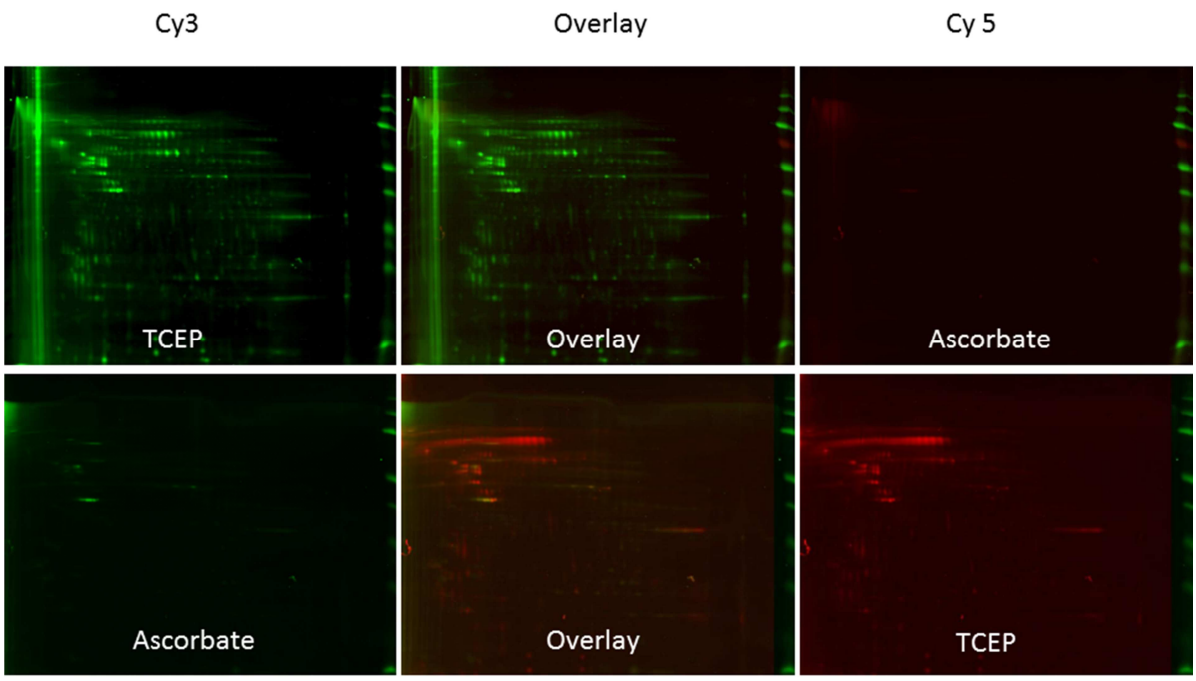

Figure 11 Specificty of Ascorbate reduction
A comparison of the selectivity of ascorbate reduction vs. TCEP reduction in protein homogenate from NOS free 3T3 fibroblasts shows that ascorbate reduction and subsequent CyDye labeling is selective for nitrosylations.

The scans of the gels show that when proteins are reduced with TCEP the CyDye label is able to react with the free thiol groups on the protein. However, when the proteins are reacted with ascorbate the labeling does not happen as there are no S-nitrosylations to be reduced to free thiols by ascorbate.

The results show (see Figure 11) that the labeling is specific, for Cy5, the label used for the labeling of samples in the SNO-DIGE while Cy3 was used for the internal standard.

3.5.2 Interference of ascorbate with CyDye labeling

To test if reduction with ascorbate was possibly interfering with the CyDye labeling dyes were incubated with SHSY-5Y cell protein homogenate treated with the NO donor DEA/NO and either reduced with ascorbate first and then labeled with CyDye or reduced and labeled simultaneously.

The scans of the gels show that the simultaneous reduction and labeling is slightly better, though not significantly, than two separate steps. The results also show that the ascorbate does not interfere with the CyDye labeling.

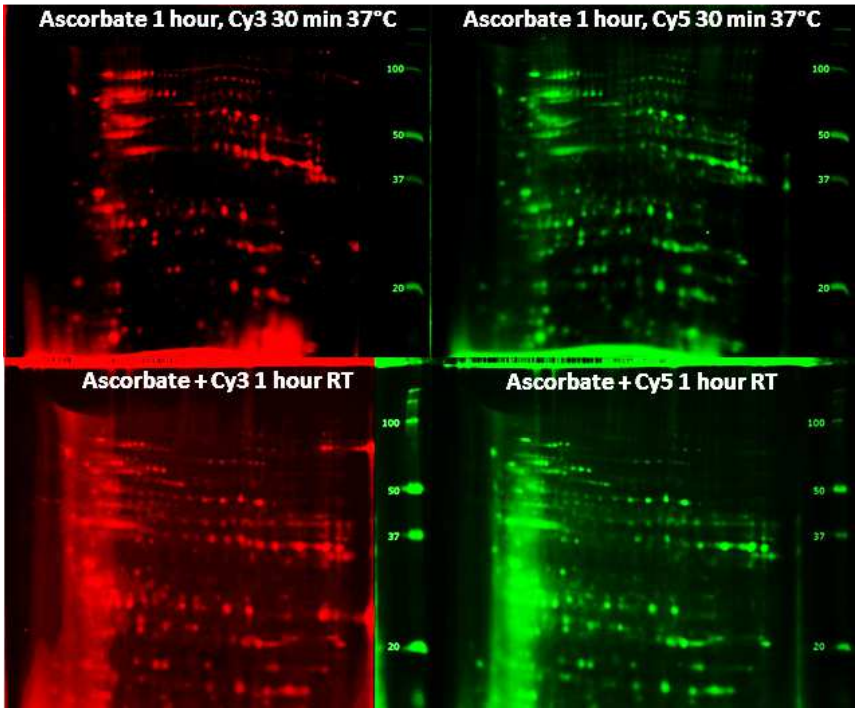

Figure 12 Separate or simultaneous reduction or labeling
A test of the effects of separate or simultaneous reduction and labeling steps on the efficiency of labeling show that ascorbate did not interfere with the labeling.

3.6 S-nitrosylation and autophagy

In light of the effects of the SNI operation on the S-nitrosylation of proteins involved in protein metabolism and folding, the next step was to assess whether and how S-Nitrosylation is involved in these processes. For this a cell model of neuroblastoma cells (SHSY-5Y) and induced autophagy by stimulation with rapamycin was used.

3.6.1 nNOS over-expression

SHSY-5Y neuroblastoma cells were transduced with a Lentiviral vector for mouse neuronal NOS (NOS1, nNOS) in which nNOS was under control of the cytomegalo virus (CMV) promoter and transduction monitored by eGFP expression under the control of the Ires-2 promoter. A stable cell line was produced by cell sorting. Figure 13 shows a western blot for nNOS in wild type and nNOS-overexpressing cells. The blot confirmed nNOS overepression.

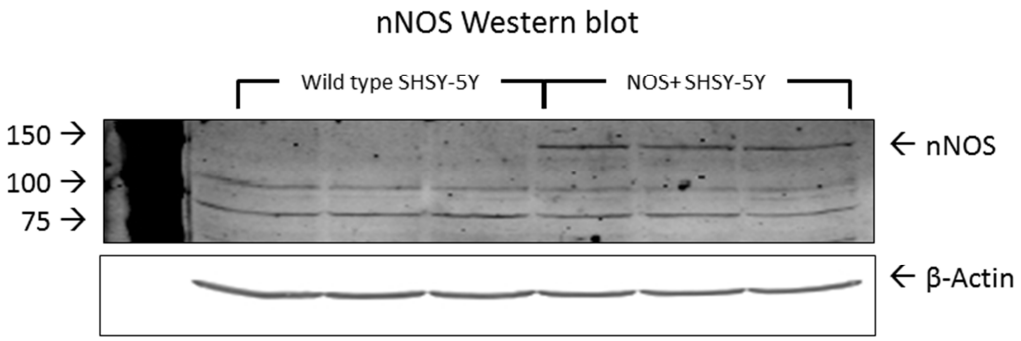

Figure 13 nNOS over-expression in SHSY-5Y cells
Western blot for nNOS in the two cell types used: wild type and nNOS over-expressing cells. β-actin was used as loading control.

3.6.2 NO production

NO production of the neuroblastoma cells was measured using the Saville-Griess method adapted for microtiterplate. Stimulation with rapamycin did not affect nitric oxide content but NO was found to be increased by the overexpression of nNOS by 25% ($p < 0.05$). See Figure 14.

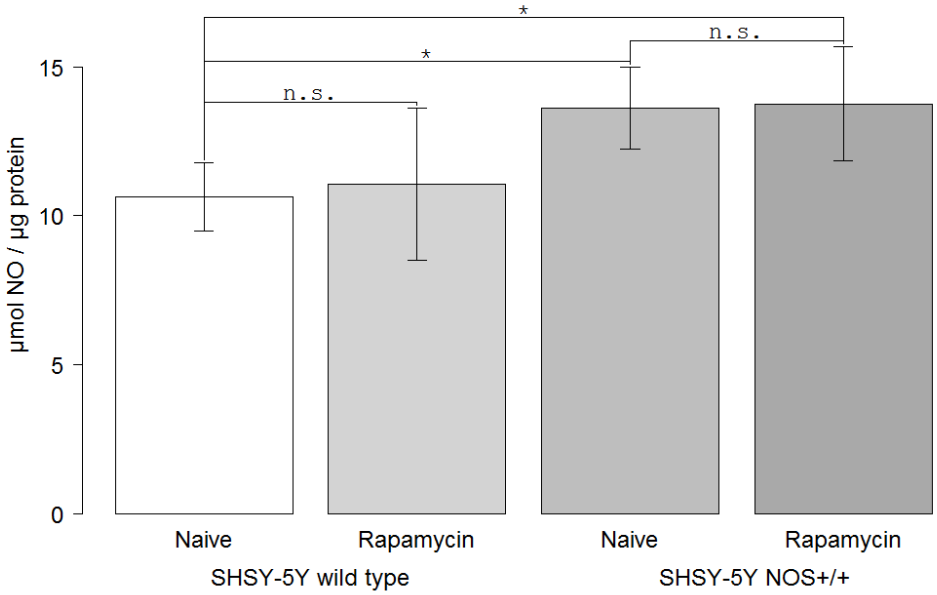

Figure 14 Nitric oxide content of protein after stimulation with rapamycin
Nitric oxide content of protein from wild type and nNOS over-expressing SHSY-5Y cells after stimulation with rapamycin (1 µM, 6 hours).

3.6.3 Markers for autophagy

To test the effects of the nNOS over-expression on the autophagy processes, western blots were performed for known autophagy markers after stimulation of wild type as well as nNOS over-expressing cells with rapamycin (1 µM, 6 hours).

3.6.3.1 Ratio of LC3-I and LC3-II

The ratio of LC3-I / LC3-II was significantly increased (+233%, $p < 0.05$) in the wild type cells after stimulation with Rapamycin and dramatically increased (+100%, $p < 0.05$) after stimulation in nNOS over-expressing cells. nNOS over-expressing cells had a higher basal ratio than the wild type (+144%, $p < 0.05$). See Figure 15, Figure 16, and Table 10.

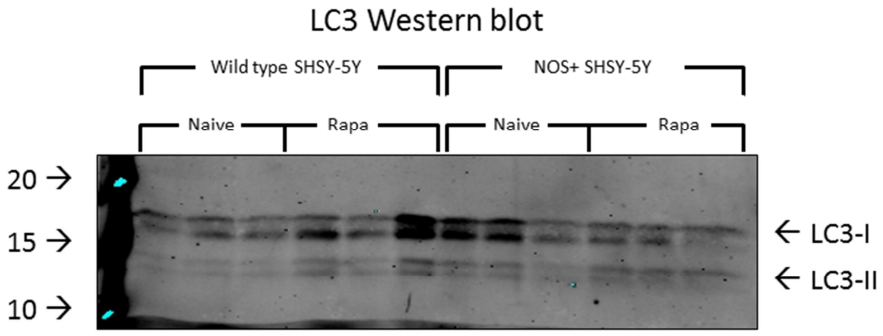

Figure 15 LC3-I and LC3-II after rapamycin stimulation western blot
Total protein homogenate western blot of LC3-I and LC3-II in wild type and nNOS over-expressing SHSY-5Y cells after stimulation with rapamycin (1 µM, 6 hours).

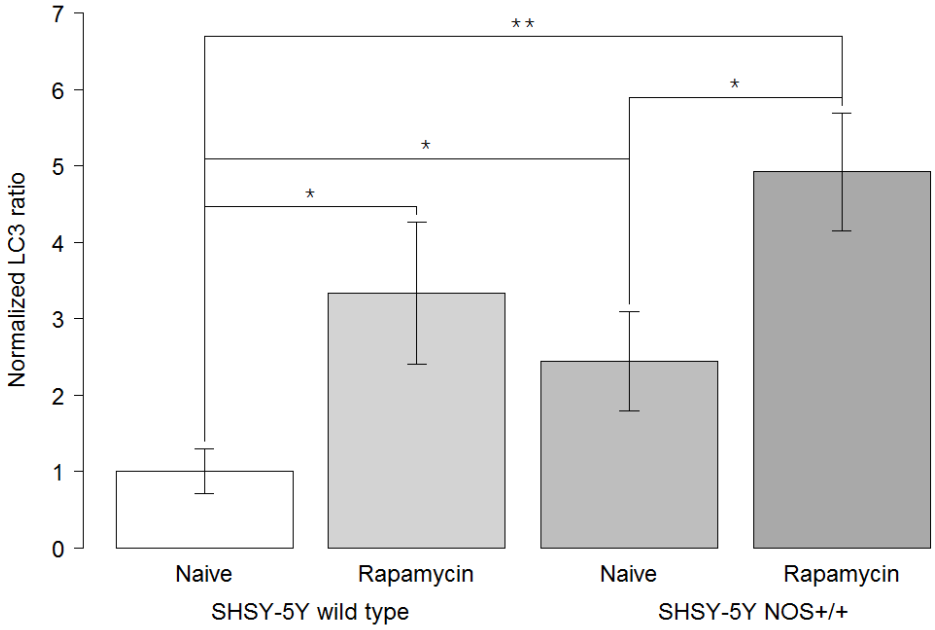

Figure 16 Ratio of LC3-I/LC3-II after rapamycin stimulation
Ratio of LC3-I/LC3-II after stimulation with rapamycin (1 µM, 6 hours). Average values are normalized to Naïve cells = 1. Significance markers: * $p < 0.05$, ** $p < 0.01$, *** $p < 0.001$.

3.6.3.2 Ubiquitination

Total ubiquitination was significantly reduced (-28%, $p < 0.01$) in the wild type cells after stimulation with rapamycin but was dramatically increased (+99%, $p < 0.001$) after stimulation in nNOS over-expressing cells, with no significant basal difference between the two cell types. See Figure 17, Figure 18, and Table 10.

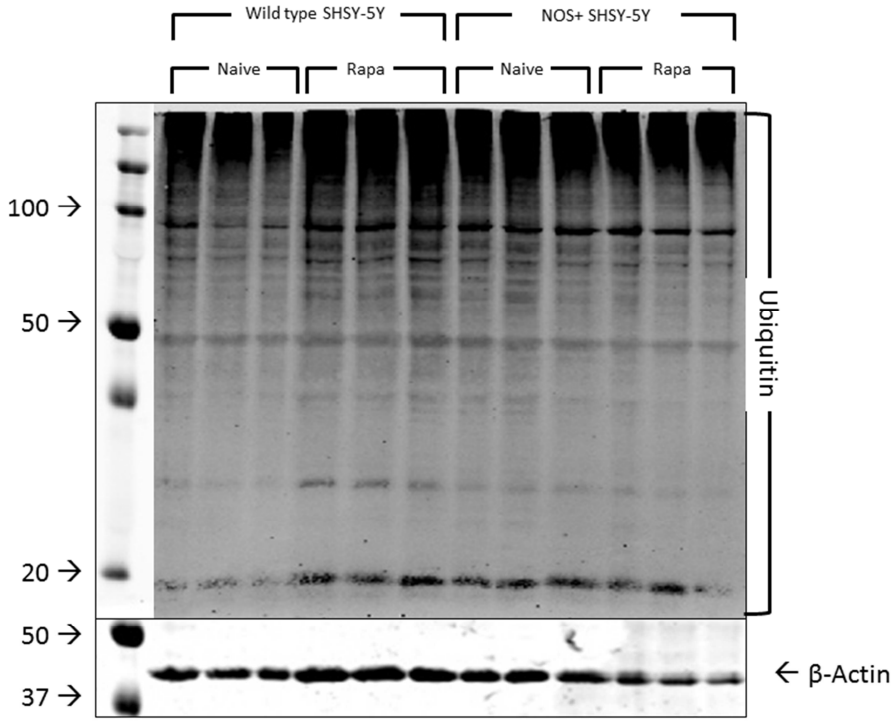

Figure 17 Ubiquitinylation after rapamycin stimulation western blot
Total protein homogenate western blot of ubiquitinylation in wild type and nNOS over-expressing SHSY-5Y cells after stimulation with rapamycin (1 µM, 6 hours).

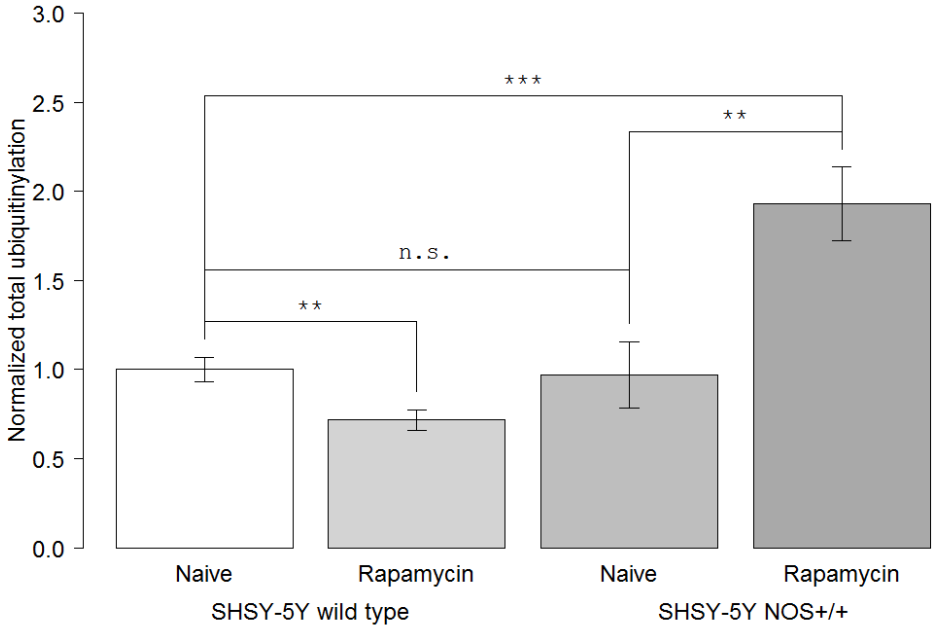

Figure 18 Total ubiquitinylation after rapamycin stimulation
Total ubiquitinylation in wild type and nNOS over-expressing SHSY-5Y cells after stimulation with rapamycin (1 µM, 6 hours). Average values are normalized to Naïve cells = 1. Significance markers: * $p < 0.05$, ** $p < 0.01$, *** $p < 0.001$.

3.6.3.3 HSC-70

The level of HSC-70 was slightly but significantly decreased (-25%, $p < 0.01$) in the wild type cells after stimulation with rapamycin and doubled (+117%, $p < 0.001$) after stimulation in nNOS over-expressing cells. No significant basal difference between the two cell types was observed. See Figure 19, Figure 20, and Table 10.

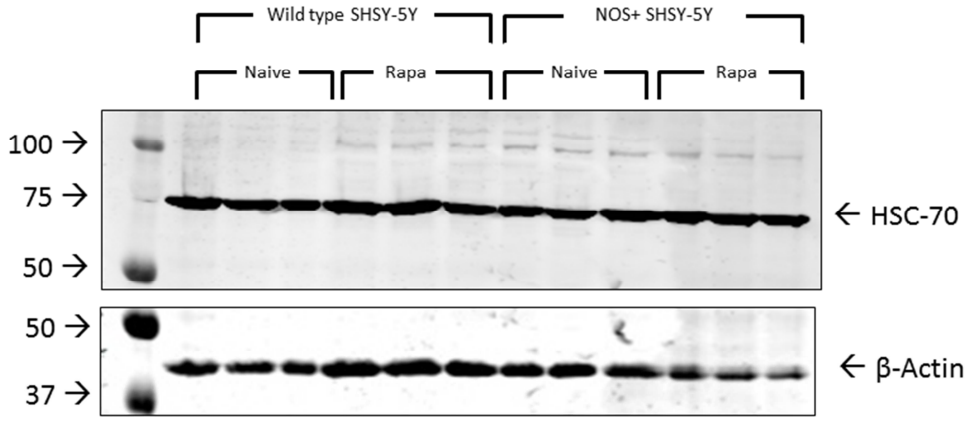

Figure 19 HSC70 after rapamycin stimulation western blot
Total protein homogenate western blot of HSC70 in wild type and nNOS over-expressing SHSY-5Y cells after stimulation with rapamycin (1 µM, 6 hours).

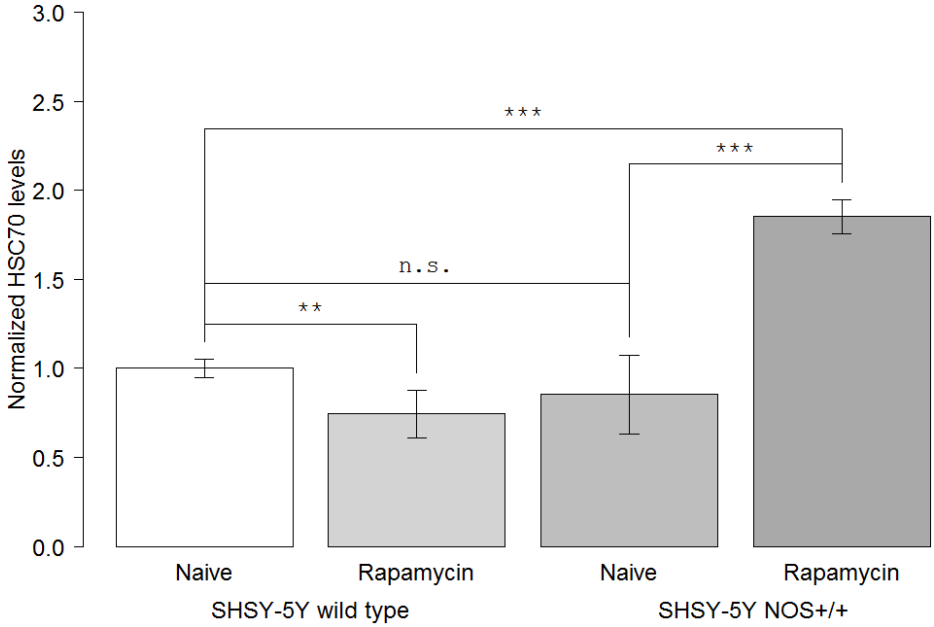

Figure 20 HSC70 after rapamycin stimulation
HSC70 expression in wild type and nNOS over-expressing SHSY-5Y cells after stimulation with rapamycin (1 µM, 6 hours). Average values are normalized to Naïve cells = 1. Significance markers: * $p < 0.05$, ** $p < 0.01$, *** $p < 0.001$.

3.6.3.4 p62 (SQSTM1)

The level of p62 was significantly increased (+14%, $p < 0.05$) in the wild type cells after stimulation with rapamycin but not significantly modified after stimulation in nNOS over-expressing cells. No significant basal difference between the two cell types was observed. See Figure 21, Figure 22, and Table 10.

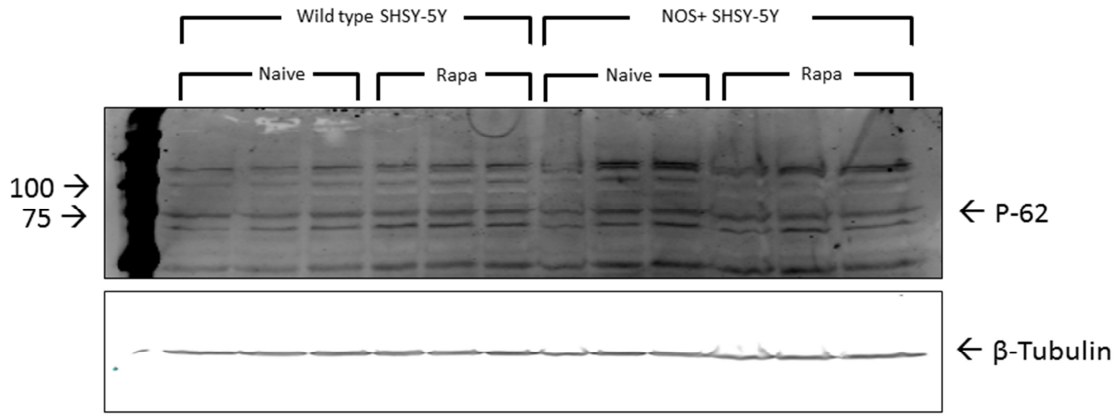

Figure 21 p62 (SQSTM1) after rapamycin stimulation western blot
Total protein homogenate western blot of p62 (SQSTM1) in wild type and nNOS over-expressing SHSY-5Y cells after stimulation with rapamycin (1 µM, 6 hours).

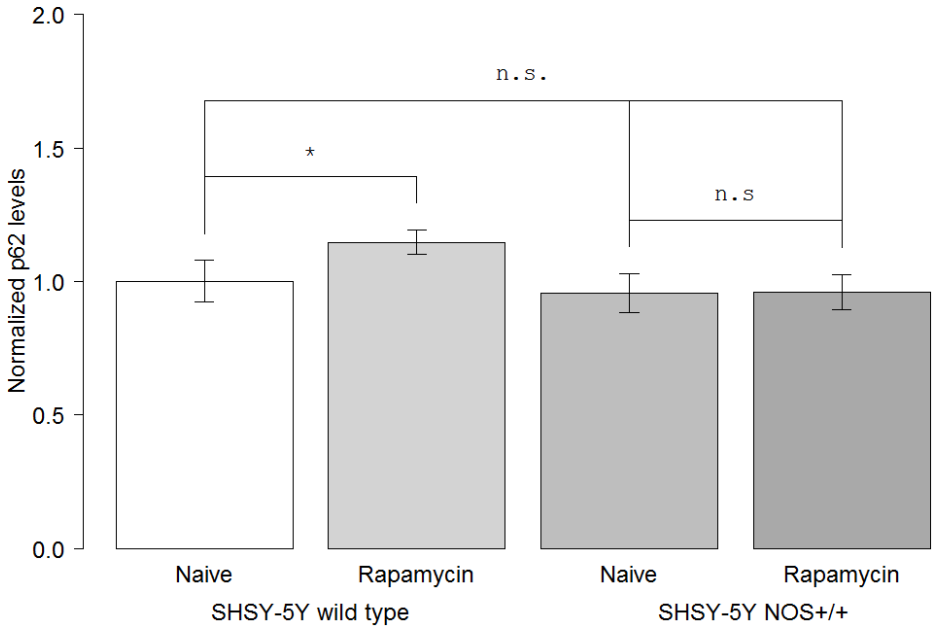

Figure 22 p62 (SQSTM1) after rapamycin stimulation
p62 (SQSTM1) expression in wild type and nNOS over-expressing SHSY-5Y cells after stimulation with rapamycin (1 µM, 6 hours). Average values are normalized to Naïve cells = 1. Significance markers: * $p < 0.05$, ** $p < 0.01$, *** $p < 0.001$.

Table 10 Autophagy markers after stimulation with rapamycin

Cell type	Treatment	Ubiquitin	HSC70	p62	LC3-I / LC3-II
WT	Naïve	1.00	1.00	1.00	1.00
	Rapamycin	0.72 **	0.74 **	1.14 *	3.33 *
nNOS+	Vehicle	0.97	0.85	0.96	2.44 *
	Naïve	1.93 ***	1.85 ***	0.96	4.92 **

Autophagy markers in wild type and nNOS over-expressing SHSY-5Y cells after stimulation with rapamycin (1 µM, 6 hours). Average values are normalized to Naïve cells = 1. Asterisks indicate significance (ANOVA) of change from wild type naïve: * $p < 0.05$, ** $p < 0.01$, *** $p < 0.001$.

3.6.3.5 Loading controls

To test if the β-actin was possibly regulated by the nNOS overexpression or rapamycin stimulation two other separate loading controls were tested, HSP70 and GAPDH. Neither HSP70 nor GAPDH was significantly modified by the nNOS overexpression or rapamycin stimulation. See Figure 23 and Figure 24.

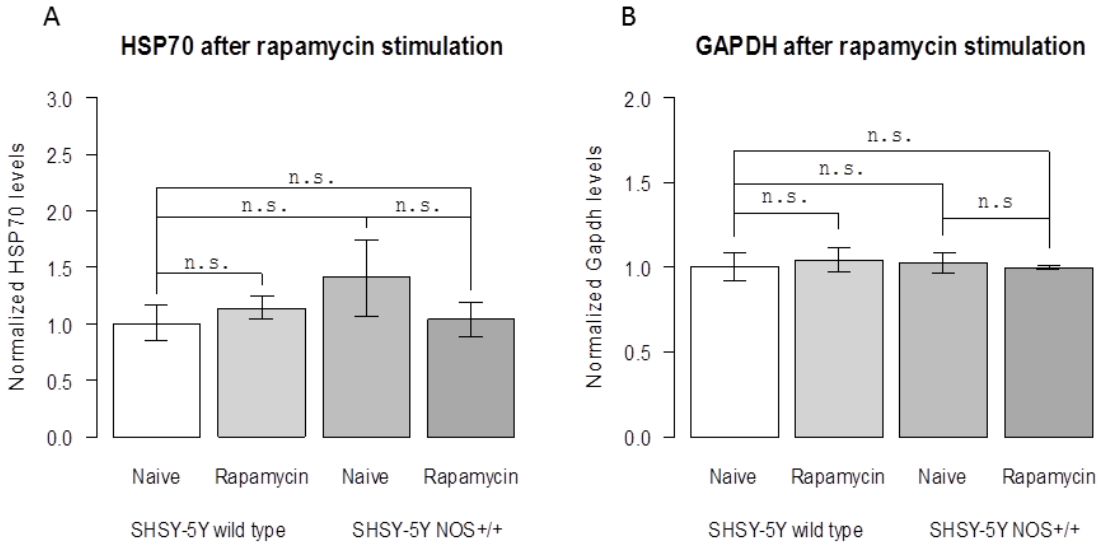

Figure 23 Loading controls HSP70 and GAPDH
Loading control in wild type and nNOS over-expressing SHSY-5Y cells after stimulation with rapamycin (1 µM, 6 hours). Neither HSP70 (A) nor GAPDH (B) was significantly modified by the nNOS overexpression or rapamycin stimulation.

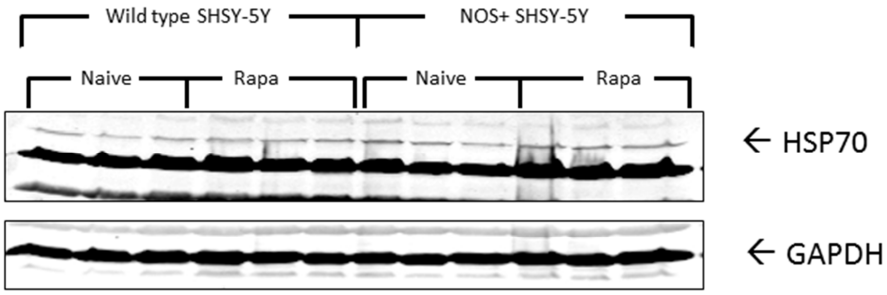

Figure 24 Loading controls HSP70 and GAPDH blots
Total protein homogenate western blot of HSP70 and GAPDH in wild type and nNOS over-expressing SHSY-5Y cells after stimulation with rapamycin (1 µM, 6 hours).

3.6.4 SNO-DIGE

To investigate the progress of S-nitrosylation in autophagy a timeline of S-nitrosylation changes was made using the SNO-DIGE method after stimulation of nNOS over-expressing cells with rapamycin (0.2 µM, 0-24 hours). Twenty two unique proteins in 27 spots were found to show time dependent changes in nitrosylation. The greatest changes occurred in the range of 4 and 8 hours after stimulation with rapamycin. Based on these results a time point of 6 hours was selected for further investigations. See Table 12.

At the four hour time point the most profound increases in nitrosylation were found to be in the proteins WD repeat-containing protein 1 (*wdr1*, ratio 1.72 after 4 hours compared with naive, 1.34 after 8 hours), Elongation factor 2 (*eef2*, 1.66 after 4 hours, 0.98 after 8 hours), and Methionine aminopeptidase 1 (*metap1*, 1.62 after 4 hours, 0.98 after 8 hours). The greatest decrease in nitrosylation was found in Heat shock cognate 71 kDa protein (*hspa8*, 0.46 after 4 hours, 0.42 after 8 hours), Calreticulin (*calr*, 0.67 after 4 hours, 0.65 after 8 hours), and Zyxin (*zyx*, 0.73 after 4 hours, 0.73 after 8 hours).

Heat shock cognate 71 kDa protein and Pyruvate kinase isozymes M1/M2 were also found to be nitrosylated after SNI operation. Actin, cytoplasmic 1 (actb), Elongation factor 2 (eef2), Far upstream element-binding protein 1 (fubp1), Heat shock cognate 71 kDa protein (hspa8), Pyruvate kinase isozymes M1/M2 (pkm2), and T-complex protein 1 subunit epsilon (cct5) were also found in the SNOSID method. See below.

Far upstream element-binding protein 1 and Pyruvate kinase isozymes M1/M2 were also found to be nitrosylated with the SNO-SILAC method. See below.

3.6.5 SNO-SILAC and SNOSID

To investigate the potential targets of S-nitrosylation in autophagy the SNO-SILAC and SNOSID methods were employed after stimulation of wild type as well as nNOS over-expressing cells with rapamycin (1 µM, 6 hours).

The SNOSID method revealed 27 nitrosylation sites in 17 different proteins. See Table 11.

Table 11 S-Nitrosylation sites after induction of autophagy with rapamycin in nNOS overexpressing SHSY-5Y found by the SNOSID method.

Protein Name	Gene	Cysteine	Control	Rapamycin
Elongation factor 2	eef2	290	√	√
Alpha-enolase	eno1	357	√	√
Glyceraldehyde-3-phosphate dehydrogenase	gapdh	152, 156	√	√
Glyceraldehyde-3-phosphate dehydrogenase	gapdh	247	√	√
Heat shock cognate 71 kDa protein	hspa8	17	√	√
Phosphoglycerate kinase 1	pgk1	108	√	√
Enolase	eno3	357	√	√
Tubulin alpha-1B chain	tuba1b	347	√	√
Malate dehydrogenase, mitochondrial	mdh2	89	√	X
GTP-binding nuclear protein Ran	ran	112, 120	√	X
Echinoderm microtubule-ass. protein-like 4	eml4	461	X	√
Heterogeneous nuclear ribonucleoprotein H	hnrnph1	22	X	√
Pyruvate kinase isozymes M1/M2	pkm2	423, 424	X	√
Malate dehydrogenase, mitochondrial	mdh2	212	X	√
Polypyrimidine tract-binding protein 1	ptbp1	250, 251	X	√
40S ribosomal protein S26	rps26	74, 77	X	√
Superoxide dismutase [Cu-Zn	sod1	7	X	√
Tubulin alpha-1A chain	tuba1a	347	X	√
Tubulin beta chain	tubbp2	12	X	√
Ubiquitin-conjugating enzyme E2 D1	ube2d1	85	X	√

Several proteins were found in two or three approaches these are listed in Table 14.

The SNO-SILAC revealed 29 proteins with alteration of S-nitrosylation. A summary of these proteins can be found in Table 13 and Figure 26.

Although few S-nitrosylated proteins were found with this method the SILAC experiment revealed 513 proteins of which 185 were significantly modified by rapamycin stimulation, overexpression of nNOS, or

both. The full list of proteins identified with the SILAC method can be found in Appendix VII. A list of ER-stress proteins from the silac data can be found in Table 16.

3.6.6 SNO-Elisa

To confirm the nitrosylation of some targets found in the SNOSID the SNO-Elisa method was employed as described above. Antibodies were directed against Glyceraldehyde-3-phosphate dehydrogenase (gapdh, 1:1000, Ambion, AM 4300) as loading control and ubiquitin-conjugating enzyme E2-D1 (ube2d1, 1:1000, abcam, ab76652). Ube2d1 showed a 20% up-nitrosylation after induction of autophagy ($p = 0.029$). See Figure 25.

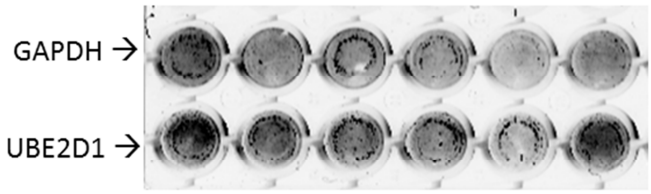

	Naïve			Rapamycin		
UBE2D1	43.42	34.44	33.06	31.84	20.79	39.49
GAPDH	43.04	28.74	31.35	25.86	16.32	27.22
Ratio	1.01	1.20	1.05	1.23	1.27	1.45

Figure 25 SNO-Elisa of UBE2D1
SNO-Elisa of Ubiquitin-conjugating enzyme E2-D1 in nNOS over-expressing SHSY-5Y cells after stimulation with rapamycin (1 µM, 6 hours) using GAPDH as loading control.

Table 12 Protein modification by S-nitrosylation after induction of autophagy by rapamycin stimulation as analyzed by SNO-DIGE

Spot no.	Uniprot ID	Protein Name	Gene	0 h	0.5 h	4 h	8 h	16 h	24 h	Spark plot	MW	PI	SNO sites
1	CSDE1_HUMAN	Cold shock domain-containing protein E1	csde1	1	0.86	0.85	0.96	0.36	0.81		88885	5.82	
2	ZYX_HUMAN	Zyxin	zyx	1	0.79	0.73	0.73		0.67		61277	6.23	
3	UBA1_HUMAN	Ubiquitin-like modifier-activating enzyme 1	uba1	1	1.35	1.23	0.88	0.66	0.99		117849	5.33	
4	EF2_HUMAN	Elongation factor 2	eef2	1	1.03	1.66	0.98	0.55			95338	6.41	290
5	FUBP1_HUMAN	Far upstream element-binding protein 1	fubp1	1	1.21	1.22	1.34	1.06	1.51		67560	7.35	148
7	XRCC5_HUMAN	X-ray repair cross-complementing protein 5	xrcc5	1	1.33	1.32	1.57		1.60		82705	5.39	
8	WDR1_HUMAN	WD repeat-containing protein 1	wdr1	1	1.34	1.72	1.34		1.48		66194	6.21	
9	KPYM_HUMAN	Pyruvate kinase isozymes M1/M2	pkm2	1	1.06	0.97	1.12	1.52	0.89		57937	7.60	49, 423, 424
11	HSP7C_HUMAN	Heat shock cognate 71 kDa protein	hspa8	1	0.59	0.46	0.42	0.44	0.62		70898	5.12	17
12	HSP7C_HUMAN	Heat shock cognate 71 kDa protein	hspa8	1	1.25	1.39	1.28	1.19	1.36		70898	5.12	17
13	CALR_HUMAN	Calreticulin	calr	1	0.80	0.67	0.65	0.64	0.93		48142	4.03	
14	ACTB_HUMAN	Actin, cytoplasmic 1	actb	1	1.24	1.24	1.72	1.02	1.51		41737	5.07	217, 257, 272
15	CALR_HUMAN	Calreticulin	calr	1	1.54	1.43	1.42		1.64		48142	4.03	
16	DHE3_HUMAN	Glutamate dehydrogenase 1, mitochondrial	glud1	1	1.03	1.33	1.00		0.83		61398	7.58	
17	TCPE_HUMAN	T-complex protein 1 subunit epsilon	cct5	1	1.11	1.36	0.90	0.76	0.92		59671	5.24	450
18	HNRPK_HUMAN	Heterogeneous nuclear ribonucleoprotein K	hnrnpk	1	1.31	1.15	0.82		0.82		50976	5.14	
19	CTBP2_HUMAN	C-terminal-binding protein 2	ctbp2	1	1.26	1.16	1.10		1.03		48945	6.51	
20	AMPM1_HUMAN	Methionine aminopeptidase 1	metap1	1	1.16	1.62	0.98	1.08	1.01		43215	6.77	
21	NP1L1_HUMAN	Nucleosome assembly protein 1-like 1	nap1l1	1	1.30	1.17	1.30		1.23		45374	4.08	
22	CALR_HUMAN	Calreticulin	calr	1	1.38	1.16	1.28		1.39		48142	4.03	
23	RUVB2_HUMAN	RuvB-like 2	ruvbl2	1	1.05	1.26	1.07	0.80	1.09		51157	5.25	
24	ECH1_HUMAN	Delta(3,5)-Delta(2,4)-dienoyl-CoA isomerase	ech1	1	0.96	0.83	1.01	0.49	1.00		35816	7.80	
25	HSPB1_HUMAN	Heat shock protein beta-1	hspb1	1	1.11	1.35	1.09		0.94		22783	5.97	
26	HSPB1_HUMAN	Heat shock protein beta-1	hspb1	1	1.00	1.22	1.03	0.99	1.07		22783	5.97	
27	RABL3_HUMAN	Rab-like protein 3	rabl3	1	1.36	1.15	1.42	1.28	1.81	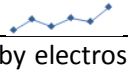	26423	6.71	

S-nitrosylation after rapamycin stimulation was assessed by 2D SNO-DIGE analysis and subsequent identification by electrospray ionization mass spectrometry (ESI-MS/MS). SNO Upregulation is shown in blue, SNO down regulation in red, numbers indicate ratio compared to 0 hour (naïve). Identification of the modified cysteines was done with the SNOSID or SNO-SILAC. Abbreviations: pI, isoelectric point; MW, protein molecular weight; h, hours after stimulation.

Table 13 Protein modification by S-nitrosylation after induction of autophagy with rapamycin in wild type and nNOS overexpressing SHSY-5Y cells as analyzed by SNO-SILAC

Protein ID	Protein	Gene	Cysteine	WT	WT+R	nNOS+	nNOS++R
ROA2_HUMAN	Heterogeneous nuclear ribonucleop. A2/B1	hnrnpa2b1	50	56.3	56.7	51.0	59.5
HNRPD_HUMAN	Heterogeneous nuclear ribonucleoprotein D0	hnrnpd	126	53.8	58.8	54.8	41.5
RTN4_HUMAN	Reticulon-4	rtn4	1101	28.3	34.7		32.2
NHP2_HUMAN	H/ACA ribonucleoprotein complex subunit 2	nhp2	18	21.2	29.2		
DOPO_HUMAN	Dopamine beta-hydroxylase	dbh	596	5.5		5.8	5.7
PPIA_HUMAN	Peptidyl-prolyl cis-trans isomerase A	ppia	161	3.6		4.3	
KPYM_HUMAN	Pyruvate kinase isozymes M1/M2	pkm2	49	0.8			0.6
RLA0_HUMAN	60S acidic ribosomal protein P0	rplp0	119	20.8			
HDGF_HUMAN	Hepatoma-derived growth factor	hdgf	108	14.1			
TCPD_HUMAN	T-complex protein 1 subunit delta	cct4	450	8.3			
RL7A_HUMAN	60S ribosomal protein L7a	rpl7a	199		39.8	32.8	42.4
NOP58_HUMAN	Nucleolar protein 58	nop58	439		26.7	24.4	28.6
FUBP1_HUMAN	Far upstream element-binding protein 1	fubp1	148			10.0	21.8
CRIP2_HUMAN	Cysteine-rich protein 2	crip2	126			9.8	
VDAC2_HUMAN	VDAC-2	vdac2	47			49.4	
RS3_HUMAN	40S ribosomal protein S3	rps3	97				20.9
RL30_HUMAN	60S ribosomal protein L30	rpl30	85				40.2
RL32_HUMAN	60S ribosomal protein L32	rpl32	96				36.6
ACTB_HUMAN	Actin, cytoplasmic 1	actb	217				84.8
PRKDC_HUMAN	DNA-dependent protein kinase catalytic subunit	prkdc	4061				60.7
G3P_HUMAN	Glyceraldehyde-3-phosphate dehydrogenase	gapdh	152; 156				0.1
HNRPU_HUMAN	Heterogeneous nuclear ribonucleoprotein U	hnrnpu	497				38.2
LRC59_HUMAN	Leucine-rich repeat-containing protein 59	lrrc59	59				75.5
KDM5A_HUMAN	Lysine-specific demethylase 5A	kdm5a	626; 636				32.7
NDKA_HUMAN	Nucleoside diphosphate kinase A	nme1	109				5.1
TBB4B_HUMAN	Tubulin beta-4B chain	tubb4b	12				22.7
VDAC3_HUMAN	VDAC-3	vdac3	36				35.6
VIME_HUMAN	Vimentin	vim	328				41.0

Nitrosylated cysteins identified by the SNO-SILAC method. WT: Wild type SHSY-5Y cells, nNOS+: nNOS overexpressing SHSY-5Y cells, rapa: Rapamycin stimulation (1 µM, 6 hours). Numerical values indicate ratio of silac heavy amino acids to light.

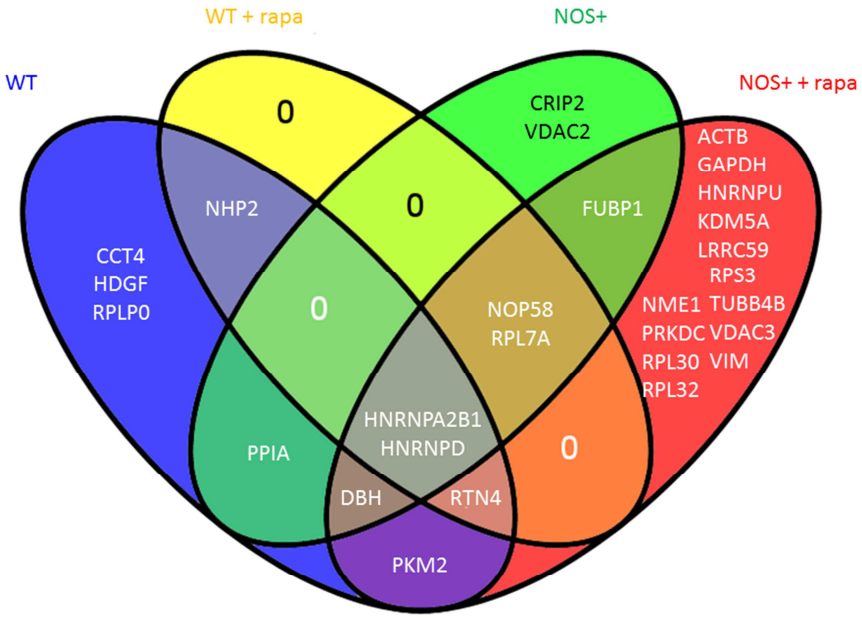

Figure 26 Venn diagram of proteins identified by SNO-SILAC
Venn diagram of nitrosylated proteins identified by SNO-SILAC

Table 14 Protein S-nitrosylation in multiple methods

Protein ID	Protein name	Gene	Cysteine	SNO-DIGE	SNOSID	SNO-SILAC
ACTB_HUMAN	Actin, cytoplasmic 1	actb	217	√	X	√
EF2_HUMAN	Elongation factor 2	eef2	290	√	√	X
FUBP1_HUMAN	Far upstream element-binding protein 1	fubp1	148	√	X	√
G3P_HUMAN	Glyceraldehyde-3-phosphate dehydrogenase	gapdh	152, 156	X	√	√
HSP7C_HUMAN	Heat shock cognate 71 kDa protein	hspa8	17	√	√	X
KPYM_HUMAN	Pyruvate kinase isozymes M1/M2	pkm2	49, 423, 424	√	√	√

Proteins found nitrosylated after autophagy induction using 2 or more approaches

Table 15 Protein expression of proteins found nitrosylated by multiple methods

Protein ID	Protein	Gene	WT	WT + Rapa	nNOS	nNOS + Rapa
EF2_HUMAN	Elongation factor 2	eef2	1.00	1.37	1.38	**0.57 ***
HSP7C_HUMAN	Heat shock cognate 71 kDa protein	hspa8	1.00	0.94	0.90	**0.89 ***
ACTB_HUMAN	Actin, cytoplasmic 1	actb	1.00	1.43	1.32	1.33
FUBP1_HUMAN	Far upstream element-binding protein 1	fubp1	1.00	0.98	0.98	1.15
G3P_HUMAN	Glyceraldehyde-3-phosphate dehydrogenase	gapdh	1.00	1.06	1.00	0.97
KPYM_HUMAN	Pyruvate kinase isozymes M1/M2	pkm2	1.00	0.60	1.25	0.89

Whole protein expression after rapamycin stimulation was assessed by SNO-SILAC. WT: Wild type SHSY-5Y cells, nNOS+: nNOS overexpressing SHSY-5Y cells, rapa: Rapamycin stimulation (1 µM, 6 hours). Expression is normalized to wild-type naïve. * Significant Anova $p < 0.05$.

Table 16 ER-stress proteins from SNO-SILAC data

Protein ID	Protein	Gene	WT	WT vs WT+Rapa	WT vs nNOS+	nNOS+ vs nNOS+ +Rapa
GRP78_HUMAN	78 kDa glucose-regulated protein	hspa5	1.00	1.27	1.19	1.26
PDIA1_HUMAN	Protein disulfide-isomerase	p4hb	1.00	1.20	1.14	1.63 *
CALX_HUMAN	Calnexin	canx	1.00	0.92	0.85 *	0.85
ERO1A_HUMAN	ERO1-like protein alpha	ero1l	1.00	0.18	0.25	0.29

Results on four known ER-stress protein markers from the SNO-SILAC method. WT: Wild type SHSY-5Y cells, nNOS+: nNOS overexpressing SHSY-5Y cells, Rapa: Rapamycin stimulation (1 µM, 6 hours). * Significant Anova $p < 0.05$.

4. Discussion

4.1 S-nitrosylation in neuropathic pain

This study shows substantial protein S-nitrosylation and denitrosylation in the spinal cord upon sciatic nerve injury in mice on the side ipsilateral to the injury. In addition the results show that the impact of sciatic nerve injury on hyperalgesia can be abolished by eliminating nitric oxide production with the unspecific NOS inhibitor L-NAME. This suggests that NO-mediated post-translational protein modifications contribute to the neuronal and glial adaptations to the damage of the afferent neurons.

4.1.1 Results of screening for S-nitrosylation

The initial investigation into the targets of nitric oxide using 2D SNO-DIGE screening revealed 31 proteins with increased nitrosylation and 22 with a decrease in SNO. This indicates that there is substantial constitutive S-nitrosylation in the spinal cord. In contrast, sham surgery only resulted in SNO-modifications of 15 proteins out of which only three showed an increase of S-nitrosylation suggesting that most of the observed alterations after SNI were elicited by the axonal injury.

Time course analyses of candidate proteins revealed that some early SNO-modifications observed at one day after the injury had returned to baseline at 7 days. This was true for protein disulfide isomerase and glutathione synthetase where the SNO had been reduced after one day. On the other hand, S-nitrosylation of the mitochondrial aconitase 2 was mainly increased at 7 days suggesting that S-nitrosylation of some targets may impact on the chronic phase. It is conceivable that SNO-modifications of mitochondrial targets may outlast cytoplasmic or ER SNO modifications because of the more sustained disturbance of the redox balance at the mitochondria.

In order to confirm the observed S-nitrosylation of some candidate proteins the biotin switch technique was applied. The BST was able to confirm that GSS, PDI, Aco2, Tuba, Tubb, and Prdx6 were S-nitrosylated after nerve injury. SNO down-regulation of PDI in BST, though the other proteins did not show a significant difference between naïve and SNI-treated mice. Because the quantification of Western Blots has limitations an ELISA based version of the BST, called biotin switch ELISA (BSE), was established. This technical modification still does not allow for a differentiation between multiple SNO sites in one protein and relies on the specificity of the antibody. The quantitative readout however, was suitable to assess time courses of SNO modifications of target proteins and may be an advancement of the original method. The SNOSID method provided information about the site of S-nitrosylation in the amino acid

sequence as well as changes in the number or location of SNO sites, but did not provide quantitative data. As shown in Fig. 4, SNOSID identified many SNO sites that were not affected by the sciatic nerve injury. SNOSID and 2D SNO-DIGE therefore provided complimentary information of the SNO-proteome. However, as for 2D-SNO-DIGE, the SNOSID screen mainly detected SNO-sites in highly abundant cytosolic proteins.

4.1.2 Context of results with current literature

The current understanding of NO mediated effects in nociceptive and nerve injury models suggests that glutamate release from the injured or stimulated afferent neurons activates NMDA receptors of the postsynaptic neurons which is linked to activation of neuronal NOS in the postsynaptic density and subsequent NO release. NO may then act on several targets in its vicinity (Schmidtko et al. 2009, Tegeder et al. 2011). This idea is supported by the observed increase of protein S-nitrosylation after sciatic nerve injury which was in part reversible upon treatment with L-NAME and paralleled by L-NAME mediated reversal of hyperalgesia. However, the observed decrease of S-nitrosylation of several proteins is not readily explained in this context. The decrease may be due to complex changes in the redox status, in redoxin functions (Benhar et al. 2008) and intracellular levels of glutathione (Romero and Bizzozero 2009, Benhar, Forrester and Stamler 2009). The apparent decrease of SNO-sites may also result from trans-nitrosylation and formation of disulfide bonds or stronger oxidation of thiol groups to form sulfinic and sulfonic acid derivatives of cysteine. Such changes occur upon reaction with hydrogen peroxide (Lim et al. 2008, Noh et al. 2009, Burgoyne et al. 2007, Charles et al. 2007, Saurin et al. 2004) which may compete with NO for the cysteines. NOS catalytic activity depends on the oxidation-reduction cycle at its catalytic site. Redox imbalances lead to uncoupling and production of H_2O_2 instead of NO (Sun, Druhan and Zweier 2008, Landmesser et al. 2003) so that posttranslational reversible S-nitrosylation of critical cysteines may shift to irreversible thiol oxidations upon axonal injury.

Out of the 53 proteins found in the first SNO-DIGE, 19 proteins have been previously reported to be S-nitrosylated in different contexts. For example, S-nitrosylation of protein disulfide isomerase (PDI) was shown to affect its chaperone activity resulting in protein misfolding, accumulation of polyubiquitinated proteins, and neurodegeneration (Uehara et al. 2006, Walker et al. 2010). In these experiments PDI was denitrosylated after sciatic nerve injury suggesting that this may be a protective adaptive response and an attempt to prevent further ER stress. Based on the SNO site predictions and the SNOSID results PDI was S-nitrosylated at its active sites at cysteines 57, 60, 406, and 409, sites that are known to be redox active (Maattanen et al. 2006). S-nitrosylation may affect the function of several other enzymes which

were identified by SNO-DIGE and SNOSID. Based on the localization of S-nitrosylated cysteines, it is conceivable that catalytic functions of glutathione synthetase (GSS), mitochondrial aconitase (ACO2) and peroxiredoxin-6 (Prdx6) were changed after nerve injury. GSS has an ATP binding site in glutamic acid 425 in the vicinity of the SNO site Cys422, which upon its nitrosylation might interfere with ATP binding. For Prdx6 cysteine 47 in the catalytic center of the enzyme is a SNO site and hence may affect its oxidoreductase activity (Fisher 2011) and S-nitrosylation of Aco2 at Cys448 and Cys541 may compete with iron-sulphur binding of these cysteines and lead to mitochondrial iron overload and dysfunctions (Cairo et al. 2002, Bulteau et al. 2004). Indeed several of the proteins which were SNO-modified are localized in mitochondria and involved in glucose metabolism and ATP synthesis or transport. Synapses are enriched with mitochondria to meet the high demand of energy for maintenance of synaptic activity. Upon nerve injury axonal transport of mitochondria and the physiological fusion and fission processes are strongly impaired suggesting that mitochondrial pathology is reflected by the SNO-modifications of mitochondrial proteins (Barsoum et al. 2006, Westermann 2009, Ferrari et al. 2011) and may be contributed by S-nitrosylation mediated changes of cytoskeletal dynamics and axonal transport (Lu et al. 2009, Thom et al. 2008). It is of note that S-nitrosylation of the mitochondrial aconitase 2 was further increased 7 days after nerve injury whereas SNO-alterations of the ER localized PDI and the cytosolic GSS were normalized suggesting that SNO events at the mitochondria may indeed extend to the chronic phase.

4.1.3 Methodological limitations

Although the 2D SNO-DIGE revealed many SNO protein modifications the method has limitations in that it mostly detects abundant cytosolic proteins while underrepresenting membrane proteins and highly hydrophobic proteins. In addition, insufficient protein separation resulting in false positive results and the variability of the electrophoretic process may affect results. Further difficulties arise, if posttranslational modifications of proteins, such as phosphorylation or protein cleavage impact on their isoelectric point and mass so that one protein may be represented in more than one spot. Such double representations occurred for dihydropyrimidinase-related protein 2 (spot 13 and 14), which is known to be phosphorylated (Sweet et al. 2009), for ATP synthase subunit d and leukocyte elastase inhibitor A (no. 56 and no. 57, and no. 39 and no. 41 respectively) and mitochondrial aconitase (Aco2) (no. 2 and no. 5). S-nitrosylation was consistent for all these double represented proteins so that the result was not confounded. Identification of the correct protein from excised gel spots can be precarious. Traces of proteins from neighboring spots may interfere with identification by mass spectrometry. To eliminate

this interference the protein spot location was matched with the mass and theoretical pI as well as the emPAI values from the MS data (Ishihama et al. 2005), which gave an estimation of protein abundance. Based on these values the prime candidate for each spot was selected.

The present study did not assess the detailed toponomical aspects of S-nitrosylation or the cell types in which these changes occurred. In the spinal cord neuronal NOS is mainly expressed in the terminals of primary afferent neurons in laminae I and II and in some interneurons in laminae III, IV and V (Maihofner et al. 2000). Glial cells do not express NOS isoenzymes at baseline and 24 hours after SNI, but may upregulate inducible NOS at later time points (Maihofner et al. 2000, Zhang et al. 1993). It is therefore assumed that most of the observed SNO modifications are localized in neurons in laminae I-V of the dorsal horn. However, endothelial NOS may contribute to the SNO-proteome and since NO is a diffusible molecule it may also cause S-nitrosylation at neighboring glial cells or of matrix proteins. For detailed SNO-toponomics laser microdissection of dorsal horn regions and cell sorting prior to 2D SNO-DIGE may answer these questions in the future. Knock-in models are required to assess the functional relevance of individual SNO-sites in individual proteins. In order to improve the proteomic analyses the SILAC technique could be exploited.

4.1.4 Conclusion

Despite the limitations this is the first study showing that S-nitrosylation and denitrosylation in the spinal cord contribute to the adaptive post-translational changes after peripheral nerve injury. The observed partial L-NAME-mediated reversibility of the SNO-modifications and reversal of hyperalgesia suggest that the SNO-modifications contribute to the development of neuropathic pain. This study provides a list of potentially interesting candidate targets for S-nitrosylation that may play a role in the development of neuronal hyperexcitability. In this context NO apparently acts as a posttranslational modifier that, according to the prime candidates revealed by 2D SNO-DIGE and SNOSID, is likely to impact on mitochondrial functions, protein folding and misfolding, redox control and cytoskeletal remodeling.

4.2 S-nitrosylation in Autophagy

In light of the results of the investigation into neuropathic pain that S-nitrosylation was likely to impact on protein folding and misfolding the next step was to further investigate the effect of S-nitrosylation on these processes. For this a cellular model of neuronal nitric oxide synthase (nNOS) over-expressing neuroblastoma cell culture, as well as wild type cells of the same type, stimulated with rapamycin to induce the process of autophagy was used. The effects of nNOS overexpression on autophagic processes were evaluated by western blotting with antibodies for known markers of autophagy. S-nitrosylation was evaluated using a combination of SNO-DIGE, SNOSID, SNO-SILAC, and SNO-ELISA methods.

4.2.1 Evaluation of Autophagy progression

An initial analysis of autophagy markers on the effects of rapamycin on the two cell lines revealed that there is substantial basal increase (+ 144%, $p < 0.05$) in the ratio of LC3-I / LC3-II in the nNOS over-expressing cells compared to the wild type after stimulation with rapamycin. Under stressful conditions (e.g. starvation, pharmacological stimulation) LC3-I is converted to LC3-II by conjugation with phosphatidylethanolamine and then the conjugate form is recruited to autophagosomal membranes (Sou et al. 2006). The autophagosomes then fuse with lysosomes to form autolysosomes, and intra-autophagosomal components are degraded by lysosomal hydrolases (Sou et al. 2006). At the same time, LC3-II in autolysosomal lumen is degraded. Thus an increase in the ratio of LC3-I / LC3-II indicates an increased autophagic activity or impairment of lysosomal degradation (Tanida, Ueno and Kominami 2008, Mizushima and Yoshimori 2007). A lower increase of the LC3-I/LC3-II ratio after stimulation with rapamycin in the nNOS over-expressing cells (+233% in WT, +100% in nNOS+) suggests that the autophagic activity may be impaired by the increase of NO and possibly by an increase of direct protein S-nitrosylation. Alternatively, an increase of NO may also stimulate sGC mediated production of cGMP, followed by subsequent activation of protein kinase G (PKG). However, no direct link between autophagy and PKG has been reported in the literature, supporting the theory that S-nitrosylation might be the main mediator of the effects of NO on autophagy.

A second important marker for degradation of protein aggregates is the ubiquitination of proteins. Ubiquitin is a small protein consisting of 76 amino acids that is covalently bound to lysines of proteins to mark them for degradation in a process called ubiquitination. Ubiquitination utilized a cascade of three different types of ubiquitin ligases, the E1 ubiquitin-activating enzyme that uses ATP to activate ubiquitin for conjugation and transfers it to an E2 ubiquitin-conjugating enzyme. The E2 the enzymes then interact with a specific E3 partner. The E3 finally transfers the ubiquitin to the target protein via attachment to a

lysine residue thus marking the target protein for degradation by targeting them to the proteasome, the lysosome, and the autophagosome (Shaid et al. 2013).

In the nNOS over-expressing cells the total ubiquitination was increased (+100%, $p < 0.01$) while it was decreased (-30%, $p < 0.01$)) in the wild type cells after rapamycin stimulation. This indicates that the targeting or degradation processes may be impaired by the increase in S-nitrosylation of the E1, E2 or E3 ubiquitin ligases. Indeed these results are consistent with previous results by Sarkar et al. who showed that NO inhibits autophagy by two distinct mechanisms. Primarily by S-nitrosylation of JNK1 inhibits the formation of autophagosomes by reduced Bcl-2 phosphorylation, leading to an increase in interaction of Bcl-2 with Beclin-1, and disrupting Beclin 1–hVps34 association, which is essential to the initiation of autophagic processes (Li and Fan 2010, Sarkar et al. 2011). Secondly Sarkar et al showed that NO activates the mammalian target of rapamycin receptor 1 (mTORC1) leading to an inhibition of autophagy processes (Sarkar et al. 2011). This further supports that the effects of NO on the autophagy process are not mediated directly through the sGC and PKG pathway.

Heat shock cognate 71 kDa protein (HSC70, gene: hspa8) is chaperone that binds to nascent polypeptides to facilitate correct protein folding. An increase in HSC70 expression is indicative of increased protein misfolding (Liu, Daniels and Cao 2012). Indeed the increase in HSC70 expression (+120%, $p < 0.001$) seen in nNOS over-expressing cells after stimulation with rapamycin, while there was a decrease in HSC70 expression in wild type cells after stimulation, suggests that there may be a significant increase of misfolding and/or disruption of the targeting of misfolded proteins to degradation caused by increased S-nitrosylation or redox stress of newly generated proteins due to S-nitrosylation.

4.2.2 Targets of S-nitrosylation after autophagy induction

Thus there are clear effects of the increased nitric oxide production induced by the over-expression of nNOS on the processes of protein degradation. The next question that arises is what might be the targets of nitric oxide. To screen for targets of S-nitrosylation the same approaches as in the investigation of S-nitrosylation in neuropathic pain were used, namely SNO-DIGE and SNOSID. Due to the transient nature of proteins during a process such as autophagy a SILAC based approach was also assessed to analyze protein S-nitrosylation and total protein expression simultaneously. The main drawback of the SNO-DIGE approach is the mimicry of nitrosylation events by changes in protein expression. Thus a simultaneous down-regulation in the expression of a protein and increase in nitrosylation might be seen as little or no change in nitrosylation in the SNO-DIGE and vice versa. When inducing a process that increases protein

degradation and turnover such as autophagy it is essential to obtain protein expression information to account for changes that might produce false positive or false negative results.

To investigate the progress of S-nitrosylation in autophagy a timeline of S-nitrosylation changes was made using the SNO-DIGE method after stimulation of nNOS over-expressing cells with rapamycin. Twenty two unique proteins in 27 spots were found to show time dependent changes in nitrosylation. The greatest changes occurred in the range of 4 and 8 hours after stimulation with rapamycin. Based on these results a time point of 6 hours was selected for further investigations of nitrosylation events after rapamycin stimulation.

The results suggested that NO impacts on the autophagy process as indicated by the autophagy markers, but this study found only a few direct alterations of autophagy-proteins by S-nitrosylation suggesting that NO did not directly interfere with the autophagy processes.

4.2.3 Context of results with current literature

Currently only one study assessed the involvement of S-nitrosylation in autophagy. Sarkar et al, showed as previously described, that S-nitrosylation of JNK1 inhibits the formation of autophagosomes by reduced Bcl-2 phosphorylation (Sarkar et al. 2011). Using an autophagy database published by Homma et al. (Homma, Suzuki and Sugawara 2011) and the S-nitrosylation prediction algorithm GPS-SNO (Xue et al. 2010), revealed that out of 387 proteins listed (with sufficient information to acquire their sequence) 259 proteins were predicted to be S-nitrosylated. In fact this study found four proteins listed in the autophagy database to be nitrosylated, namely Actin (actb), Pyruvate kinase isozymes M1/M2 (pkm), DNA-dependent protein kinase catalytic subunit (prkdc), and Ubiquitin-like modifier-activating enzyme 1 (uba1).

The SNO-SILAC revealed that cysteine 217 of Actin is nitrosylated. Right next to this cysteine is a phosphorylation site at tyrosine 218 (Rush et al. 2005) indicating that the phosphorylation of that site could be affected by S-nitrosylation events, potentially affecting the proteins function. Aguilera et al. showed that actin participates in the early events of cytoskeletal autophagosome formation upon starvation induced autophagy, and that actin is necessary for starvation-mediated autophagy (Aguilera, Beron and Colombo 2012). Also actin S-nitrosylation is believed to influence neurotransmitter release in inflammatory pain leading to disinhibition of synaptic transmission in the spinal dorsal horn (Lu et al. 2009, Lu et al. 2011). Thus S-nitrosylation of actin may indeed both have detrimental implications

immediately after neuronal injury through disinhibition of signal transduction as well as long term effects through inhibition of autophagosome formation.

DNA-dependent protein kinase catalytic subunit (PRKDC) is a serine/threonine-protein kinase that acts as a molecular sensor for DNA damage and also phosphorylates the autophagy protein JNK1 (Ma et al. 2004, Soubeyrand et al. 2003, Yavuzer et al. 1998). In this study PRKDC was found to be nitrosylated at cysteine 4061 in the SNO-DIGE after rapamycin stimulation of nNOS over-expressing cells though no currently known functional site is nearby. Knockdown of PRKDC has been shown to induce massive autophagic cell death after ionizing radiation injury of glioblasoma cells, indicating a protective role of the protein in response to DNA damage (Zhuang et al. 2011). Recent studies have revealed that S-nitrosylation of DNA repair proteins may enhance their activity (Tang, Wei and Liu 2012) and that PRKDC S-nitrosylation is mediated through GAPDH (Kornberg et al. 2010). The effect of S-nitrosylation on the function of PRKDC remains to be determined.

Ubiquitin-like modifier-activating enzyme 1 (UBA1) is an ubiquitin-activating E1 enzyme. UBA1 activates ubiquitin by first adenylating its C-terminal glycine residue with ATP, followed by linking this residue to the side chain of a cysteine residue in E1, yielding an ubiquitin-E1 thioester and free AMP. UBA1 has two active sites within the E1 molecule, allowing it to accommodate two ubiquitin moieties at a time. S-nitrosylation of the active thiol could affect the ability of UBA1 to carry out the transfer of ubiquitin to the E2 as discussed above.

The results suggest that S-nitrosylation may regulate protein folding, ubiquitination, and possibly de novo protein generation. In this study several proteins have emerged as major candidates for being targets of S-nitrosylation and consequentially impacting the autophagic processes, namely Heat shock cognate 71 kDa protein (abbreviation: HSC70, gene: hspa8) and Pyruvate kinase isozymes M1/M2 (PKM2, gene: pkm2), Calreticulin (gene:calr), Ubiquitin-conjugating enzyme E2 D1 (UBE2D1, gene: ube2d1), and Elongation factor 2 (EF2, gene: eef2).

HSC70 and PKM2 were found to be nitrosylated after induction of autophagy by rapamycin as well as in mouse spinal cord after SNI operation. These proteins mutually interact and, though the interaction site has not been described, nitrosylation of either protein could interfere with their interaction. Acetylation of PKM2 at K305 decreases PKM2 enzyme activity and increases PKM2 interaction with HSC70 (Lv et al. 2011). HSC70 is a chaperone for chaperone-mediated autophagy and through interaction with PKM2 association of PKM2 with lysosomes is promoted and subsequently also promotes the lysosomal-

dependent degradation of PKM2 (Lv et al. 2011). In addition S-nitrosylation of PKM2 cysteines 423 and 424 could theoretically impact on the proteins ability to bind with D-fructose 1,6-bisphosphate (FBP). FBP allosterically activates the M2 isoform while selective binding to tyrosine-phosphorylated peptides releases the allosteric activator FBP, leading to inhibition of PKM enzymatic activity (Lv et al. 2011). This diverts glucose metabolites from energy production to anabolic processes when cells are stimulated by certain growth factors. FBP has allosteric binding sites in region 432 – 437 and region 514 – 521. Nitrosylation of nearby cysteines could thus interfere with the binding of FBP and inhibiting the activation of PKM2 possibly further influencing the interaction with HSC70 and subsequent chaperone-mediated autophagy of PKM2. Thus S-nitrosylation of PKM2 and HSC70 may influence the long term adaption of neurons to neuronal damage by inhibition of the autophagic processes.

Calreticulin is a calcium-binding chaperone that promotes folding, oligomeric assembly, and quality control in the endoplasmic reticulum (ER) via the calreticulin/calnexin cycle (Michalak et al. 2009). Calreticulin binds to misfolded proteins and prevents them from being exported from the endoplasmic reticulum to the Golgi apparatus (Holaska et al. 2001, Nauseef, McCormick and Clark 1995).

Calreticulin has 3 cysteines (C105, C137, and C163) with C105 and C137 forming a disulfide bridge, leaving C163 as the likely candidate for nitrosylation. Nitrosylation of calreticulin has been shown to lead to an increase in its externalization from the ER in conjunction with phosphatidylserine (PS) under apoptotic stress suggesting that calreticulin acts as a bridging molecule during apoptotic cell clearance (Tarr et al. 2010). Although they share many components (e.g. the proteins Becliin-1, p62, and Atg5) and appear to be highly connected processes no direct causal relationship has been convincingly shown between autophagy and apoptosis (Gump and Thorburn 2011). S-nitrosylation of Calreticulin during autophagy could, similarly to its effects in apoptosis, lead to an increased externalization of misfolded protein and subsequently their transfer to degradation by the autophagic processes.

The process of ubiquitination requires an ubiquitin-activating E1 enzyme, an E2 conjugating enzyme and an E3 ubiquitin ligase. Following activation of ubiquitin by formation of a thioester bond with the E1 the ubiquitin moiety is transferred to the E2. The E2 then transfers the ubiquitin to either an E3 ligase or mediates the attachment of ubiquitin to a lysine residue of the substrate protein through a RING or U-box E3 ligases (Windheim, Peggle and Cohen 2008). UBE2D1 accepts ubiquitin from the E1 complex through cysteine 85 and catalyzes its attachment to other proteins. Indeed UBE2D1 was found to be nitrosylated at cysteine 85 by the SNOSID method. Nitrosylation of the active site C85 might affect its

ability to ubiquitinylate proteins and thus interfere with targeting of certain proteins to degradation. Thus S-nitrosylation might catalyze the reaction in a manner depicted in Figure 27.

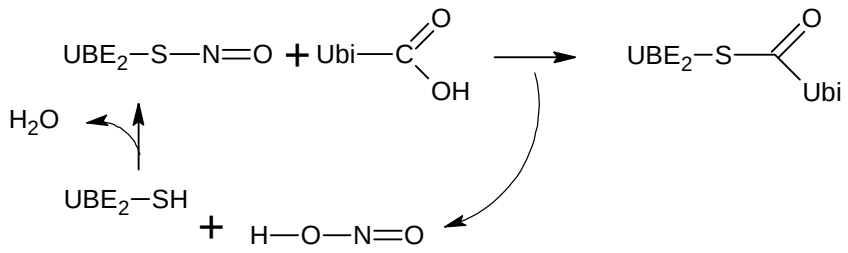

Figure 27 Catalysis of E2 ubiquitination by NO
Figure shows the reaction when ubiquitin is transferred to the E2 ligase by formation of a thioester bond. UBE_2:E2 ubiquitin conjugating enzyme, Ubi: ubiquitin.

This catalysis might lead to the strong increase in ubiquitination seen in nNOS over-expressing cells, compared to a decrease in wild type, after stimulation with rapamycin. This could further indicate that although there is increased ubiquitination the proteins are not being transferred to degradation, suggesting an impairment of the ubiquitination degradation pathway at another step. However, no evaluation of protein aggregates was conducted in this study and this remains to be investigated in future studies.

In addition ubiquitination not only marks proteins for degradation but is also important for regulation of receptor presentation at the cell membrane, such as AMPA-R. Therefore, alteration of ubiquitin may also affect e.g. glutamate sensitivity which is relevant for pain signaling.

It is important to note that nNOS itself is regulated by ubiquitination (Clapp et al. 2012, Clapp et al. 2010, Oustwani et al. 2011). This could lead to a feedback loop where an increase in NO leads to increased ubiquitination of nNOS and subsequent decrease in NO. Also increased activity of the ubiquitin pathway possibly decreases NO production and thus limiting the inhibitory effects of NO on protein degradation.

While Ube2D and Hsc70 control protein stability and quality, EF2 may be a potential NO target involved in protein synthesis being an essential factor for protein synthesis. Phosphorylation by EF-2 kinase completely inactivates EF-2, and such might also be true of nitrosylation (Hizli et al. 2013). Nitrosylation might interfere with the proteins ability to be phosphorylated or its interaction with ribosomes. EF is under the control of the mTOR system and rapamycin increases the level of phosphorylated EF2 (Ji et al. 2009). EF2 was found to be nitrosylated at cysteine 290 and was found nitrosylated in the SNO-DIGE

after rapamycin stimulation. Nitrosylation of EF2 was increased after 4 hours but then decreased back to its initial value after 8 hours, to 55% of its initial value after 16 hours, and was no longer nitrosylated after 24 hours.

From this evidence it appears that NO may use multiple mechanisms to modulate cell survival under stress conditions:

1. Interfering with chaperone mediated autophagy.
2. Interfering with protein degradation and receptor presentation through ubiquitination.
3. Control of de novo protein synthesis and regulation of energy/calcium homeostasis.

4.2.4 Methodological limitations

For the autophagy through rapamycin stimulation part of this study, the disadvantages of SNO-DIGE for screening for S-nitrosylation are particularly important. A process such as autophagy involves a high level of protein modifications, such as phosphorylation as well as changes in expression and degradation. Such changes may mask the changes in nitrosylation events. Identification of the correct protein from each excised gel spot is problematic and requires statistical approaches as described above.

To correct for these changes the usefulness of a SILAC based method for the identification of S-nitrosylated proteins was assessed. Using this approach it is theoretically possible to simultaneously detect nitrosylated proteins and non-nitrosylated proteins and calculate the level of nitrosylation as a ratio of expressed proteins. However the approach did reveal only few nitrosylated proteins though total protein expression patterns of around 500 proteins were successfully mapped. This information is nevertheless helpful to evaluate the true changes in nitrosylation of proteins identified by SNO-DIGE.

The main limitations of this method revolve around the complexity of samples. The samples are not purified for S-nitrosylated proteins and thus contain a high amount of non-nitrosylated proteins leading to a difficult evaluation of the sample. Better sample fractionation of the samples, for example by cellular components, could reduce the sample complexity. Also improvements in mass spectrometry and improved peptide search algorithms may also improve sample analysis. A better SILAC standard could be made by mixing naïve SILAC cells and SILAC treated with rapamycin to improve expression profile of proteins whose expression may be dormant before induction.

This study was limited to the use of rapamycin for autophagic stimulation. Rapamycin is a direct inhibitor of mTOR. Glucagon is also another inhibitor of mTOR and autophagy induction can also be induced independent of mTOR by lithium, sodium valproate and carbamazepine (Sarkar et al. 2011). Thus further exploration could include different stimulators of autophagy as well as utilizing proteasome the proteasomal inhibitor MG-132. Tamoxifen is also believed to induce autophagy by increasing the expression of Beclin-1 (Zhang et al. 2007). A multifaceted approach could possibly better reveal which role S-nitrosylation may play in the induction of distinct autophagy pathways. Inhibition of autophagic processes would also add another dimension to such studies. Several inhibitors of autophagy are known though most of them are not entirely specific. This includes the sequestration inhibitors 3-MA, LY294002, and wortmannin; phosphatidylinositol-3-kinase inhibitors such as lime okadaic acid; compounds that raise the lysosomal pH like bafilomycin; chloroquine that increases the formation of autophagosomes; single gene deletions or RNAi interference (e.g. Atg genes) (Klionsky et al. 2008).

To evaluate the progression of autophagy this study utilized western blotting for LC3-I/LC3-II ratios, p62, HSC70, ubiquitin, as well as SILAC based data of protein expression levels. Several other methods have been described to monitor the progression of autophagy. This includes electron microscopy of autophagosomes, fluorescence microscopy with GFP tagged LC3, TOR and Atg1 kinase activity assays, monitoring of transcriptional regulation of autophagy genes, protein degradation assays, GFP-Atg8/LC3 lysosomal delivery and proteolysis, autophagosome-lysosome colocalization, and more (Klionsky et al. 2008). A more varied approach to determine the progress of autophagy would enhance the knowledge on how NO, through S-nitrosylation, interferes with the process.

Using a cellular model may not fully reveal potential changes that occur *in vivo* upon exposure to certain types of stress and the response may be site and tissue specific. This study employed neuroblastoma cells which share some features of neuronal cells but do not allow an assessment of the complex interplay of neurons, glia, immune and endothelial cells which all contribute to the production and scavenging of NO. Although overexpression of nNOS in culture was used to mimic the nerve injury evoked induction of nNOS *in vivo*, the neuroblastoma model cannot mimic the specific functions of nNOS at the presynaptic terminal and in the postsynaptic density where modification of protein stability and quality may be crucial for synaptic signaling. Nevertheless, the results suggest that NO modifies protein folding and ubiquitination through direct S-nitrosylation though the *in vivo* relevance has to be addressed in future studies.

4.2.5 Conclusion

This study provides a list of potentially interesting candidate targets for S-nitrosylation that may play a role in the ability of neurons to recover from injury (e.g. SNI) by impairing the cells ability to adapt to the stressful situation. Impairment of the injured neuron to adapt to increased stress leads to neuronal death, a crucial part of the development of neuropathic pain. Autophagy may be an important protective adaptive response which, by promoting the removal of protein waste in injured neurons, may enhance the likelihood for neuronal survival. Further studies may reveal whether alteration of direct protein S-nitrosylation of target proteins in autophagy pathways improves the outcome in terms of neuronal survival and neuropathic pain. Thus the results suggest that NO, in addition to its known regulation of cGMP signaling, may contribute to the fine tuning of protein folding and degradation which are key mechanisms for allowing neurons to recover stability after axonal injury.

5. Summary

Neuropathic pain is a maladaptive form of chronic pain caused by a primary injury or lesions in the central or peripheral nervous systems. Recently nitric oxide (NO) has emerged as important pro-nociceptive signaling molecule in pain signaling and processing. Chemical inhibiton or deletion of Nitric oxide synthase (NOS), as well and inhibition of the NOS-coenzyme tetrahydrobiopterin is known to reduce or inhibit neuropathic pain. NO exert its influence through two major pathways: by stimulation of sGC and by direct S-nitrosylation (SNO) of target proteins. This study assessed in the spinal cord the SNO-proteome with two methods, two-dimensional S-nitrosothiol difference gel electrophoresis (2D SNO-DIGE) and SNO-site identification (SNOSID) at baseline and 24 h after sciatic nerve injury with/without pretreatment with the nitric oxide synthase inhibitor L-NAME. At 24h after nerve injury, SNO-DIGE revealed 30 proteins with increased S-nitrosylation and 23 proteins with decreased S-nitrosylation. SNO-sites were identified for 17 out of these 53 proteins. L-NAME pretreatment substantially reduced both constitutive and nerve injury evoked up-S-nitrosylation. For the top candidates S-nitrosylation was confirmed with the biotin switch technique and time course analyses at 1 and 7 days after nerve injury showed that SNO modifications of protein disulfide isomerase (PDI), glutathione synthase (GSS) and peroxiredoxin-6 (Prdx6) had returned to baseline within 7 days whereas S-nitrosylation of mitochondrial aconitase 2 (Aco2) was further increased. The identified SNO modified proteins are primarily involved in mitochondrial function, protein folding and transport, synaptic signaling and redox control.

Several targets, including PDI, Heat shock cognate 71 kDa protein, and Serpin B6, indicated that NO might play a role in protein quality control, metabolism, and folding. Subsequently an investigation into the potential role of NO and SNO in proteasomal degradation and autophagy was performed. Autophagy is a basic catabolic mechanism involving the degradation of unnecessary or dysfunctional cellular components through the lysosomal machinery and is an important factor in the recovery of neurons after injury. A cellular model of neuronal nitric oxide synthase (nNOS) over-expressing neuroblastoma cell culture stimulated with rapamycin to induce autophagy was used. The effects of nNOS overexpression on autophagic processes were evaluated by western blotting with antibodies for known markers of autophagy. S-nitrosylation was evaluated using a combination of SNO-DIGE, SNOSID, SNO-SILAC, and SNO-ELISA methods. Increased (+ 144%, $p < 0.05$) LC3-I / LC3-II ratio in the nNOS over-expressing cells compared to the wild type after stimulation with rapamycin suggested that the autophagic activity may be impaired by the increase of NO and possibly by an increase of direct protein S-nitrosylation. In the nNOS over-expressing cells the total ubiquitination was increased (+100%, p <

0.01) while it was decreased (-30%, $p < 0.01$)) in the wild type cells after rapamycin stimulation. This indicates that the targeting or degradation processes may be impaired by the increase in S-nitrosylation of the E1, E2 or E3 ubiquitin ligases. The results suggest that S-nitrosylation may regulate protein folding, ubiquitination, and possibly de novo protein generation. In this study several proteins have emerged as major candidates for being targets of S-nitrosylation and consequentially may affect the autophagic processes, namely heat shock cognate 71 kDa protein and pyruvate kinase isozymes M1/M2, calreticulin, ubiquitin-conjugating enzyme E2 D1, and elongation factor 2.

The results suggest that NO, in addition to its known regulation of cGMP signaling, may contribute to the fine tuning of protein folding and degradation which are key mechanisms for allowing neurons to recover stability after axonal injury.

6. Zusammenfassung auf Deutch

Neuropathischer Schmerz ist eine Form von chronischem Schmerz, verursacht durch eine Verletzung oder Läsion im zentralen oder peripheren Nervensystem. Schneiden oder Quetschen sind häufige Ursachen von neuropathischen Schmerzen, z.B. nach Amputation einer Extremität oder einem Bandscheibenvorfall. Einige Krankheiten wie Multiple Sklerose, HIV/AIDS und Diabetes können Nervendegeneration verursachen und die Verarbeitung von Schmerzsignalen stören, was zu Schmerzen führt. Ebenso können neurotoxische Chemikalien und Medikamente, wie Beispielsweise die in der Chemotherapie bei Krebs eingesetzten (z.B. Cisplatin, Oxaliplatin, and Vincristine), Schmerzen durch Schädigung von Neuronen. Die Hauptmerkmale von neuropathischem Schmerz sind unangenehmen und anormalen Gefühle, wie erhöhte Antwort auf schmerzhafte Stimuli (Hyperalgesie) und schmerzhafte Antwort auf benigne Stimulation (Allodynie).

Es hat sich gezeigt, dass NO ein wichtiges pro-nozizeptives Signalmolekül ist, NO entfaltet seine Wirkungen teilweise , indem es durch Stimulation der löslichen Guanylylcyclase die Produktion von cGMP steigert. NO moduliert zudem Enzymfunktionen oder Protein-Interaktionen und –Transport durch direkte Protein S-Nitrosylierung (SNO) von entscheidenden Cysteinresten. SNO ist eine post-translationale kovalente Addition von Stickoxid zur Thiol-Gruppe des Cysteins. Die Funktion direkter S-Nitrosylierungen für die Entstehung chronischer Schmerzen ist weitestgehend unbekannt. In dieser Studie wurde daher untersucht.

Daher kann die NO vermittelte S-Nitrosylierung der Übertragung von Schmerzsignalen dienen, ähnlich wie die Regulation durch Phosphorylierung und De-Phosphorylierung und kann Einfluß auf die nozizeptive Antwort und Adaptation von lang anhaltenden Verletzungen, wie axonale Verletzungen haben.

Angesichts des erhöhten NO-Gehalt von Neuronen nach einer Verletzung und der Tatsache das der cGMP/PKG-Signalweg nicht komplett den Effekt von NO im Schmerz erklärt, lässt es vermuten das die pro-nozizeptiven Effekte von NO auch durch direkte S-Nitrosylierung von Proteinen vermittelt wird. Der Hauptmechanismus der S-Nitrosylierung in der Adaptation auf Schmerzsignale begründet sich sehr wahrscheinlich in Ionenkanälen, Rezeptoren, mitochondrialer Qualitätskontrolle, sowie bei Proteinen welche beim Protein-Recycling beteiligt sind. Daher ist es interessant das S-Nitrosoproteom des

neuropathischen Schmerzmodels zu untersuchen, um herauszufinden welche Proteine wichtige Ziele der SNO sind.

Diese Studie zeigt eine beachtliche Protein S-Nitrosylierung und De-Nitrosylierung im Rückenmark nach SNI in Mäusen auf der ipsilateralen Seite der Verletzung. Zusätzlich zeigen die Ergebnisse das der Einfluss der SNI auf Hyperalgesie durch Unterdrückung der Stickoxid-Produktion, durch den unspezifischen NOS-Inhibitor L-NAME beseitigt werden kann. Daraus lässt sich schließen, dass die NO-vermittelte post-translationalen Proteinmodifikationen zu neuronale und gliale Adaptationen, nach Schädigung der afferenten Neuronen, beitragen.

Die anfänglichen Untersuchungen auf die Ziele des Stickoxids mittels 2D SNO-DIGE Screening zeigen 31 Proteine mit erhöhter Nitrosylierung und 22 mit einer Abnahme in der SNO. Dies zeigt, dass es eine beachtliche konstitutive S-Nitrosylierung im Rückenmark gibt. Im Gegensatz dazu kommt es bei Schein-Operationen zur Modifikation von 15 Proteinen, von denen nur drei eine erhöhte S-Nitrosylierung aufweisen, was nahelegt, dass die meisten Änderungen nach SNI durch die axonale Verletzung ausgelöst werden.

Um die beobachtete S-Nitrosylierung von einigen beteiligten Proteinen zu bestätigen, wurde die Biotin-Switch-Technik (BST) angewandt. Diese zeigte, dass Aconitate hydratase, mitochondrial (Aco2), Glutathione synthetase (Gss), Peroxiredoxin-6 (Prdx6), Protein disulfide-isomerase A3 (PDI), Tubulin alpha-4A chain (Tuba), und Tubulin beta-5 chain (Tubb) nach Nervenläsion S-nitrosyliert werden. Zur besseren Quantifizierung wurde eine ELISA basierte Version des BST etabliert, der Biotin-Switch ELISA.

Um zu untersuchen ob S-Nitrosylierung nach SNI eine kurzlebige frühe Erscheinung ist oder einen langlebigen Anpassungsmechanismus darstellt, überprüften wir S-Nitrosylierungen von bekannten Zielgenen (GSS, PDI, GAPDH, TUBB, PRX-6, ACO2) ein und sieben Tage nach SNI unter Verwendung des zuvor beschriebenen ELISAs. Für PDI, GSS und PRX6 normalisierten sich die S-Nitrosylierungen, die nach einem Tag sichtbar waren, nach sieben Tagen wieder. Im Gegensatz dazu war bei ACO2 die S-Nitrosylierung nach einem Tag noch unverändert aber sieben Tage nach SNI signifikant erhöht, was vermuten lässt, dass ACO2 S-Nitrosylierung eine chronische Modifikation darstellt.

Die SNOSID-Methode liefert Informationen über das modifizierte Cystein sowie Änderungen in der Zahl oder Lokalisation der SNO-Stelle. SNOSID liefert jedoch keine quantitativen Daten. Die Hauptziele von SNOSID beinhalten die Akonitat-Hydratase (mitochondriales Protein), die Fruktose-Bisphosphat-Aldolase

C, das Pyruvatkinase-Isoenzym M1/M2, die Malatdehydrogenase (mitochondriales Protein), das NADH-Dehydroganse-(Ubiquinon)-Flavoprotein 1 (mitochondriales Protein) und Phosphoglyceratmutase 1.

Die Untersuchungen zeigen, dass S-Nitrosylierung und Denitrosylierung bei den adaptiven post-translationalen Änderungen im Rückenmark nach Nervenläsion mitwirken. Die beobachtete partielle L-NAME-vermittelte Reversibilität der SNO-Modifikationen und die Umkehr der Hyperalgesie legen nahe, dass die SNO-Modifikationen zur Entstehung von neuropathischem Schmerz beitragen könnten. NO könnte hierbei durch die direkte posttranslationale Modifikation verschiedene Anpassungsprozesse modulieren. Bei den Haupt-SNO Kandidaten handelte es sich um Protein der Mitochondrien, des Zytoskeletts, Chaperone und am Proteinabbau beteiligte Proteine sowie einige Enyzme. Die Ergebnissen deuten darauf hin, dass NO für die Qualitätskontrolle von Proteinen und Mitochondrien bedeutsam sein könnte.

Da die Ergebnisse der Untersuchungen neuropathischer Schmerzen vermuten ließen, dass S-Nitrosylierung Proteinfaltung positiv als auch negativ beeinflussen könnte, wurde anschließend der Effekt der S-Nitrosylierung auf Autophagie-Prozesse untersucht. Die Autophagie ist neben einer Proteasom-vermittelten Proteindegradation ein wesentlicher Proteinabbauweg. Hierzu wurde eine neuronale Stickstoffmonoxid-Synthase (nNOS) überexprimierende Neuroblastom Zelllinie, als auch wildtypische Zellen des gleichen Zelltyps, mit Rapamycin stimuliert, um den Vorgang der Autophagie zu induzieren. Die Auswirkungen der nNOS- Überexprimierung auf autophagische Vorgänge wurden unter Verwendung einer Kombination von SNO-DIGE, SNOSID, SNO-ELISA, und SNO-SILACMethoden eruiert. SNO-SILAC nutzt den Einbau einer zugeführten „schweren“ Form von Aminosäuren in Proteine mit stabilen isotopischen Nuklei (z.B. Deuterium, 13C, 15N). Nach dem Wachstum der Zielorganismen in „schwerem“ Nährmedium wird das „schwere“ Protein extrahiert. Durch das Vermischen mit extrahiertem Protein aus dem gleichen oder ähnlichen Organismus aus irgendeinem anderen expermimentellen Versuchsaufbau, wird ein interner Standard gewonnen. Nach massenspektrometrischer Analyse kann der Quotient aus schweren und leichten Proteinen je Probe berechnet und innerhalb der experimentellen Gruppen verglichen werden. Durch das Kennzeichnen der Cysteine mit Thiolreaktiven Markern kann der Quotient für unterschiedlich gekennzeichnete Cysteine reduziert und dadurch der Grad der Nitrosylierungen oder Redox-Modifikationen unterschiedlicher Proben verglichen werden.

Erste Analysen des Effektes von Rapamyzin mittels Markern für Autophagie ergaben, dass eine starke basale Zunahme (+144 %, $p < 0,05$) des LC3-I / LC3-II Quotienten in den nNOS überexprimierenden Zellen im Vergleich zur wildtypischen Kontrolle nach Stimulation mit Rapamycin besteht. Die Zunahme des LC3-I / LC3-II Quotienten weist auf eine Zunahme der autophagischen Aktivität oder auf eine Beeinträchtigung des lysosomalen Abbaus hin. Ein verminderter Anstieg des LC3-I / LC3-II Quotienten nach Stimulation mit Rapamycin in nNOS überexprimierenden Zellen (+233 % in WT, + 100 % in nNOS+) deutete an, dass die autophagische Aktivität aufgrund der NO-Überproduktionund vermutlich durch die Zunahme direkter Protein S-Nitrosylierung beeinträchtigt sein könnte.

Ein weiterer wichtiger Marker für die Degradierung von Proteinaggregaten ist die Ubiquitinylierung von Proteinen. Ubiquitin ist ein kleines Protein bestehend aus 76 Aminosäuren. Während der sogenannten Ubiquitinylierung wird es kovalent an Lysin-Reste der Proteine gebunden, um diese für die Degradierung zu kennzeichnen. In den nNOS überexprimierenden Zellen war die Summe der Ubiquitinylierungen erhöht (+100 %, $p < 0,01$), während sie in den wildtypischen Zellen nach Stimulation mit Rapamyzin reduziert war (-30 %, $p < 0,01$). Dies lässt vermuten, dass die Markierungs- bzw. Degradierungsvorgänge durch die vermehrte S-Nitrosylierung der Ubiquitin Ligasen verändert sein könnten.

Heat shock cognate 71 kDa proteinm (HSC70, *hspa8*) ist ein Chaperon, dass an wachsende Polypeptidketten bindet, um eine fehlerfreie Proteinfaltung zu gewährleisten. Es konnte eine erhöhte HSC70 Expression (+120 %, $p < 0,001$) in nNOS überexprimierenden Zellen nach Stimulation mit Rapamycin beobachtet werden, während in wildtypischen Zellen HSC70 nach Stimulation abnahm. Dies impliziert, dass die Fehlfaltung von Proteinen signifikant steigt und / oder die Markierung fehlgefalteter Proteine zur Degradierung gestört ist, was wiederum durch die vermehrte S-Nitrosylierung oder durch Redox-Stress von neu- synthetisierten Proteinen aufgrund von S-Nitrosylierungen ausgelöst wird.

Um Targets für S-Nitrosylierungen zu identifizieren, wurde die gleiche Herangehensweise wie bei der Untersuchung von S-Nitrosylierungen während neuropathischer Schmerzen verwendet: SNO-DIGE und SNOSID. Aufgrund der transienten Natur der Proteine während Vorgängen wie Autophagie, wurde eine SILAC-basierte Methode herangezogen, um die Protein S-Nitrosylierung und die Gesamtheit der Proteinexpression simultan zu analysieren.

Zur Untersuchung des Fortschreitens der S-Nitrosylierung nach Induktion von Autophagy wurde unter Verwendung der SNO-DIGE Methode eine Zeitreihe über die Veränderungen von S-Nitrosylierungen nach Stimulation von nNOS überexprimierenden Zellen mit Rapamycin erstellt. 22 unterschiedliche Proteine in

27 ‚spots' wurden gefunden, die zeitabhängige Veränderungen der Nitrosylierungen zeigten. Die bedeutendsten Modifikationen ereigneten sich zwischen 4 und 8 Stunden nach Stimulation mit Rapamycin.

Die SNO-SILACUntersuchung ergab nur wenige nitrosylierte Proteine, obgleich die Gesamtheit der Proteinexpressionsmuster von etwa 500 Proteinen identifiert werden konnte. Die Resultate implizieren, dass NO autophagische Vorgänge beeinflusst, wie durch die Autophagie-Marker aufgezeigt werden konnte. Allerdings wurden in dieser Studie nur wenige direkte Modifikationen von Autophagie-Proteinen durch S-Nitrosylierungen gefunden, was darauf hindeutet, dass NO eher indirekt in die Vorgänge der Autophagie eingreift. Die S-Nitrosylierung reguliert womöglich die Proteinfaltung, Ubiquitinierung und wahrscheinlich auch die *de novo* Proteinsynthese. In dieser Studie konnten einige Proteine als Hauptkandidaten für die S-Nitrosylierung identifiziert werden, die autophagische Vorgänge beeinflussen. Zu ihnen zählen HSC70, das Pyruvat-Kinase-Isoenzym M1/M2 (PKM2, Gen:*pkm2*), Calreticulin (Gen: *calr*), das Ubiquitin-konjugierende Enzym E2 D1 (UBE2D1, Gen: *ube2d1*) und der Elongationsfaktor 2 (EF2, Gen: *eef2*).

Die Untersuchungen zeigen eine direkteS-Nitrosylierung verschiedener Proteine im Rückenmark nach Schädigung des Ischiasnerven. Diese posttranslationale NO-vermittelte Modifikation könnte für die Anpassungen der Neuronen an die axonale Schädigung, insbesondere im Hinblick auf die Wiederherstellung neuronaler Stabilität und damit fürdie Entstehung neuropathischer Schmerzen von Bedeutung sein. . Weitere Studien könnten aufklären, ob spezifische SNO-Targetproteine hierbei eine herausragende Rolle spielen und therapeutisch beeinflussbar sind.

7. List of Abbreviations

2-D DIGE	Two-dimensional difference gel electrophoresis
ACO2	Aconitate hydratase 2 (mitochondrial)
ACTB	Actin, cytoplasmic 1
ACTR3	actin related protein 3
ALDOC	Fructose-bisphosphate aldolase C
ANOVA	Analyis of Variance
ASM	Ammonium sulfamate
ASR	astroglial serine racemase
ATP5H	ATP synthase subunit d, mitochondrial
BH4	tetrahydrobiopterin
BSE	Biotin switch ELISA
BST	Biotin-Switch-Technique
CALR	Calreticulin
CCT5	T-complex protein 1 subunit epsilon
CMV	Cytomegalo virus
CYS	cysteine
DIGE	Difference gel electrophoresis
DNM1	dynamin-1
EF2	Elongation factor 2
ER	Endoplasmic reticulum
ESI-MS/MS	electrospray ionization mass spectrometry
FBP	D-fructose 1,6-bisphosphate
FUBP1	Far upstream element-binding protein 1
GAPDH	Glyceraldehyde-3-phosphate dehydrogenase
GCH1	GTP cyclohydrolase 1
GPS-SNO	Group-based Prediction System
GSNO	S-nitrosoglutathione
GSS	Glutathione S-synthetase
GSTM1	Glutathione S-transferase Mu 1
HIF-1	Hypoxia-inducible factor 1
HSC70	Heat shock cognate 71 kDa protein
HSPA8	Heat shock cognate 71 kDa protein
IAM	iodoacetamide
IASP	International Association for the Study of Pain
ICAT	isotope-coded affinity tags
L-NAME	Nω-Nitro-L-arginine methyl ester hydrochloride
MDH2	Malate dehydrogenase, mitochondrial
METAP1	Methionine aminopeptidase 1
MS	mass spectrometry
mTORC1	mammalian target of rapamycin receptor 1
NEFM	Neurofilament medium polypeptide

NEM	N-ethyl-maleimide
NICE	National Institute for Health and Clinical Excellence
NMDA	N-Methyl-D-aspartic acid
nNOS	Neuronal nitric oxide synthase
NO	Nitric Oxide
NOS	Nitric oxide synthase
Nox5	NADPH oxidase 5
NSF	*N-ethylmaleimide-sensitive factor*
PBS	Phosphate buffered saline
PDI	Protein disulfide isomerase
PITPNA	Phosphatidylinositol transfer protein alpha isoform
PKG	Protein kinase G
PKM2	Pyruvate kinase isozymes M1/M2
PRDX1	Peroxiredoxin-1
PRDX6	Peroxiredoxin-6
PRKDC	DNA-dependent protein kinase catalytic subunit
PS	phosphatidylserine
SDS-PAGE	SDS-polyacrylamide gel electrophoresis
sGC	soluble guanylylcyclase
SHSY-4Y	Human Neuroblastoma cells
SILAC	stable isotope labeling by amino acids in cell culture
SNARE	soluble NSF attachment protein receptor
SNI,	spared nerve injury
SNO	S-Nitrosylation
SNO-ELISA	Biotin switch ELISA
SNOSID	SNO-Site Identification
TBS	Tris buffered saline
TUBB	Tubulin-beta
UBA1	Ubiquitin-like modifier-activating enzyme 1
UBE2D1	Ubiquitin-conjugating enzyme E2 D1
WDR1	WD repeat-containing protein 1
ZYX	Zyxin

8. Bibliography

Aguilera, M. O., W. Beron & M. I. Colombo (2012) The actin cytoskeleton participates in the early events of autophagosome formation upon starvation induced autophagy. *Autophagy,* 8**,** 1590-1603.

Aley, K. O., G. McCarter & J. D. Levine (1998) Nitric oxide signaling in pain and nociceptor sensitization in the rat. *J Neurosci,* 18**,** 7008-14.

Aracena-Parks, P., S. A. Goonasekera, C. P. Gilman, R. T. Dirksen, C. Hidalgo & S. L. Hamilton (2006) Identification of cysteines involved in S-nitrosylation, S-glutathionylation, and oxidation to disulfides in ryanodine receptor type 1. *Journal of Biological Chemistry,* 281**,** 40354-40368.

Asada, K., J. Kurokawa & T. Furukawa (2009) Redox- and Calmodulin-dependent S-Nitrosylation of the KCNQ1 Channel. *Journal of Biological Chemistry,* 284**,** 6014-6020.

Barsoum, M. J., H. Yuan, A. A. Gerencser, G. Liot, Y. Kushnareva, S. Graber, I. Kovacs, W. D. Lee, J. Waggoner, J. Cui, A. D. White, B. Bossy, J. C. Martinou, R. J. Youle, S. A. Lipton, M. H. Ellisman, G. A. Perkins & E. Bossy-Wetzel (2006) Nitric oxide-induced mitochondrial fission is regulated by dynamin-related GTPases in neurons. *Embo J,* 25**,** 3900-11.

Beers, M. H. & R. Berkow. 2012. The Merck Manual for Professionals [Internet]. In *Neurologic Disorders - Pain,* eds. B. MH, J. TV, B. M, K. JL & P. R. Whitehouse Station (NJ): Merck Research Laboratories.

Bellinger, A. M., S. Reiken, C. Carlson, M. Mongillo, X. P. Liu, L. Rothman, S. Matecki, A. Lacampagne & A. R. Marks (2009) Hypernitrosylated ryanodine receptor calcium release channels are leaky in dystrophic muscle. *Nature Medicine,* 15**,** 325-330.

Benhar, M., M. T. Forrester, D. T. Hess & J. S. Stamler (2008) Regulated protein denitrosylation by cytosolic and mitochondrial thioredoxins. *Science,* 320**,** 1050-4.

Benhar, M., M. T. Forrester & J. S. Stamler (2009) Protein denitrosylation: enzymatic mechanisms and cellular functions. *Nat Rev Mol Cell Biol,* 10**,** 721-32.

Benn, S. C., D. Perrelet, A. C. Kato, J. Scholz, I. Decosterd, R. J. Mannion, J. C. Bakowska & C. J. Woolf (2002) Hsp27 upregulation and phosphorylation is required for injured sensory and motor neuron survival. *Neuron,* 36**,** 45-56.

Bingol, B. & E. M. Schuman (2005) Synaptic protein degradation by the ubiquitin proteasome system. *Current Opinion in Neurobiology,* 15**,** 536-541.

Boettger, M. K., N. Uceyler, M. Zelenka, A. Schmitt, A. Reif, Y. Chen & C. Sommer (2007) Differences in inflammatory pain in nNOS-, iNOS- and eNOS-deficient mice. *Eur J Pain,* 11**,** 810-8.

Bouhassira, D., M. Lanteri-Minet, N. Attal, B. Laurent & C. Touboul (2008) Prevalence of chronic pain with neuropathic characteristics in the general population. *Pain,* 136**,** 380-387.

Bourquin, A.-F., M. Suveges, M. Pertin, N. Gilliard, S. Sardy, A. C. Davison, D. R. Spahn & I. Decosterd (2006) Assessment and analysis of mechanical allodynia-like behavior induced by spared nerve injury (SNI) in the mouse. *Pain,* 122**,** 14.e1-14.

Boyce-Rustay, J. M. & M. F. Jarvis (2009) Neuropathic Pain: Models and Mechanisms. *Current Pharmaceutical Design,* 15**,** 1711-1716.

Broillet, M. C. (2000) A single intracellular cysteine residue is responsible for the activation of the olfactory cyclic nucleotide-gated channel by NO. *Journal of Biological Chemistry,* 275**,** 15135-15141.

Bulteau, A. L., H. A. O'Neill, M. C. Kennedy, M. Ikeda-Saito, G. Isaya & L. I. Szweda (2004) Frataxin acts as an iron chaperone protein to modulate mitochondrial aconitase activity. *Science,* 305**,** 242-5.

Burgoyne, J. R., M. Madhani, F. Cuello, R. L. Charles, J. P. Brennan, E. Schroder, D. D. Browning & P. Eaton (2007) Cysteine redox sensor in PKGIa enables oxidant-induced activation. *Science,* 317**,** 1393-7.

Burnette, W. N. (1981) WESTERN BLOTTING - ELECTROPHORETIC TRANSFER OF PROTEINS FROM SODIUM DODECYL SULFATE-POLYACRYLAMIDE GELS TO UNMODIFIED NITROCELLULOSE AND RADIOGRAPHIC DETECTION WITH ANTIBODY AND RADIOIODINATED PROTEIN-A. *Analytical Biochemistry,* 112**,** 195-203.

Butterfield, D. A., A. Gnjec, H. F. Poon, A. Castegna, W. M. Pierce, J. B. Klein & R. N. Martins (2006) Redox proteomics identification of oxidatively modified brain proteins in inherited Alzheimer's disease: An initial assessment. *Journal of Alzheimers Disease,* 10**,** 391-397.

Cairo, G., R. Ronchi, S. Recalcati, A. Campanella & G. Minotti (2002) Nitric oxide and peroxynitrite activate the iron regulatory protein-1 of J774A.1 macrophages by direct disassembly of the Fe-S cluster of cytoplasmic aconitase. *Biochemistry,* 41**,** 7435-42.

Camerini, S., M. L. Polci, U. Restuccia, V. Usuelli, A. Malgaroli & A. Bachi (2007) A novel approach to identify proteins modified by nitric oxide: the HIS-TAG switch method. *Journal of Proteome Research,* 6**,** 3224-3231.

Charles, R. L., E. Schroder, G. May, P. Free, P. R. Gaffney, R. Wait, S. Begum, R. J. Heads & P. Eaton (2007) Protein sulfenation as a redox sensor: proteomics studies using a novel biotinylated dimedone analogue. *Mol Cell Proteomics,* 6**,** 1473-84.

Cheah, J. H., S. F. Kim, L. D. Hester, K. W. Clancy, S. E. Patterson, V. Papadopoulos & S. H. Snyder (2006) NMDA receptor-nitric oxide transmission mediates neuronal iron homeostasis via the GTPase Dexras1. *Neuron,* 51**,** 431-440.

Chiang, C. Y., J. Wang, Y. F. Xie, S. Zhang, J. W. Hu, J. O. Dostrovsky & B. J. Sessle (2007) Astroglial glutamate-glutamine shuttle is involved in central sensitization of nociceptive neurons in rat medullary dorsal horn. *Journal of Neuroscience,* 27**,** 9068-9076.

Choi, Y. B., L. Tenneti, D. A. Le, J. Ortiz, G. Bai, H. S. V. Chen & S. A. Lipton (2000) Molecular basis of NMDA receptor-coupled ion channel modulation by S-nitrosylation. *Nature Neuroscience,* 3**,** 15-21.

Chouchani, E. T., T. R. Hurd, S. M. Nadtochiy, P. S. Brookes, I. M. Fearnley, K. S. Lilley, R. A. J. Smith & M. P. Murphy (2010) Identification of S-nitrosated mitochondrial proteins by S-nitrosothiol difference in gel electrophoresis (SNO-DIGE): implications for the regulation of mitochondrial function by reversible S-nitrosation. *Biochemical Journal,* 430**,** 49-59.

Clapp, K. M., H.-M. Peng, G. J. Jenkins, M. J. Ford, Y. Morishima, M. Lau & Y. Osawa (2012) Ubiquitination of Neuronal Nitric-oxide Synthase in the Calmodulin-binding Site Triggers Proteasomal Degradation of the Protein. *Journal of Biological Chemistry,* 287**,** 42601-42610.

Clapp, K. M., H. M. Peng, Y. Morishima, M. Lau, V. J. Walker, W. B. Pratt & Y. Osawa (2010) C331A Mutant of Neuronal Nitric-oxide Synthase Is Labilized for Hsp70/CHIP (C Terminus of HSC70-interacting Protein)-dependent Ubiquitination. *Journal of Biological Chemistry,* 285**,** 33642-33651.

Collins, P. J., G. McMahon, P. O'Brien & B. O'Connor (2004) Purification, identification and characterisation of seprase from bovine serum. *Int J Biochem Cell Biol,* 36**,** 2320-33.

Cox, J. J., F. Reimann, A. K. Nicholas, G. Thornton, E. Roberts, K. Springell, G. Karbani, H. Jafri, J. Mannan, Y. Raashid, L. Al-Gazali, H. Hamamy, E. M. Valente, S. Gorman, R. Williams, D. P. McHale, J. N. Wood, F. M. Gribble & C. G. Woods (2006) An SCN9A channelopathy causes congenital inability to experience pain. *Nature.,* 444**,** 894-8.

Dall'Agnol, M., C. Bernstein, H. Bernstein, H. Garewal & C. M. Payne (2006) Identification of S-nitrosylated proteins after chronic exposure of colon epithelial cells to deoxycholate. *Proteomics,* 6**,** 1654-1662.

Decosterd, I. & C. J. Woolf (2000) Spared nerve injury: an animal model of persistent peripheral neuropathic pain. *Pain,* 87**,** 149-158.

Derakhshan, B., P. C. Wille & S. S. Gross (2007) Unbiased identification of cysteine S-nitrosylation sites on proteins. *Nature Protocols,* 2**,** 1685-1691.

DiAntonio, A. & L. Hicke (2004) Ubiquitin-dependent regulation of the synapse. *Annual Review of Neuroscience,* 27**,** 223-246.

Doulias, P. T., J. L. Greene, T. M. Greco, M. Tenopoulou, S. H. Seeholzer, R. L. Dunbrack & H. Ischiropoulos (2010) Structural profiling of endogenous S-nitrosocysteine residues reveals unique features that accommodate diverse mechanisms for protein S-nitrosylation. *Proceedings of the National Academy of Sciences of the United States of America,* 107**,** 16958-16963.

Evans, J. R. & K. Bielefeldt (2000) Regulation of sodium currents through oxidation and reduction of thiol residues. *Neuroscience,* 101**,** 229-236.

Farquhar-Smith, P. (2011) Chemotherapy-induced neuropathic pain. *Current opinion in supportive and palliative care,* 5**,** 1-7.

Ferrari, L. F., A. Chum, O. Bogen, D. B. Reichling & J. D. Levine (2011) Role of Drp1, a key mitochondrial fission protein, in neuropathic pain. *J Neurosci,* 31**,** 11404-10.

Fisher, A. B. (2011) Peroxiredoxin 6: A Bifunctional Enzyme with Glutathione Peroxidase and Phospholipase A(2) Activities. *Antioxidants & Redox Signaling,* 15**,** 831-844.

Goerg, B., N. Qvartskhava, P. Voss, T. Grune, D. Haeussinger & F. Schliess (2007) Reversible inhibition of mammalian glutamine synthetase by tyrosine nitration. *Febs Letters,* 581**,** 84-90.

Gonzalez, D. R., F. Beigi, A. V. Treuer & J. M. Hare (2007) Deficient ryanodine receptor S-nitrosylation increases sarcoplasmic reticulum calcium leak and arrhythmogenesis in cardiomyocytes. *Proceedings of the National Academy of Sciences of the United States of America,* 104**,** 20612-20617.

Gow, A. J. & J. S. Stamler (1998) Reactions between nitric oxide and haemoglobin under physiological conditions. *Nature,* 391**,** 169-173.

Gu, Z. Z., M. Kaul, B. X. Yan, S. J. Kridel, J. K. Cui, A. Strongin, J. W. Smith, R. C. Liddington & S. A. Lipton (2002) S-nitrosylation of matrix metalloproteinases: Signaling pathway to neuronal cell death. *Science,* 297**,** 1186-1190.

Guhring, H., M. Gorig, M. Ates, O. Coste, H. U. Zeilhofer, A. Pahl, K. Rehse & K. Brune (2000) Suppressed injury-induced rise in spinal prostaglandin E2 production and reduced early thermal hyperalgesia in iNOS-deficient mice. *J Neurosci,* 20**,** 6714-20.

Gump, J. M. & A. Thorburn (2011) Autophagy and apoptosis: what is the connection? *Trends in Cell Biology,* 21**,** 387-392.

Gygi, S. P., B. Rist, S. A. Gerber, F. Turecek, M. H. Gelb & R. Aebersold (1999) Quantitative analysis of complex protein mixtures using isotope-coded affinity tags. *Nature Biotechnology,* 17**,** 994-999.

Hao, G., B. Derakhshan, L. Shi, F. Campagne & S. S. Gross (2006) SNOSID, a proteomic method for identification of cysteine S-nitrosylation sites in complex protein mixtures. *Proceedings of the National Academy of Sciences of the United States of America,* 103**,** 1012-1017.

Hao, G. & S. S. Gross (2006) Electrospray tandem mass spectrometry analysis of S- and N-nitrosopeptides: Facile loss of NO and radical-induced fragmentation. *Journal of the American Society for Mass Spectrometry,* 17**,** 1725-1730.

Hara, M. R., N. Agrawal, S. F. Kim, M. B. Cascio, M. Fujimuro, Y. Ozeki, M. Takahashi, J. H. Cheah, S. K. Tankou, L. D. Hester, C. D. Ferris, S. D. Hayward, S. H. Snyder & A. Sawa (2005) S-nitrosylated GAPDH initiates apoptotic cell death by nuclear translocation following Siah1 binding. *Nature Cell Biology,* 7**,** 665-U40.

Hizli, A. A., Y. Chi, J. Swanger, J. H. Carter, Y. Liao, M. Welcker, A. G. Ryazanov & B. E. Clurman (2013) Phosphorylation of Eukaryotic Elongation Factor 2 (eEF2) by Cyclin A-Cyclin-Dependent Kinase 2 Regulates Its Inhibition by eEF2 Kinase. *Molecular and cellular biology,* 33**,** 596-604.

Holaska, J. M., B. E. Black, D. C. Love, J. A. Hanover, J. Leszyk & B. M. Paschal (2001) Calreticulin is a receptor for nuclear export. *Journal of Cell Biology,* 152**,** 127-140.

Homma, K., K. Suzuki & H. Sugawara (2011) The Autophagy Database: an all-inclusive information resource on autophagy that provides nourishment for research. *Nucleic Acids Research,* 39**,** D986-D990.

Huang, Y., H. Y. Man, Y. Sekine-Aizawa, Y. F. Han, K. Juluri, H. B. Luo, J. Cheah, C. Lowenstein, R. L. Huganir & S. H. Snyder (2005) S-nitrosylation of N-ethylmaleimide sensitive factor mediates surface expression of AMPA receptors. *Neuron,* 46**,** 533-540.

Inoue, K., T. Akaike, Y. Miyamoto, T. Okamoto, T. Sawa, M. Otagiri, S. Suzuki, T. Yoshimura & H. Maeda (1999) Nitrosothiol formation catalyzed by ceruloplasmin - Implication for cytoprotective mechanism in vivo. *Journal of Biological Chemistry,* 274**,** 27069-27075.

Ishihama, Y., Y. Oda, T. Tabata, T. Sato, T. Nagasu, J. Rappsilber & M. Mann (2005) Exponentially modified protein abundance index (emPAI) for estimation of absolute protein amount in proteomics by the number of sequenced peptides per protein. *Molecular & Cellular Proteomics,* 4**,** 1265-1272.

Itoh, Y., F. H. Ma, H. Hoshi, M. Oka, K. Noda, Y. Ukai, H. Kojima, T. Nagano & N. Toda (2000) Determination and bioimaging method for nitric oxide in biological specimens by diaminofluorescein fluorometry. *Analytical Biochemistry,* 287**,** 203-209.

Jaffrey, S. R., H. Erdjument-Bromage, C. D. Ferris, P. Tempst & S. H. Snyder (2001) Protein S-nitrosylation: a physiological signal for neuronal nitric oxide. *Nature Cell Biology,* 3**,** 193-197.

Jaffrey, S. R., M. Fang & S. H. Snyder (2002) Nitrosopeptide mapping: A novel methodology reveals S-nitrosylation of Dexras1 on a single cysteine residue. *Chemistry & Biology,* 9**,** 1329-1335.

Jaggi, A. S., V. Jain & N. Singh (2011) Animal models of neuropathic pain. *Fundamental & Clinical Pharmacology,* 25**,** 1-28.

Ji, W. T., L. Wang, R. C. Lin, W. R. Huang & H. J. Liu (2009) Avian reovirus influences phosphorylation of several factors involved in host protein translation including eukaryotic translation elongation factor 2 (eEF2) in Vero cells. *Biochemical and Biophysical Research Communications,* 384**,** 301-305.

Jian, K. H., M. Chen, X. Cao, X. H. Zhu, M. L. Fung & T. M. Gao (2007) Nitric oxide modulation of voltage-gated calcium current by S-nitrosylation and cGMP pathway in cultured rat hippocampal neurons. *Biochemical and Biophysical Research Communications,* 359**,** 481-485.

Jin, X. G., S. R. Chen, X. H. Cao, L. Li & H. L. Pan (2011) Nitric oxide inhibits nociceptive transmission by differentially regulating glutamate and glycine release to spinal dorsal horn neurons. *J Biol Chem,* 286**,** 33190-202.

Kelleher, Z. T., A. Matsumoto, J. S. Stamler & H. E. Marshall (2007) NOS2 regulation of NF-kappa B by S-nitrosylation of p65. *Journal of Biological Chemistry,* 282**,** 30667-30672.

Kettenhofen, N. J., X. Wang, M. T. Gladwin & N. Hogg. 2008. In[hyphen (true graphic)]Gel Detection of S[hyphen (true graphic)]Nitrosated Proteins Using Fluorescence Methods. In *Methods in Enzymology,* ed. P. Enrique Cadenas and Lester, 53-71. Academic Press.

Kim, W. K., Y. B. Choi, P. V. Rayudu, P. Das, W. Asaad, D. R. Arnelle, J. S. Stamler & S. A. Lipton (1999) Attenuation of NMDA receptor activity and neurotoxicity by nitroxyl anion, NO. *Neuron,* 24**,** 461-469.

Klionsky, D. J., H. Abeliovich, P. Agostinis, D. K. Agrawal, G. Aliev, D. S. Askew, M. Baba, E. H. Baehrecke, B. A. Bahr, A. Ballabio, B. A. Bamber, D. C. Bassham, E. Bergamini, X. N. Bi, M. Biard-Piechaczyk, J. S. Blum, D. E. Breclesen, J. L. Brodsky, J. H. Brumell, U. T. Brunk, W. Bursch, N. Camougrand, E. Cebollero, F. Cecconi, Y. Y. Chen, L. S. Chin, A. Choi, C. T. Chu, J. K. Chung, P. G. H. Clarke, R. S. B. Clark, S. G. Clarke, C. Clave, J. L. Cleveland, P. Codogno, M. I. Colombo, A. Coto-Montes, J. M. Cregg, A. M. Cuervo, J. Debnath, F. Demarchi, P. B. Dennis, P. A. Dennis, V. Deretic, R. J.

Devenish, F. Di Sano, J. F. Dice, M. DiFiglia, S. Dinesh-Kumar, C. W. Distelhorst, M. Djavaheri-Mergny, F. C. Dorsey, W. Droge, M. Dron, W. A. Dunn, M. Duszenko, N. T. Eissa, Z. Elazar, A. Esclatine, E. L. Eskelinen, L. Fesues, K. D. Finley, J. M. Fuentes, J. Fueyo, K. Fujisaki, B. Galliot, F. B. Gao, D. A. Gewirtz, S. B. Gibson, A. Gohla, A. L. Goldberg, R. Gonzalez, C. Gonzalez-Estevez, S. Gorski, R. A. Gottlieb, D. Haussinger, Y. W. He, K. Heidenreich, J. A. Hill, M. Hoyer-Hansen, X. Hu, W. P. Huang, A. Iwasaki, M. Jaattela, W. T. Jackson, X. Jiang, S. K. Jin, T. Johansen, J. U. Jung, M. Kadowaki, C. Kang, A. Kelekar, D. H. Kessel, J. Kiel, H. P. Kim, A. Kimchi, T. J. Kinsella, K. Kiselyov, K. Kitamoto, E. Knecht, et al. (2008) Guidelines for the use and interpretation of assays for monitoring autophagy in higher eukaryotes. *Autophagy,* 4**,** 151-175.

Kornberg, M. D., N. Sen, M. R. Hara, K. R. Juluri, J. V. K. Nguyen, A. M. Snowman, L. Law, L. D. Hester & S. H. Snyder (2010) GAPDH mediates nitrosylation of nuclear proteins. *Nature Cell Biology,* 12**,** 1094-U89.

Landmesser, U., S. Dikalov, S. R. Price, L. McCann, T. Fukai, S. M. Holland, W. E. Mitch & D. G. Harrison (2003) Oxidation of tetrahydrobiopterin leads to uncoupling of endothelial cell nitric oxide synthase in hypertension. *J Clin Invest,* 111**,** 1201-9.

Laughlin, T. M., K. F. Kitto & G. L. Wilcox (1999) Redox manipulation of NMDA receptors in vivo: alteration of acute pain transmission and dynorphin-induced allodynia. *Pain,* 80**,** 37-43.

Lee, S. J., J. R. Lee, Y. H. Kim, Y. S. Park, S. I. Park, H. S. Park & K. P. Kim (2007) Investigation of tyrosine nitration and nitrosylation of angiotensin II and bovine serum albumin with electrospray ionization mass spectrometry. *Rapid Communications in Mass Spectrometry,* 21**,** 2797-2804.

Lewis, S. E., R. J. Mannion, F. A. White, R. E. Coggeshall, S. Beggs, M. Costigan, J. L. Martin, W. H. Dillmann & C. J. Woolf (1999) A role for HSP27 in sensory neuron survival. *Journal of Neuroscience,* 19**,** 8945-8953.

Li, F., P. Sonveaux, Z. N. Rabbani, S. L. Liu, B. Yan, Q. Huang, Z. Vujaskovic, M. W. Dewhirst & C. Y. Li (2007) Regulation of HIF-1 alpha stability through S-nitrosylation. *Molecular Cell,* 26**,** 63-74.

Li, X. Q. & Z. Fan (2010) The Epidermal Growth Factor Receptor Antibody Cetuximab Induces Autophagy in Cancer Cells by Downregulating HIF-1 alpha and Bcl-2 and Activating the Beclin 1/hVps34 Complex. *Cancer Research,* 70**,** 5942-5952.

Lim, J. C., H. I. Choi, Y. S. Park, H. W. Nam, H. A. Woo, K. S. Kwon, Y. S. Kim, S. G. Rhee, K. Kim & H. Z. Chae (2008) Irreversible oxidation of the active-site cysteine of peroxiredoxin to cysteine sulfonic acid for enhanced molecular chaperone activity. *J Biol Chem,* 283**,** 28873-80.

Lindermayr, C., S. Sell & J. Durner (2009) Generation and detection of S-nitrosothiols. *Methods in molecular biology (Clifton, N.J.),* 476**,** 210-22.

Lipton, S. A., Y. B. Choi, Z. H. Pan, S. Z. Z. Lei, H. S. V. Chen, N. J. Sucher, J. Loscalzo, D. J. Singel & J. S. Stamler (1993) A REDOX-BASED MECHANISM FOR THE NEUROPROTECTIVE AND NEURODESTRUCTIVE EFFECTS OF NITRIC-OXIDE AND RELATED NITROSO-COMPOUNDS. *Nature,* 364**,** 626-632.

Liu, T., C. K. Daniels & S. S. Cao (2012) Comprehensive review on the HSC70 functions, interactions with related molecules and involvement in clinical diseases and therapeutic potential. *Pharmacology & Therapeutics,* 136**,** 354-374.

Lowry, O. H., N. J. Rosebrough, A. L. Farr & R. J. Randall (1951) PROTEIN MEASUREMENT WITH THE FOLIN PHENOL REAGENT. *Journal of Biological Chemistry,* 193**,** 265-275.

Lu, J. S., T. Katano, E. Okuda-Ashitaka, Y. Oishi, Y. Urade & S. Ito (2009) Involvement of S-nitrosylation of actin in inhibition of neurotransmitter release by nitric oxide. *Molecular Pain,* 5**,** 12.

Lu, J. S., T. Katano, D. Uta, H. Furue & S. Ito (2011) Rapid S-nitrosylation of actin by NO-generating donors and in inflammatory pain model mice. *Molecular Pain,* 7**,** 13.

Lv, L., D. Li, D. Zhao, R. T. Lin, Y. J. Chu, H. Zhang, Z. Y. Zha, Y. Liu, Z. Li, Y. P. Xu, G. Wang, Y. R. Huang, Y. Xiong, K. L. Guan & Q. Y. Lei (2011) Acetylation Targets the M2 Isoform of Pyruvate Kinase for Degradation through Chaperone-Mediated Autophagy and Promotes Tumor Growth. *Molecular Cell,* 42**,** 719-730.

Ma, Y. M., H. H. Lu, B. Tippin, M. F. Goodman, N. Shimazaki, O. Koiwai, C. L. Hsieh, K. Schwarz & M. R. Lieber (2004) A biochemically defined system for mammalian nonhomologous DNA end joining. *Molecular Cell,* 16**,** 701-713.

Maattanen, P., G. Kozlov, K. Gehring & D. Y. Thomas (2006) ERp57 and PDI: multifunctional protein disulfide isomerases with similar domain architectures but differing substrate-partner associations. *Biochem Cell Biol,* 84**,** 881-9.

Maihofner, C., C. Euchenhofer, I. Tegeder, K. F. Beck, J. Pfeilschifter & G. Geisslinger (2000) Regulation and immunhistochemical localization of nitric oxide synthases and soluble guanylyl cyclase in mouse spinal cord following nociceptive stimulation. *Neurosci Lett,* 290**,** 71-5.

Manas, A., J. L. Monroy, A. A. Ramos, C. Cano, V. Lopez-Gomez, X. Masramon, M. Perez & T. c. s. group (2011) Prevalence of neuropathic pain in radiotherapy oncology units. *International journal of radiation oncology, biology, physics,* 81**,** 511-20.

Manfredi, M., G. Bini, G. Cruccu, N. Accornero, A. Berardelli & L. Medolago (1981) CONGENITAL ABSENCE OF PAIN. *Archives of Neurology,* 38**,** 507-511.

Mannick, J. B., C. Schonhoff, N. Papeta, P. Ghafourifar, M. Szibor, K. Z. Fang & B. Gaston (2001) S-nitrosylation of mitochondrial caspases. *Journal of Cell Biology,* 154**,** 1111-1116.

Marion M, B. (1976) A rapid and sensitive method for the quantitation of microgram quantities of protein utilizing the principle of protein-dye binding. *Analytical Biochemistry,* 72**,** 248-254.

Martinez-Ruiz, A., L. Villanueva, C. G. de Orduna, D. Lopez-Ferrer, M. A. Higueras, C. Tarin, I. Rodriguez-Crespo, J. Vazquez & S. Lamas (2005) S-nitrosylation of Hsp90 promotes the inhibition of its ATPase and endothelial nitric oxide synthase regulatory activities. *Proceedings of the National Academy of Sciences of the United States of America,* 102**,** 8525-8530.

Matsushita, K., C. N. Morrell, B. Cambien, S. X. Yang, M. Yamakuchi, C. Bao, M. R. Hara, R. A. Quick, W. Cao, B. O'Rourke, J. M. Lowenstein, J. Pevsner, D. D. Wagner & C. J. Lowenstein (2003) Nitric oxide regulates exocytosis by S-nitrosylation of N-ethylmaleimide-sensitive factor. *Cell,* 115**,** 139-50.

Meller, S. T., S. J. Lewis, J. N. Bates, M. J. Brody & G. F. Gebhart (1990) Is there a role for an endothelium-derived relaxing factor in nociception? *Brain Res,* 531**,** 342-5.

Michalak, M., J. Groenendyk, E. Szabo, L. I. Gold & M. Opas (2009) Calreticulin, a multi-process calcium-buffering chaperone of the endoplasmic reticulum. *Biochemical Journal,* 417**,** 651-666.

Minami, T., M. Onaka, E. Okuda-Ashitaka, H. Mori, S. Ito & O. Hayaishi (1995) L-NAME, an inhibitor of nitric oxide synthase, blocks the established allodynia induced by intrathecal administration of prostaglandin E2. *Neurosci Lett,* 201**,** 239-42.

Mirza, U. A., B. T. Chait & H. M. Lander (1995) MONITORING REACTIONS OF NITRIC-OXIDE WITH PEPTIDES AND PROTEINS BY ELECTROSPRAY-IONIZATION MASS-SPECTROMETRY. *Journal of Biological Chemistry,* 270**,** 17185-17188.

Miyamoto, T., A. E. Dubin, M. J. Petrus & A. Patapoutian (2009) TRPV1 and TRPA1 mediate peripheral nitric oxide-induced nociception in mice. *PLoS ONE,* 4**,** e7596.

Mizushima, N. & T. Yoshimori (2007) How to interpret LC3 immunoblotting. *Autophagy,* 3**,** 542-545.

Mohr, S., J. S. Stamler & B. Brune (1996) Posttranslational modification of glyceraldehyde-3-phosphate dehydrogenase by S-nitrosylation and subsequent NADH attachment. *Journal of Biological Chemistry,* 271**,** 4209-4214.

Mustafa, A. K., M. Kumar, B. Selvakumar, G. P. H. Ho, J. T. Ehmsen, R. K. Barrow, L. M. Amzel & S. H. Snyder (2007) Nitric oxide S-nitrosylates serine racemase, mediating feedback inhibition of D-serine formation. *Proceedings of the National Academy of Sciences of the United States of America,* 104**,** 2950-2955.

Nauseef, W. M., S. J. McCormick & R. A. Clark (1995) CALRETICULIN FUNCTIONS AS A MOLECULAR CHAPERONE IN THE BIOSYNTHESIS OF MYELOPEROXIDASE. *Journal of Biological Chemistry,* 270**,** 4741-4747.

NICE. 2010. CG96 Neuropathic pain - pharmacological management: NICE guideline. In *www.nice.org.uk/cg96*, ed. N. I. f. H. a. C. Excellence. London: National Institute for Health and Clinical Excellence.

Nickel, F. T., F. Seifert, S. Lanz & C. Maihofner (2012) Mechanisms of neuropathic pain. *European Neuropsychopharmacology,* 22**,** 81-91.

Noh, Y. H., J. Y. Baek, W. Jeong, S. G. Rhee & T. S. Chang (2009) Sulfiredoxin Translocation into Mitochondria Plays a Crucial Role in Reducing Hyperoxidized Peroxiredoxin III. *J Biol Chem,* 284**,** 8470-7.

Nott, A., P. M. Watson, J. D. Robinson, L. Crepaldi & A. Riccio (2008) S-Nitrosylation of histone deacetylase 2 induces chromatin remodelling in neurons. *Nature,* 455**,** 411-5.

Nunez, L., M. Vaquero, R. Gomez, R. Caballero, P. Mateos-Caceres, C. Macaya, I. Iriepa, E. Galvez, A. Lopez-Farre, J. Tamargo & E. Delpon (2006) Nitric oxide blocks hKv1.5 channels by S-nitrosylation and by a cyclic GMP-dependent mechanism. *Cardiovascular Research,* 72**,** 80-89.

Ong, S. E., B. Blagoev, I. Kratchmarova, D. B. Kristensen, H. Steen, A. Pandey & M. Mann (2002) Stable isotope labeling by amino acids in cell culture, SILAC, as a simple and accurate approach to expression proteomics. *Molecular & Cellular Proteomics,* 1**,** 376-386.

Oustwani, C. S., N. D. Tsihlis, A. K. Vavra, Q. Jiang, J. Martinez & M. R. Kibbe (2011) Nitric Oxide Increases Lysine 48-Linked Ubiquitination Following Arterial Injury. *Journal of Surgical Research,* 170**,** E169-E177.

Ozawa, K., E. J. Whalen, C. D. Nelson, Y. Y. Mu, D. T. Hess, R. J. Lefkowitz & J. S. Stamler (2008) S-nitrosylation of beta-arrestin regulates beta-adrenergic receptor trafficking. *Molecular Cell,* 31**,** 395-405.

Palmer, Z. J., R. R. Duncan, J. R. Johnson, L. Y. Lian, L. V. Mello, D. Booth, J. W. Barclay, M. E. Graham, R. D. Burgoyne, I. A. Prior & A. Morgan (2008) S-nitrosylation of syntaxin 1 at Cys(145) is a regulatory switch controlling Munc18-1 binding. *Biochemical Journal,* 413**,** 479-491.

Qian, J., F. Chen, Y. Kovalenkov, D. Pandey, M. A. Moseley, M. W. Foster, S. M. Black, R. C. Venema, D. W. Stepp & D. J. R. Fulton (2012) Nitric oxide reduces NADPH oxidase 5 (Nox5) activity by reversible S-nitrosylation. *Free Radical Biology and Medicine,* 52**,** 1806-1819.

Reynaert, N. L., K. Ckless, S. H. Korn, N. Vos, A. S. Guala, E. F. M. Wouters, A. van der Vliet & Y. M. W. Janssen-Heininger (2004) Nitric oxide represses inhibitory kB kinase through S-nitrosylation. *Proceedings of the National Academy of Sciences of the United States of America,* 101**,** 8945-8950.

Rodriguez-Muela, N., F. Germain, G. Marino, P. S. Fitze & P. Boya (2012) Autophagy promotes survival of retinal ganglion cells after optic nerve axotomy in mice. *Cell Death and Differentiation,* 19**,** 162-169.

Romero, J. M. & O. A. Bizzozero (2009) Intracellular glutathione mediates the denitrosylation of protein nitrosothiols in the rat spinal cord. *J Neurosci Res,* 87**,** 701-9.

Rush, J., A. Moritz, K. A. Lee, A. Guo, V. L. Goss, E. J. Spek, H. Zhang, X. M. Zha, R. D. Polakiewicz & M. J. Comb (2005) Immunoaffinity profiling of tyrosine phosphorylation in cancer cells. *Nature Biotechnology,* 23**,** 94-101.

Salanova, M., G. Schiffl, J. Rittweger, D. Felsenberg & D. Blottner (2008) Ryanodine receptor type-1 (RyR1) expression and protein S-nitrosylation pattern in human soleus myofibres following bed rest and exercise countermeasure. *Histochemistry and Cell Biology,* 130**,** 105-118.

Sarkar, S., V. I. Korolchuk, M. Renna, S. Imarisio, A. Fleming, A. Williams, M. Garcia-Arencibia, C. Rose, S. Q. Luo, B. R. Underwood, G. Kroemer, C. J. O'Kane & D. C. Rubinsztein (2011) Complex Inhibitory Effects of Nitric Oxide on Autophagy. *Molecular Cell,* 43**,** 19-32.

Saurin, A. T., H. Neubert, J. P. Brennan & P. Eaton (2004) Widespread sulfenic acid formation in tissues in response to hydrogen peroxide. *Proc Natl Acad Sci U S A,* 101**,** 17982-7.

Saville, B. (1958) A SCHEME FOR THE COLORIMETRIC DETERMINATION OF MICROGRAM AMOUNTS OF THIOLS. *Analyst,* 83**,** 670-672.

Scheving, R., I. Wittig, H. Heide, B. Albuquerque, M. Steger, U. Brandt & I. Tegeder (2012) Protein S-nitrosylation and denitrosylation in the mouse spinal cord upon injury of the sciatic nerve. *Journal of Proteomics,* 75**,** 3987-4004.

Schmidt, H., H. Hofmann, U. Schindler, Z. S. Shutenko, D. D. Cunningham & M. Feelisch (1996) No center dot NO from NO synthase. *Proceedings of the National Academy of Sciences of the United States of America,* 93**,** 14492-14497.

Schmidtko, A., W. Gao, P. Konig, S. Heine, R. Motterlini, P. Ruth, J. Schlossmann, D. Koesling, E. Niederberger, I. Tegeder, A. Friebe & G. Geisslinger (2008) cGMP produced by NO-sensitive guanylyl cyclase essentially contributes to inflammatory and neuropathic pain by using targets different from cGMP-dependent protein kinase I. *J Neurosci,* 28**,** 8568-76.

Schmidtko, A., P. Ruth, G. Geisslinger & I. Tegeder (2003) Inhibition of cyclic guanosine 5'-monophosphate-dependent protein kinase I (PKG-I) in lumbar spinal cord reduces formalin-induced hyperalgesia and PKG upregulation. *Nitric Oxide,* 8**,** 89-94.

Schmidtko, A., I. Tegeder & G. Geisslinger (2009) No NO, no pain? The role of nitric oxide and cGMP in spinal pain processing. *Trends in Neurosciences,* 32**,** 339-346.

Scholz, J., D. C. Broom, D. H. Youn, C. D. Mills, T. Kohno, M. R. Suter, K. A. Moore, I. Decosterd, R. E. Coggeshall & C. J. Woolf (2005) Blocking caspase activity prevents transsynaptic neuronal apoptosis and the loss of inhibition in lamina II of the dorsal horn after peripheral nerve injury. *Journal of Neuroscience,* 25**,** 7317-7323.

Selvakumar, B., R. L. Huganir & S. H. Snyder (2009) S-nitrosylation of stargazin regulates surface expression of AMPA-glutamate neurotransmitter receptors. *Proceedings of the National Academy of Sciences of the United States of America,* 106**,** 16440-16445.

Sen, N., M. R. Hara, A. S. Ahmad, M. B. Cascio, A. Kamiya, J. T. Ehmsen, N. Aggrawal, L. Hester, S. Dore, S. H. Snyder & A. Sawa (2009) GOSPEL: A Neuroprotective Protein that Binds to GAPDH upon S-Nitrosylation. *Neuron,* 63**,** 81-91.

Shaid, S., C. H. Brandts, H. Serve & I. Dikic (2013) Ubiquitination and selective autophagy. *Cell Death and Differentiation,* 20**,** 21-30.

Sollner, T. H. & S. Sequeira (2003) S-nitrosylation of NSF controls membrane trafficking. *Cell,* 115**,** 127-129.

Sou, Y., I. Tanida, M. Komatsu, T. Ueno & E. Kominami (2006) Phosphatidylserine in addition to phosphatidylethanolamine is an in vitro target of the mammalian Atg8 modifiers, LC3, GABARAP, and GATE-16. *Journal of Biological Chemistry,* 281**,** 3017-3024.

Soubeyrand, S., L. Pope, B. Pakuts & R. J. G. Hache (2003) Threonines 2638/2647 in DNA-PK are essential for cellular resistance to ionizing radiation. *Cancer Research,* 63**,** 1198-1201.

Sun, J., L. J. Druhan & J. L. Zweier (2008) Dose dependent effects of reactive oxygen and nitrogen species on the function of neuronal nitric oxide synthase. *Arch Biochem Biophys,* 471**,** 126-33.

Sun, J. H., C. L. Xin, J. P. Eu, J. S. Stamler & G. Meissner (2001) Cysteine-3635 is responsible for skeletal muscle ryanodine receptor modulation by NO. *Proceedings of the National Academy of Sciences of the United States of America,* 98**,** 11158-11162.

Sutton, M. A. & E. M. Schuman (2006) Dendritic protein synthesis, synaptic plasticity, and memory. *Cell,* 127**,** 49-58.

Sweet, S. M., C. M. Bailey, D. L. Cunningham, J. K. Heath & H. J. Cooper (2009) Large scale localization of protein phosphorylation by use of electron capture dissociation mass spectrometry. *Mol Cell Proteomics,* 8**,** 904-12.

Takahashi, H., Y. Shin, S. J. Cho, W. M. Zago, T. Nakamura, Z. Z. Gu, Y. L. Ma, H. Furukawa, R. Liddington, D. X. Zhang, G. Tong, H. S. V. Chen & S. A. Lipton (2007) Hypoxia enhances S-nitrosylation-mediated NMDA receptor inhibition via a thiol oxygen sensor motif. *Neuron,* 53**,** 53-64.

Takasusuki, T., T. Fujiwara, S. Yamaguchi, T. Fukushima, K. Akagawa & Y. Hori (2007) Enhancement of synaptic transmission and nociceptive behaviour in HPC-1/syntaxin 1A knockout mice following peripheral nerve injury. *European Journal of Neuroscience,* 26**,** 2179-2187.

Tang, C.-H., W. Wei & L. Liu (2012) Regulation of DNA repair by S-nitrosylation. *Biochimica Et Biophysica Acta-General Subjects,* 1820**,** 730-735.

Tang, Z., J. A. Bauer, B. Morrison & D. J. Lindner (2006) Nitrosylcobalamin promotes cell death via S nitrosylation of Apo2L/TRAIL receptor DR4. *Molecular and Cellular Biology,* 26**,** 5588-5594.

Tanida, I., T. Ueno & E. Kominami (2008) LC3 and Autophagy. *Methods in molecular biology (Clifton, N.J.),* 445**,** 77-88.

Tarr, J. M., P. J. Young, R. Morse, D. J. Shaw, R. Haigh, P. G. Petrov, S. J. Johnson, P. G. Winyard & P. Eggleton (2010) A Mechanism of Release of Calreticulin from Cells During Apoptosis. *Journal of Molecular Biology,* 401**,** 799-812.

Tegeder, I., M. Costigan, R. S. Griffin, A. Abele, I. Belfer, H. Schmidt, C. Ehnert, J. Nejim, C. Marian, J. Scholz, T. Wu, A. Allchorne, L. Diatchenko, A. M. Binshtok, D. Goldman, J. Adolph, S. Sama, S. J. Atlas, W. A. Carlezon, A. Parsegian, J. Lotsch, R. B. Fillingim, W. Maixner, G. Geisslinger, M. B. Max & C. J. Woolf (2006) GTP cyclohydrolase and tetrahydrobiopterin regulate pain sensitivity and persistence. *Nat Med,* 12**,** 1269-1277.

Tegeder, I., R. Scheving, I. Wittig & G. Geisslinger (2011) SNO-ing at the Nociceptive Synapse? *Pharmacological Reviews,* 63**,** 366-389.

Tegeder, I., A. Schmidtko, E. Niederberger, P. Ruth & G. Geisslinger (2002) Dual effects of spinally delivered 8-bromo-cyclic guanosine monophosphate (8-bromo-cGMP) in formalin-induced nociception in rats. *Neuroscience Letters,* 332**,** 146-150.

Thom, S. R., V. M. Bhopale, D. J. Mancini & T. N. Milovanova (2008) Actin S-nitrosylation inhibits neutrophil beta2 integrin function. *J Biol Chem,* 283**,** 10822-34.

Tian, J., S. F. Kim, L. Hester & S. H. Snyder (2008) S-nitrosylation/activation of COX-2 mediates NMDA neurotoxicity. *Proc Natl Acad Sci U S A,* 105**,** 10537-40.

Torrance, N., B. H. Smith, M. I. Bennett & A. J. Lee (2006) The epidemiology of chronic pain of predominantly neuropathic origin. Results from a general population survey. *Journal of Pain,* 7**,** 281-289.

Torta, F., V. Usuelli, A. Malgaroli & A. Bachi (2008) Proteomic analysis of protein S-nitrosylation. *Proteomics,* 8**,** 4484-4494.

Tsang, A. H. K., Y. I. Lee, H. S. Ko, J. M. Savitt, O. Pletnikova, J. C. Troncoso, V. L. Dawson, T. M. Dawson & K. K. K. Chung (2009) S-nitrosylation of XIAP compromises neuronal survival in Parkinson's disease. *Proceedings of the National Academy of Sciences of the United States of America,* 106**,** 4900-4905.

Uehara, T., T. Nakamura, D. D. Yao, Z. Q. Shi, Z. Z. Gu, Y. L. Ma, E. Masliah, Y. Nomura & S. A. Lipton (2006) S-Nitrosylated protein-disulphide isomerase links protein misfolding to neurodegeneration. *Nature,* 441**,** 513-517.

Walker, A. K., M. A. Farg, C. R. Bye, C. A. McLean, M. K. Horne & J. D. Atkin (2010) Protein disulphide isomerase protects against protein aggregation and is S-nitrosylated in amyotrophic lateral sclerosis. *Brain,* 133**,** 105-116.

Westermann, B. (2009) Nitric oxide links mitochondrial fission to Alzheimer's disease. *Sci Signal,* 2**,** pe29.

Whalen, E. J., M. W. Foster, A. Matsumoto, K. Ozawa, J. D. Violin, L. G. Que, C. D. Nelson, M. Benhar, J. R. Keys, H. A. Rockman, W. J. Koch, Y. Daaka, R. J. Lefkowitz & J. S. Stamler (2007) Regulation of beta-adrenergic receptor signaling by S-nitrosylation of G-protein-coupled receptor kinase 2. *Cell,* 129**,** 511-522.

Windebank, A. J. & W. G. Grisold (2008) Chemotherapy-induced neuropathy. *Journal of the Peripheral Nervous System,* 13**,** 27-46.

Windheim, M., M. Peggle & P. Cohen (2008) Two different classes of E2 ubiquitin-conjugating enzymes are required for the mono-ubiquitination of proteins and elongation by polyubiquitin chains with a specific topology. *Biochemical Journal,* 409**,** 723-729.

Xue, Y., Z. X. Liu, X. J. Gao, C. J. Jin, L. P. Wen, X. B. Yao & J. A. Ren (2010) GPS-SNO: Computational Prediction of Protein S-Nitrosylation Sites with a Modified GPS Algorithm. *Plos One,* 5**,** 7.

Yavuzer, U., G. C. M. Smith, T. Bliss, D. Werner & S. P. Jackson (1998) DNA end-independent activation of DNA-PK mediated via association with the DNA-binding protein C1D. *Genes & Development,* 12**,** 2188-2199.

Yoshida, T., R. Inoue, T. Morii, N. Takahashi, S. Yamamoto, Y. Hara, M. Tominaga, S. Shimizu, Y. Sato & Y. Mori (2006) Nitric oxide activates TRP channels by cysteine S-nitrosylation. *Nature Chemical Biology,* 2**,** 596-607.

Yu, H. M., J. Xu, C. Li, C. Zhou, F. Zhang, D. Han & G. Y. Zhang (2008) Coupling between neuronal nitric oxide synthase and glutamate receptor 6-mediated c-Jun N-terminal kinase signaling pathway via S-nitrosylation contributes to ischemia neuronal death. *Neuroscience,* 155**,** 1120-1132.

Zhang, L., J. Yu, H. Pan, P. Hu, Y. Hao, W. Cai, H. Zhu, A. D. Yu, X. Xie, D. Ma & J. Yuan (2007) Small molecule regulators of autophagy identified by an image-based high-throughput screen. *Proceedings of the National Academy of Sciences of the United States of America,* 104**,** 19023-19028.

Zhang, X., V. Verge, Z. Wiesenfeld-Hallin, G. Ju, D. Bredt, S. H. Synder & T. Hokfelt (1993) Nitric oxide synthase-like immunoreactivity in lumbar dorsal root ganglia and spinal cord of rat and monkey and effect of peripheral axotomy. *J Comp Neurol,* 335**,** 563-75.

Zhu, H. N., S. Q. Pan, S. Gu, E. M. Bradbury & X. Chen (2002) Amino acid residue specific stable isotope labeling for quantitative proteomics. *Rapid Communications in Mass Spectrometry,* 16**,** 2115-2123.

Zhuang, W., B. Li, L. Long, L. Chen, Q. Huang & Z.-q. Liang (2011) Knockdown of the DNA-dependent protein kinase catalytic subunit radiosensitizes glioma-initiating cells by inducing autophagy. *Brain Research,* 1371**,** 7-15.

9. Appendixes

9.1 Appendix I - Acknowledgements

My thanks to Prof. Dr. Irmgard Tegeder for giving me the opportunity to work on this project and whose guidance and mentorship was instrumental in the success of this work.

Thanks to Prof. Dr. Jochen Klein for his co-supervision and participation as the primary supervisor.

Thanks to Prof. Dr. Dr. Geisslinger for providing me with the job and working place at the Institut für Klinische Pharmakologie as well as the excellent working conditions.

Many thanks to Annett Häussler, Thekla Myrczek, and Max Mattil for their excellent technical assistance and invaluable help.

I thank Dr. Ilka Wittig for her priceless advice and guidance on all things “proteomics” as well as excellent companionship. Thanks also to Dr. Heinrich Heide and Mirco Steger for their help with the mass spectrometry analysis of my samples.

My thanks to my working group AG Tegeder: Annett, Boris, Geetha, Hee-young, Katja, Maike, Philipp, and Thekla, thanks for all the fun we´ve had. And extra thanks to Dr. Hee-Young Lim for her help with all things molecular biology and cloning, Boris Albuquerque for his help with behavioral experiments and translations, and Maike Kanngießer for help with translations.

On a more personal note I would like extend special thanks to Kristin Helgadóttir for joining me on this wonderful adventure to Germany and all her ceaseless support and motivation. Also I would like to give special thanks to my parents whose support and encouragement for my education and welfare through the years has been priceless.

To all my friends and family in Iceland, sorry for being away for so long.

9.2 Appendix II – Publications resulting from this work

Publications

Scheving R, Wittig I, Heide H, Albuquerque B, Steger M, Brandt U, Tegeder I, Protein S-nitrosylation in autophagy. (*In preparation*)

Scheving R, Wittig I, Heide H, Albuquerque B, Steger M, Brandt U, Tegeder I, Protein S-nitrosylation and denitrosylation in the mouse spinal cord upon injury of the sciatic nerve. (Journal of Proteomics, May 2012)

Tegeder I; **Scheving R**, Wittig I, Geisslinger G. SNO-ing at the Nociceptive Synapse? Pharmacological Reviews, Jun 2011

Presentations

Scheving R, Wittig I, Heide H, Albuquerque B, Steger M, Brandt U, Tegeder I, Protein S-nitrosylation and denitrosylation in the mouse spinal cord upon injury of the sciatic nerve. Poster presentation at the European Proteomics Association Proteomics meeting Glasgow, Scotland, 9-12 July 2012.

Scheving R, Wittig I, Heide H, Steger M, Brandt U, Tegeder I, Protein S-nitrosylation and denitrosylation in the mouse spinal cord upon injury of the sciatic nerve. Poster presentation at the Deutsche Gesellschaft für experimentelle und klinische Pharmakologie (DGPT) 77th annual meeting, Frankfurt am Main, Germany, 31. March - 01. April 2011.

9.3 Appendix III – Curriculum Vitae

Personal information

	Reynir Scheving Letzter Hasenpfad 13 60598 Frankfurt am Main Germany Born in Reykjavik, Iceland

Education

Since September 2009	J.W. Goethe University Hospital • Institute of Clinical Pharmacology • PhD Student of Prof. Dr. Irmgard Tegeder
2002 to 2007	University of Iceland • Master of Science in Pharmacy • Master's thesis: Optimization of the physical properties of silicone as a drug delivery system.
1995 – 1999	Menntaskólinn við Hamrahlíð • High school degree in Natural Sciences.

Employment

2007 to 2009	Actavis, Iceland • Research Scientist in Analytical Development
1999 - 2002	Securitas, Iceland • Software and web-based solutions development

9.4 Appendix IV - Effects of L-NAME treatment

Spot	UniProt ID2	Gene Name	Name	SNI VS Control		L-NAME VS Control		MW [kDa]	calc. pI	Function	SNOSID Site
				TTEST	Ratio	TTEST	Ratio				
1	MATR3_MOUSE	*matr3*	Matrin-3	0.0115	-1.18	0.0138	-1.29	94.6	6.25	May play a role in transcription or may interact with other nuclear matrix proteins to form the internal fibrogranular network	
2	DYN1_MOUSE	*dnm1*	Dynamin-1	0.3365	1.09	0.8963	-1.01	97.7	7.74	Microtubule-associated force-producing protein involved in producing microtubule bundles and able to bind and hydrolyze GTP.	
3	DYN1_MOUSE	*dnm1*	Dynamin-1	0.3249	-1.15	0.0498	-1.62	97.7	7.74	(see above)	
4	UBP5_MOUSE	*usp5*	Ubiquitin carboxyl-terminal hydrolase 5	0.6382	1.05	0.3796	-1.10	95.8	5.01	Involved in unanchored 'Lys-48'-linked polyubiquitin disassembly.	
5	K6PP_MOUSE	*pfkp*	6-phosphofructokinase type C	0.1585	-1.05	0.0220	-1.12	85.4	7.11	Catalytic activity: ATP + D-fructose 6-phosphate = ADP + D-fructose 1,6-bisphosphate.	
6	GAS6_MOUSE	*gas6*	Growth arrest-specific protein 6	0.6728	-1.03	0.0072	-1.23	74.6	5.52	Ligand for tyrosine-protein kinase receptors AXL, TYRO3 and MER whose signaling is implicated in cell growth and survival, cell adhesion and cell migration	
7	DYN1_MOUSE	*dnm1*	Dynamin-1	0.1581	1.07	0.0004	-1.32	97.7	7.74		
8	ACON_MOUSE	*aco2*	Aconitate hydratase, mitochondrial	0.0520	1.15	0.1471	-1.12	85.4	7.93	Catalyzes the isomerization of citrate to isocitrate via cis-aconitat	126, 448, 451
9	NSF_MOUSE	*nsf*	Vesicle-fusing ATPase	0.0482	-1.14	0.0597	1.10	82.6	6.95	Required for vesicle-mediated transport.	11, 21, 599
10	NSF_MOUSE	*nsf*	Vesicle-fusing ATPase	0.0995	-1.16	0.8249	1.02	82.6	6.95		11, 21, 599
11	NDUS1_MOUSE	*ndufs1*	NADH-ubiquinone oxidoreductase 75 kDa subunit, mitochondrial	0.0158	-1.10	0.0001	-1.50	79.7	5.72	Core subunit of the mitochondrial membrane respiratory chain NADH dehydrogenase (Complex I).	
12	NDUS1_MOUSE	*ndufs1*	NADH-ubiquinone oxidoreductase 75 kDa subunit, mitochondrial	0.0118	-1.12	0.0660	-1.10	79.7	5.72	(see above)	
13	NDUS1_MOUSE	*ndufs1*	NADH-ubiquinone oxidoreductase 75 kDa subunit, mitochondrial	0.1530	-1.15	0.0438	1.35	79.7	5.72	(see above)	
14	MCCA_MOUSE	*mccc1*	Methylcrotonoyl-CoA carboxylase subunit alpha, mitochondrial	0.7789	-1.02	0.0828	1.19	79.3	7.83	Catalytic activity: ATP + 3-methylcrotonoyl-CoA + HCO3- = ADP + phosphate + 3-methylglutaconyl-CoA.	
15	GRP78_MOUSE	*hspa5*	78 kDa glucose-regulated protein	0.0074	-1.22	0.0198	-1.17	72.4	5.16	Probably plays a role in facilitating the	

Spot	UniProt ID2	Gene Name	Name	SNI VS Control		L-NAME VS Control		MW [kDa]	calc. pI	Function	SNOSID Site
										assembly of multimeric protein complexes inside the ER.	
16	SYG_MOUSE	*gars*	Glycyl-tRNA synthetase	0.0286	1.49	0.0015	1.60	81.8	6.65	Catalyzes the attachment of glycine to tRNA(Gly).	
17	VATA_MOUSE	*atp6v1a*	V-type proton ATPase catalytic subunit A	0.4758	-1.02	0.0347	-1.14	68.3	5.58	V-ATPase vacuolar ATPase is responsible for acidifying a variety of intracellular compartments in eukaryotic cells.	
18	SPTB2_MOUSE	*spnb2*	Spectrin beta chain, brain 1	0.6780	1.04	0.0655	-1.22	274.1	5.58	Interacts with calmodulin in a calcium-dependent manner and is thus candidate for the calcium-dependent movement of the cytoskeleton at the membrane.	
19	HSP7C_MOUSE	*hspa8*	Heat shock cognate 71 kDa protein	0.1600	1.48	0.3320	-1.28	70.8	5.52	Chaperone.	
20	GPDM_MOUSE	*gpd2*	Glycerol-3-phosphate dehydrogenase, mitochondrial	0.0058	-1.24	0.0117	-1.77	80.9	6.61	Catalytic activity: sn-glycerol 3-phosphate + a quinone = glycerone phosphate + a quinol.	
21	GPDM_MOUSE	*gpd2*	Glycerol-3-phosphate dehydrogenase, mitochondrial	0.8122	1.01	0.0013	1.58	80.9	6.61	Catalytic activity: sn-glycerol 3-phosphate + a quinone = glycerone phosphate + a quinol.	
22	LMNB1_MOUSE	*lmnb1*	Lamin-B1	0.0549	-1.24	0.0017	-1.26	66.7	5.16	Lamins are components of the nuclear lamina, a fibrous layer on the nucleoplasmic side of the inner nuclear membrane	
23	TKT_MOUSE	*tkt*	Transketolase	0.5558	-1.03	0.1893	1.08	67.6	7.50	Sedoheptulose 7-phosphate + D-glyceraldehyde 3-phosphate = D-ribose 5-phosphate + D-xylulose 5-phosphate.	
24	STXB1_MOUSE	*stxbp1*	Syntaxin-binding protein 1	0.1303	-1.15	0.4313	1.08	67.5	6.96	May participate in the regulation of synaptic vesicle docking and fusion, possibly through interaction with GTP-binding proteins.	
25	NFL_MOUSE	*nefl*	Neurofilament light polypeptide		-1.10		2.03	61.5	4.64	Involved in the maintenance of neuronal caliber.	
26	TCPG_MOUSE	*cct3*	T-complex protein 1 subunit gamma	0.6839	1.02	0.0504	1.26	60.6	6.70	Molecular chaperone	
27	KPYM_MOUSE	*pkm2*	Pyruvate kinase isozymes M1/M2	0.0128	-1.12	0.0197	1.10	57.8	7.47	Glycolytic enzyme that catalyzes the transfer of a phosphoryl group from phosphoenolpyruvate (PEP) to ADP, generating ATP.	49, 152
28	KPYM_MOUSE	*pkm2*	Pyruvate kinase isozymes M1/M2	0.0032	1.24	0.0427	-1.16	57.8	7.47	(see above)	49, 152
29	KPYM_MOUSE	*pkm2*	Pyruvate kinase isozymes M1/M2	0.4317	-1.02	0.0762	1.08	57.8	7.47	(see above)	49, 152

Spot	UniProt ID2	Gene Name	Name	SNI VS Control		L-NAME VS Control		MW [kDa]	calc. pI	Function	SNOSID Site
30	SYDC_MOUSE	*dars*	Aspartyl-tRNA synthetase, cytoplasmic	0.0495	-1.06	0.0351	-1.27	57.1	6.49	Catalyzes the specific attachment of an amino acid to its cognate tRNA.	
31	AMPL_MOUSE	*lap3*	Cytosol aminopeptidase	0.6623	-1.03	0.0175	-1.32	56.1	7.72	Presumably involved in the processing and regular turnover of intracellular proteins.	
32	DHE3_MOUSE	*glud1*	Glutamate dehydrogenase 1, mitochondrial	0.0168	1.11	0.3585	-1.04	61.3	8.00	May be involved in learning and memory reactions by increasing the turnover of the excitatory neurotransmitter glutamate (By similarity).	327, 376
33	ATPA_MOUSE	*atp5a1*	ATP synthase subunit alpha, mitochondrial	0.1241	-1.13	0.0034	-1.29	59.7	9.19	Produces ATP from ADP in the presence of a proton gradient across the membrane which is generated by electron transport complexes of the respiratory chain.	
34	DHE3_MOUSE	*glud1*	Glutamate dehydrogenase 1, mitochondrial	0.1063	-1.12	0.0028	-1.30	61.3	8.00	May be involved in learning and memory reactions by increasing the turnover of the excitatory neurotransmitter glutamate	327, 376
35	DHE3_MOUSE	*glud1*	Glutamate dehydrogenase 1, mitochondrial	0.0016	-1.24	0.0034	-1.27	61.3	8.00		327, 376
36	SSDH_MOUSE	*aldh5a1*	Succinate-semialdehyde dehydrogenase, mitochondrial	0.0232	-1.34	0.0184	-1.13	55.9	8.25	Catalyzes one step in the degradation of the inhibitory neurotransmitter gamma-aminobutyric acid (GABA)	
37	AL9A1_MOUSE	*aldh9a1*	4-trimethylaminobutyraldehyde dehydrogenase	0.0332	-1.07	0.5331	-1.01	53.5	6.98	Converts gamma-trimethylaminobutyraldehyde into gamma-butyrobetaine	
38	SSDH_MOUSE	*aldh5a1*	Succinate-semialdehyde dehydrogenase, mitochondrial	0.0216	-1.11	0.4499	1.03	55.9	8.25	(see above)	
39	NDUV1_MOUSE	*ndufv1*	NADH dehydrogenase [ubiquinone] flavoprotein 1, mitochondrial	0.0010	-1.20	0.4293	-1.05	50.8	8.21	Core subunit of the mitochondrial membrane respiratory chain NADH dehydrogenase (Complex I).	187
40	ARP3_MOUSE	*actr3*	Actin-related protein 3	0.0235	1.75	0.9286	-1.01	47.3	5.88	Functions as ATP-binding component of the Arp2/3 complex	
41	DNJA1_MOUSE	*dnaja1*	DnaJ homolog subfamily A member 1	0.7302	1.02	0.0119	1.14	44.8	7.08	Co-chaperone of Hsc70.	
42	KCRU_MOUSE	*ckmt1*	Creatine kinase, ubiquitous mitochondrial	0.0804	-1.13	0.0284	-1.32	47.0	8.16	Reversibly catalyzes the transfer of phosphate between ATP and various phosphogens.	90, 317
43	KCRU_MOUSE	*ckmt1*	Creatine kinase, ubiquitous mitochondrial	0.0426	-1.11	0.9355	-1.00	47.0	8.16	(see above)	90, 317
44	KCRB_MOUSE	*ckb*	Creatine kinase B-type	0.9585	1.00	0.0080	1.13	42.7	5.67	Reversibly catalyzes the transfer of phosphate between ATP and various phosphogens.	254

Spot	UniProt ID2	Gene Name	Name	SNI VS Control		L-NAME VS Control		MW [kDa]	calc. pI	Function	SNOSID Site
45	ODPA_MOUSE	*pdha1*	Pyruvate dehydrogenase E1 component subunit alpha, somatic form, mitochondrial	0.0892	-1.12	0.2639	1.05	43.2	8.19	Catalyzes the overall conversion of pyruvate to acetyl-CoA and CO(2).	218, 222
46	KCRU_MOUSE	*ckmt1*	Creatine kinase, ubiquitous mitochondrial	0.1008	-1.14	0.0029	-1.23	47.0	8.16	(see above)	90, 317
47	MK03_MOUSE	*mapk3*	Mitogen-activated protein kinase 3	0.0242	1.09	0.6723	-1.01	43.0	6.61	Involved in both the initiation and regulation of meiosis, mitosis, and postmitotic functions in differentiated cells by phosphorylating transcription factors .	
48	MPI_MOUSE	*mpi*	Mannose-6-phosphate isomerase	0.3258	1.28	0.3299	-1.30	46.5	5.95	Involved in the synthesis of the GDP-mannose and dolichol-phosphate-mannose.	
49	ALDOA_MOUSE	*aldoa*	Fructose-bisphosphate aldolase A	0.4874	1.03	0.0136	-1.13	39.3	8.09	Plays a key role in glycolysis and gluconeogenesis.	
50	THIL_MOUSE	*acat1*	Acetyl-CoA acetyltransferase, mitochondrial	0.5437	-1.05	0.0077	-1.32	44.8	8.51	Plays a major role in ketone body metabolism	116
51	ALDOC_MOUSE	*aldoc*	Fructose-bisphosphate aldolase C	0.5658	1.02	0.0082	1.12	39.4	7.12	Catalytic activity: D-fructose 1,6-bisphosphate = glycerone phosphate + D-glyceraldehyde 3-phosphate.	178
52	ALDOA_MOUSE	*aldoa*	Fructose-bisphosphate aldolase A	0.0304	-1.10	0.1419	-1.07	39.3	8.09	Plays a key role in glycolysis and gluconeogenesis.	
53	SNAG_MOUSE	*napg*	Gamma-soluble NSF attachment protein	0.5787	-1.06	0.0607	-1.51	34.7	5.41	Required for vesicular transport between the ER and Golgi.	
54	CNN3_MOUSE	*cnn3*	Calponin-3	0.8599	1.01	0.0329	1.22	36.4	5.72	Implicated in the regulation and modulation of smooth muscle contraction.	
55	G3P_MOUSE	*gapdh*	Glyceraldehyde-3-phosphate dehydrogenase	0.3023	1.05	0.0036	-1.23	35.8	8.25	Plays a role in glycolysis and nuclear functions	150, 154, 245
56	G3P_MOUSE	*gapdh*	Glyceraldehyde-3-phosphate dehydrogenase	0.9600	1.01	0.0221	-1.39	35.8	8.25	(see above)	150, 154, 245
57	MDHM_MOUSE	*mdh2*	Malate dehydrogenase, mitochondrial	0.0120	1.19	0.9942	-1.00	35.6	8.68	Catalytic activity: (S)-malate + NAD+ = oxaloacetate + NADH.	89, 93, 212, 275, 285
58	FAHD2_MOUSE	*fahd2a*	Fumarylacetoacetate hydrolase domain-containing protein 2A	0.1068	1.19	0.0435	1.27	34.7	8.16	May have hydrolase activity	
59	CAH2_MOUSE	*car2*	Carbonic anhydrase 2	0.0826	1.26	0.0116	1.13	29.0	7.01	Essential for bone resorption and osteoclast differentiation. Reversible hydration of carbon dioxide.	
60	PGAM1_MOUSE	*pgam1*	Phosphoglycerate mutase 1	0.0195	-1.11	0.0108	-1.14	28.8	7.18	Interconversion of 3- and 2-phosphoglycerate with 2,3-bisphosphoglycerate as the primer of the	153

Spot	UniProt ID2	Gene Name	Name	SNI VS Control		L-NAME VS Control		MW [kDa]	calc. pI	Function	SNOSID Site
										reaction.	
61	PSA7_MOUSE	*psma7*	Proteasome subunit alpha type-7	0.0701	-1.30	0.8673	1.01	27.8	8.46	The proteasome is a multicatalytic proteinase complex which is characterized by its ability to cleave peptides with Arg, Phe, Tyr, Leu, and Glu adjacent to the leaving group at neutral or slightly basic pH.	
62	RAN_MOUSE	*ran*	GTP-binding nuclear protein Ran	0.6796	-1.02	0.0067	-1.26	24.4	7.49	Involved in nucleocytoplasmic transport. Required for the import of protein into the nucleus and also for RNA export. I	112, 120
63	KAD2_MOUSE	*ak2*	Adenylate kinase 2, mitochondrial	0.1876	-1.09	0.0032	-1.72	26.5	7.39	Catalyzes the reversible transfer of the terminal phosphate group between ATP and AMP.	
64	HSPB1_MOUSE	*hspb1*	Heat shock protein beta-1	0.0269	1.28	0.0130	1.15	23.0	6.55	Involved in stress resistance and actin organization.	
65	GSTA4_MOUSE	*gsta4*	Glutathione S-transferase A4	0.0052	1.28	0.0328	1.26	25.5	7.39	Conjugation of reduced glutathione to a wide number of exogenous and endogenous hydrophobic electrophiles.	
66	SODM_MOUSE	*sod2*	Superoxide dismutase [Mn], mitochondrial	0.0744	1.12	0.0161	1.18	24.6	8.62	Destroys radicals which are normally produced within the cells and which are toxic to biological systems.	
67	TAGL3_MOUSE	*tagln3*	Transgelin-3	0.3762	1.18	0.4628	-1.13	22.5	7.33		
68	SODC_MOUSE	*sod1*	Superoxide dismutase [Cu-Zn]	0.7658	-1.02	0.0029	1.59	15.9	6.51	(see above)	
69	CYC_MOUSE	*cycs*	Cytochrome c, somatic	0.2205	-1.09	0.0022	1.42	11.6	9.58	Electron carrier protein.	

S-nitrosylation in the dorsal horn of the L4/5 mouse spinal cord was assessed by 2D SNO-DIGE analysis and subsequent identification by electrospray ionization mass spectrometry (ESI-MS/MS). SNO Upregulation is shown in blue, SNO down regulation in red. Quadruple 2D gels of naïve and SNI operated mice and SNI operated with L-NAME treatment were analyzed and statistically compared by t-tests, P was set at 0.05. Identification of the modified cysteines was done with the SNO site identification method (SNOSID). Abbreviations: pI, isoelectric point

9.5 Appendix V - Effects of Sham operation

Spot no.	UniProt ID	Gene Name	Name	Ratio	T-test	Mass	*pI*	Seq Cov	Pept	Functional description	SNOSID Site	Functional classification
1	Q6P8X1	*snx6*	Sorting nexin-6	-1.39	0.010	46649	5.73	28.8%	13	Plays a role in retrograde protein transport from endosomes to the trans-Golgi network.		Vesicle trafficking
2	Q9CZ13	*uqcrc1*	Cytochrome b-c1 complex subunit 1, mitochondrial	-1.38	0.022	52852	5.77	39.2%	32	This is a component of the ubiquinol-cytochrome c reductase complex (complex III or cytochrome b-c1 complex), which is part of the mitochondrial respiratory chain.		Energy metabolism
3	P97807	*fh*	Fumarate hydratase, mitochondrial	-1.34	0.024	54357	9.46	23.9%	15	Catalytic activity: (S)-malate = fumarate + H2O.		Energy metabolism
4	Q9CZ13	*uqcrc1*	Cytochrome b-c1 complex subunit 1, mitochondrial	-1.37	0.024	52852	5.77	10.6%	2	This is a component of the ubiquinol-cytochrome c reductase complex (complex III or cytochrome b-c1 complex), which is part of the mitochondrial respiratory chain.		Energy metabolism
5	P15105	*glul*	Glutamate decarboxylase	-1.31	0.035	42120	6.67	20.6%	9	This enzyme has 2 functions: it catalyzes the production of glutamine and GABA.	99; 346; 359	Biosynthesis
6	P15105	*glul*	Glutamate decarboxylase	-1.19	0.096	42120	6.67	55.7%	20	This enzyme has 2 functions: it catalyzes the production of glutamine and GABA.	99; 346; 359	Biosynthesis
7	P05063	*aldoc*	Aldolase 3	-1.41	0.032	39395	6.73	38.7%	54	Catalytic activity: D-fructose 1,6-bisphosphate = glycerone phosphate + D-glyceraldehyde 3-phosphate.		Energy metabolism
8	P16858	*gapdh*	Glyceraldehyde-3-phosphate dehydrogenase	-1.44	0.036	35810	8.16	35.0%	12	Has both glyceraldehyde-3-phosphate dehydrogenase and nitrosylase activities,	245; 150; 154	Energy metabolism
9	Q9D6R2	*idh3a*	Isocitric dehydrogenase subunit alpha	-1.26	0.046	39639	6.29	47.3%	27	Catalytic activity: Isocitrate + NAD+ = 2-oxoglutarate + CO2 + NADH.		Energy metabolism
10	P14152	*mdh1*	Cytosolic malate dehydrogenase	-1.24	0.032	36511	6.16	44.4%	48	Catalytic activity: (S)-malate + NAD+ = oxaloacetate + NADH.	137; 154	Energy metabolism
11	Q99LC5	*etfa*	Electron transfer flavoprotein subunit alpha, mitochondrial	1.62	0.025	35009	8.28	7.5%	15	Transfers the electrons to the main mitochondrial respiratory chain via ETF-ubiquinone oxidoreductase (ETF dehydrogenase)		Energy metabolism
12	P14152	*mdh1*	Cytosolic malate dehydrogenase	-1.51	0.022	36511	6.16	19.2%	1	Catalytic activity: (S)-malate + NAD+ = oxaloacetate + NADH.	137; 154	Energy metabolism
13	P00920	*car2*	Carbonate dehydratase II	1.65	0.007	29033	6.57	46.1%	5	Essential for bone resorption and osteoclast differentiation (By similarity). Reversible hydration of carbon dioxide.		Unknown
14	Q9DBJ1	*pgam1*	Phosphoglycerate mutase 1	-1.28	0.048	28832	6.79	17.7%	13	Interconversion of 3- and 2-phosphoglycerate with 2,3-bisphosphoglycerate as the primer of the reaction. Can also catalyze the reaction of EC 5.4.2.4 (synthase) and EC 3.1.3.13 (phosphatase), but with a reduced activity.	153	Energy metabolism
15	P16015	*car3*	Carbonate dehydratase III	-1.60	0.029	29366	6.99	79.5%	8	Reversible hydration of carbon dioxide.		Unknown
16	Q9DBJ1	*pgam1*	Phosphoglycerate	-1.53	0.041	28832	6.79	42.3%	56	Interconversion of 3- and 2-phosphoglycerate with 2,3-	153	Energy

Spot no.	UniProt ID	Gene Name	Name	Ratio	T-test	Mass	*pI*	Seq Cov	Pept	Functional description	SNOSID Site	Functional classification
			mutase 1							bisphosphoglycerate as the primer of the reaction.		metabolism
17	Q8BVI4	*qdpr*	Dihydropteridine reductase	1.29	0.044	25570	7.63	76.3%	7	The product of this enzyme, tetrahydrobiopterin (BH-4), is an essential cofactor for phenylalanine, tyrosine, and tryptophan hydroxylases (By similarity).	158	Biosynthesis
18	Q9R0Y5	*ak1*	Adenylate kinase isoenzyme 1	-1.32	0.045	21540	5.42	22.6%	29	Catalyzes the reversible transfer of the terminal phosphate group between ATP and AMP.		Energy metabolism
19	Q64152	*btf3*	RNA polymerase B transcription factor 3	-1.30	0.027	22031	10.06	28.8%	4	General transcription factor. BTF3 can form a stable complex with RNA polymerase II. Required for the initiation of transcription (By similarity).		Transcription

S-nitrosylation in the dorsal horn of the L4/5 mouse spinal cord was assessed by 2D SNO-DIGE analysis and subsequent identification by electrospray ionization mass spectrometry (ESI-MS/MS). SNO Upregulation is shown in blue, SNO down regulation in red. Quadruple 2D gels of naïve and SNI-Sham operated mice were analyzed and statistically compared by t-tests, P was set at 0.05. Identification of the modified cysteines was done with the SNO site identification method (SNOSID). Abbreviations: pI, isoelectric point

9.6 Appendix VI - The complete list of SNOSID results

Protein ID	Gene Name	Protein Name	Cysteine #	SNI	SNI + L-NAME	Control
1433T_MOUSE	*ywhaq*	14-3-3 protein theta	94			X
1433Z_MOUSE	*ywhaz*	14-3-3 protein zeta/delta	94			X
A2M_MOUSE	*a2m*	Alpha-2-macroglobulin	594			X
AATM_MOUSE	*got2*	Aspartate aminotransferase, mitochondrial	106	X		X
AATM_MOUSE	*got2*	Aspartate aminotransferase, mitochondrial	187	X		X
ACON_MOUSE	*aco2*	Aconitate hydratase, mitochondrial	126	X		
ACON_MOUSE	*aco2*	Aconitate hydratase, mitochondrial	448			X
ACON_MOUSE	*aco2*	Aconitate hydratase, mitochondrial	451			X
ADT1_MOUSE	*slc25a4*	ADP/ATP translocase 1	129			X
AINX_MOUSE	*ina*	Alpha-internexin	54	X		
ALBU_MOUSE	*alb*	Serum albumin	269	X		X
ALBU_MOUSE	*alb*	Serum albumin	270	X		X
ALBU_MOUSE	*alb*	Serum albumin	274	X		X
ALBU_MOUSE	*alb*	Serum albumin	277	X		X
ALBU_MOUSE	*alb*	Serum albumin	384			X
ALBU_MOUSE	*alb*	Serum albumin	385			X
ALBU_MOUSE	*alb*	Serum albumin	393			X
ALBU_MOUSE	*alb*	Serum albumin	472			X
ALBU_MOUSE	*alb*	Serum albumin	500	X		X
ALBU_MOUSE	*alb*	Serum albumin	501	X		X
ALBU_MOUSE	*alb*	Serum albumin	511	X	X	X
ALBU_MOUSE	*alb*	Serum albumin	538	X		X
ALBU_MOUSE	*alb*	Serum albumin	591	X	X	X
ALDOA_MOUSE	*aldoa*	Fructose-bisphosphate aldolase A	73			X
ALDOC_MOUSE	*aldoc*	Fructose-bisphosphate aldolase C	178	X		X
ANXA2_MOUSE	*anxa2*	Annexin A2	133	X		
AT1A1_MOUSE	*atp1a1*	Sodium/potassium-transporting ATPase subunit alpha-1	249	X		
AT1A1_MOUSE	*atp1a1*	Sodium/potassium-transporting ATPase subunit alpha-1	374	X	X	X
AT1A2_MOUSE	*atp1a2*	Sodium/potassium-transporting ATPase subunit alpha-2	241	X	X	X
AT1A2_MOUSE	*atp1a2*	Sodium/potassium-transporting ATPase subunit alpha-2	247	X	X	X
AT1A2_MOUSE	*atp1a2*	Sodium/potassium-transporting ATPase subunit alpha-2	372	X	X	X
AT1A2_MOUSE	*atp1a2*	Sodium/potassium-transporting ATPase subunit alpha-2	553	X		X
AT1A2_MOUSE	*atp1a2*	Sodium/potassium-transporting ATPase subunit alpha-2	702	X		X
AT1A3_MOUSE	*atp1a3*	Sodium/potassium-transporting ATPase subunit alpha-3	239	X		X
AT1A3_MOUSE	*atp1a3*	Sodium/potassium-transporting ATPase subunit alpha-3	364	X	X	X
AT1A3_MOUSE	*atp1a3*	Sodium/potassium-transporting ATPase subunit alpha-3	49	X	X	X
AT1A3_MOUSE	*atp1a3*	Sodium/potassium-transporting ATPase subunit alpha-3	546	X		X
AT1A3_MOUSE	*atp1a3*	Sodium/potassium-transporting ATPase subunit alpha-3	695	X		X
AT1B1_MOUSE	*atp1b1*	Sodium/potassium-transporting ATPase subunit beta-1	214	X	X	X
AT1B2_MOUSE	*atp1b2*	Sodium/potassium-transporting ATPase subunit beta-2	10			X
AT1B2_MOUSE	*atp1b2*	Sodium/potassium-transporting ATPase subunit beta-2	261	X		
AT1B3_MOUSE	*atp1b3*	Sodium/potassium-transporting ATPase subunit beta-3	191			X
AT2B2_MOUSE	*atp2b2*	Plasma membrane calcium-transporting ATPase 2	526	X		
ATP5H_MOUSE	*atp5h*	ATP synthase subunit d, mitochondrial	101	X		X
ATPO_MOUSE	*atp5o*	ATP synthase subunit O, mitochondrial	141	X		X
BASI_MOUSE	*bsg*	Basigin	203	X		X
CADM2_MOUSE	*cadm2*	Cell adhesion molecule 2	248	X	X	X
CADM3_MOUSE	*cadm3*	Cell adhesion molecule 3	207			X
CADM4_MOUSE	*cadm4*	Cell adhesion molecule 4	145	X		X
CADM4_MOUSE	*cadm4*	Cell adhesion molecule 4	245			X
CATB_MOUSE	*ctsb*	Cathepsin B	93	X		X
CATD_MOUSE	*ctsd*	Cathepsin D	288			X

Protein ID	Gene Name	Protein Name	Cysteine #	SNI	SNI + L-NAME	Control
CD81_MOUSE	*cd81*	CD81 antigen	156	X	X	X
CD81_MOUSE	*cd81*	CD81 antigen	157	X	X	X
CD82_MOUSE	*cd82*	CD82 antigen	174			X
CD82_MOUSE	*cd82*	CD82 antigen	176			X
CH60_MOUSE	*hspd1*	60 kDa heat shock protein, mitochondrial	442	X	X	X
CLCB_MOUSE	*cltb*	Clathrin light chain B	199	X		
CLH_MOUSE	*cltc*	Clathrin heavy chain 1	151			X
CLH_MOUSE	*cltc*	Clathrin heavy chain 1	491	X		X
CLH_MOUSE	*cltc*	Clathrin heavy chain 1	926			X
CLH_MOUSE	*cltc*	Clathrin heavy chain 1	934			X
CN37_MOUSE	*cnp*	2',3'-cyclic-nucleotide 3'-phosphodiesterase	111	X		X
CN37_MOUSE	*cnp*	2',3'-cyclic-nucleotide 3'-phosphodiesterase	334	X		X
COF1_MOUSE	*cfl1*	Cofilin-1	139	X		X
CSRP1_MOUSE	*csrp1*	Cysteine and glycine-rich protein 1	167			X
CTL1_MOUSE	*slc44a1*	Choline transporter-like protein 1	68	X		X
CX6B1_MOUSE	*cox6b1*	Cytochrome c oxidase subunit 6B1	30	X		X
CX6B1_MOUSE	*cox6b1*	Cytochrome c oxidase subunit 6B1	54	X		X
CX6B1_MOUSE	*cox6b1*	Cytochrome c oxidase subunit 6B1	65	X	X	X
CY1_MOUSE	*cyc1*	Cytochrome c1, heme protein, mitochondrial	139	X		X
DHE3_MOUSE	*glud1*	Glutamate dehydrogenase 1, mitochondrial	376			X
DHPR_MOUSE	*qdpr*	Dihydropteridine reductase	158	X		X
DHSA_MOUSE	*sdha*	Succinate dehydrogenase [ubiquinone] flavoprotein	89			X
DLDH_MOUSE	*dld*	Dihydrolipoyl dehydrogenase, mitochondrial	484			X
DOPD_MOUSE	*ddt*	D-dopachrome decarboxylase	24			X
DPP6_MOUSE	*dpp6*	Dipeptidyl aminopeptidase-like protein 6	674			X
DPYL1_MOUSE	*crmp1*	Dihydropyrimidinase-related protein 1	248			X
DPYL2_MOUSE	*dpysl2*	Dihydropyrimidinase-related protein 2	248	X	X	X
DPYL2_MOUSE	*dpysl2*	Dihydropyrimidinase-related protein 2	504	X		X
DPYL3_MOUSE	*dpysl3*	Dihydropyrimidinase-related protein 3	248	X	X	X
DPYL3_MOUSE	*dpysl3*	Dihydropyrimidinase-related protein 3	471			X
EAA2_MOUSE	*slc1a2*	Excitatory amino acid transporter 2	561	X		X
EF2_MOUSE	*eef2*	Elongation factor 2	290			X
ENDD1_MOUSE	*endod1*	Endonuclease domain-containing 1 protein	34			X
ENOA_MOUSE	*eno1*	Alpha-enolase	357	X	X	X
ENOG_MOUSE	*eno2*	Gamma-enolase	357	X	X	X
FBX2_MOUSE	*fbxo2*	F-box only protein 2	75	X		X
G3P_MOUSE	*gapdh*	Glyceraldehyde-3-phosphate dehydrogenase	150	X	X	X
G3P_MOUSE	*gapdh*	Glyceraldehyde-3-phosphate dehydrogenase	154	X	X	X
G3P_MOUSE	*gapdh*	Glyceraldehyde-3-phosphate dehydrogenase	245	X		X
GABT_MOUSE	*abat*	4-aminobutyrate aminotransferase, mitochondrial	440	X		
GBB1_MOUSE	*gnb1*	Guanine nucleotide-binding protein G(I)/G(S)/G(T)	148	X		
GBB1_MOUSE	*gnb1*	Guanine nucleotide-binding protein G(I)/G(S)/G(T)	149	X		
GBB1_MOUSE	*gnb1*	Guanine nucleotide-binding protein G(I)/G(S)/G(T)	25	X		X
GBB1_MOUSE	*gnb1*	Guanine nucleotide-binding protein G(I)/G(S)/G(T)	294	X		X
GBB2_MOUSE	*gnb2*	Guanine nucleotide-binding protein G(I)/G(S)/G(T)	148			X
GBB2_MOUSE	*gnb2*	Guanine nucleotide-binding protein G(I)/G(S)/G(T)	149			X
GBB2_MOUSE	*gnb2*	Guanine nucleotide-binding protein G(I)/G(S)/G(T)	204	X		X
GBB2_MOUSE	*gnb2*	Guanine nucleotide-binding protein G(I)/G(S)/G(T)	25	X		
GDIA_MOUSE	*gdi1*	Rab GDP dissociation inhibitor alpha	202	X		X
GDIA_MOUSE	*gdi1*	Rab GDP dissociation inhibitor alpha	282	X		X
GDIA_MOUSE	*gdi1*	Rab GDP dissociation inhibitor alpha	317			X
GFAP_MOUSE	*gfap*	Glial fibrillary acidic protein	291	X	X	X
GLNA_MOUSE	*glul*	Glutamine synthetase	346	X		X
GLNA_MOUSE	*glul*	Glutamine synthetase	359	X	X	X

Protein ID	Gene Name	Protein Name	Cysteine #	SNI	SNI + L-NAME	Control
GLRX5_MOUSE	*glrx5*	Glutaredoxin-related protein 5, mitochondrial	63			X
GNAO_MOUSE	*gnao1*	Guanine nucleotide-binding protein G(o) subunit alpha	140	X		X
GPM6A_MOUSE	*gpm6a*	Neuronal membrane glycoprotein M6-a	192			X
GPM6B_MOUSE	*gpm6b*	Neuronal membrane glycoprotein M6-b	226			X
GSLG1_MOUSE	*glg1*	Golgi apparatus protein 1	503			X
GSLG1_MOUSE	*glg1*	Golgi apparatus protein 1	511			X
HBA_MOUSE	*hba*	Hemoglobin subunit alpha	105	X		X
HBB1_MOUSE	*hbb-b1*	Hemoglobin subunit beta-1	94	X	X	X
HEMO_MOUSE	*hpx*	Hemopexin	255	X		
HNRPL_MOUSE	*hnrnpl*	Heterogeneous nuclear ribonucleoprotein L	257			X
HNRPL_MOUSE	*hnrnpl*	Heterogeneous nuclear ribonucleoprotein L	258			X
HPLN2_MOUSE	*hapln2*	Hyaluronan and proteoglycan link protein 2	291	X		X
HPLN4_MOUSE	*hapln4*	Hyaluronan and proteoglycan link protein 4	210	X		
HPLN4_MOUSE	*hapln4*	Hyaluronan and proteoglycan link protein 4	264			X
HS74L_MOUSE	*hspa4l*	Heat shock 70 kDa protein 4L	376	X	X	X
HS74L_MOUSE	*hspa4l*	Heat shock 70 kDa protein 4L	380	X	X	X
KCRB_MOUSE	*ckb*	Creatine kinase B-type	254	X		X
KCRS_MOUSE	*ckmt2*	Creatine kinase S-type, mitochondrial	317			X
KCRU_MOUSE	*ckmt1*	Creatine kinase U-type, mitochondrial	317	X	X	
KCRU_MOUSE	*ckmt1*	Creatine kinase U-type, mitochondrial	90	X		
KPYM_MOUSE	*pkm2*	Pyruvate kinase isozymes M1/M2	152	X		
KPYM_MOUSE	*pkm2*	Pyruvate kinase isozymes M1/M2	49	X	X	X
LSAMP_MOUSE	*lsamp*	Limbic system-associated membrane protein	111			X
MDHC_MOUSE	*mdh1*	Malate dehydrogenase, cytoplasmic	137	X	X	X
MDHC_MOUSE	*mdh1*	Malate dehydrogenase, cytoplasmic	154	X		X
MDHM_MOUSE	*mdh2*	Malate dehydrogenase, mitochondrial	212	X	X	X
MDHM_MOUSE	*mdh2*	Malate dehydrogenase, mitochondrial	275	X		X
MDHM_MOUSE	*mdh2*	Malate dehydrogenase, mitochondrial	285	X	X	X
MDHM_MOUSE	*mdh2*	Malate dehydrogenase, mitochondrial	89	X		X
MDHM_MOUSE	*mdh2*	Malate dehydrogenase, mitochondrial	93	X		X
MIF_MOUSE	*mif*	Macrophage migration inhibitory factor	81	X		X
MOG_MOUSE	*mog*	Myelin-oligodendrocyte glycoprotein	126	X		X
MOG_MOUSE	*mog*	Myelin-oligodendrocyte glycoprotein	52	X	X	X
MT3_MOUSE	*mt3*	Metallothionein-3	34	X		X
MT3_MOUSE	*mt3*	Metallothionein-3	35	X		X
MT3_MOUSE	*mt3*	Metallothionein-3	37	X		X
MT3_MOUSE	*mt3*	Metallothionein-3	38	X		X
MT3_MOUSE	*mt3*	Metallothionein-3	42	X		X
MYPR_MOUSE	*plp1*	Myelin proteolipid protein	201	X	X	X
NCAM1_MOUSE	*ncam1*	Neural cell adhesion molecule 1	288	X		
NCAM1_MOUSE	*ncam1*	Neural cell adhesion molecule 1	41	X		X
NCDN_MOUSE	*ncdn*	Neurochondrin	415			X
NDUA8_MOUSE	*ndufa8*	NADH dehydrogenase [ubiquinone] 1 alpha subcomplex subunit 8	66	X	X	X
NDUAA_MOUSE	*ndufa10*	NADH dehydrogenase [ubiquinone] 1 alpha subcomplex subunit 10, mitochondrial	67	X		
NDUAB_MOUSE	*ndufa11*	NADH dehydrogenase [ubiquinone] 1 alpha subcomplex subunit 11	18			X
NDUAB_MOUSE	*ndufa11*	NADH dehydrogenase [ubiquinone] 1 alpha subcomplex subunit 11	95			X
NDUS5_MOUSE	*ndufs5*	NADH dehydrogenase [ubiquinone] iron-sulfur protein 5	43			X
NDUS5_MOUSE	*ndufs5*	NADH dehydrogenase [ubiquinone] iron-sulfur protein 5	66	X	X	X
NDUS8_MOUSE	*ndufs8*	NADH dehydrogenase [ubiquinone] iron-sulfur protein 8,	119	X		
NDUS8_MOUSE	*ndufs8*	NADH dehydrogenase [ubiquinone] iron-sulfur protein 8,	123	X		

Protein ID	Gene Name	Protein Name	Cysteine #	SNI	SNI + L-NAME	Control
NDUV1_MOUSE	*ndufv1*	NADH dehydrogenase [ubiquinone] flavoprotein 1,	142			X
NFASC_MOUSE	*nfasc*	Neurofascin	452		X	X
NFH_MOUSE	*nefh*	Neurofilament heavy polypeptide	225	X		X
NPTN_MOUSE	*nptn*	Neuroplastin	217	X		X
NSF_MOUSE	*nsf*	Vesicle-fusing ATPase	599			X
ODP2_MOUSE	*dlat*	Dihydrolipoyllysine-residue acetyltransferase component of pyruvate dehydrogenase complex, mitochondrial	290	X		X
ODPA_MOUSE	*pdha1*	Pyruvate dehydrogenase E1 component subunit alpha	218	X	X	X
ODPA_MOUSE	*pdha1*	Pyruvate dehydrogenase E1 component subunit alpha	222	X	X	X
PARK7_MOUSE	*park7*	Protein DJ-1	46			X
PGAM1_MOUSE	*pgam1*	Phosphoglycerate mutase 1	153	X		X
PGCB_MOUSE	*bcan*	Brevican core protein	178			X
PGCB_MOUSE	*bcan*	Brevican core protein	834	X		X
PGCB_MOUSE	*bcan*	Brevican core protein	847	X		X
PGK1_MOUSE	*pgk1*	Phosphoglycerate kinase 1	367	X		X
PGK1_MOUSE	*pgk1*	Phosphoglycerate kinase 1	379	X		X
PGK1_MOUSE	*pgk1*	Phosphoglycerate kinase 1	380	X		X
PPIA_MOUSE	*ppia*	Peptidyl-prolyl cis-trans isomerase A	161	X		X
PRDX1_MOUSE	*prdx1*	Peroxiredoxin-1	173	X		X
PRDX3_MOUSE	*prdx3*	Thioredoxin-dependent peroxide reductase, mitochondrial	230			X
PRDX5_MOUSE	*prdx5*	Peroxiredoxin-5, mitochondrial	200			X
PRDX5_MOUSE	*prdx5*	Peroxiredoxin-5, mitochondrial	96	X	X	X
PRDX6_MOUSE	*prdx6*	Peroxiredoxin-6	47	X		X
QCR2_MOUSE	*uqcrc2*	Cytochrome b-c1 complex subunit 2, mitochondrial	192	X		X
QCR6_MOUSE	*uqcrh*	Cytochrome b-c1 complex subunit 6, mitochondrial	65	X		X
RAB3A_MOUSE	*rab3a*	Ras-related protein Rab-3A	184	X		
RAC2_MOUSE	*rac2*	Ras-related C3 botulinum toxin substrate 2	157	X		X
RAN_MOUSE	*ran*	GTP-binding nuclear protein Ran	112	X		X
RAN_MOUSE	*ran*	GTP-binding nuclear protein Ran	120	X		X
RASK_MOUSE	*kras*	GTPase KRas	80			X
ROMO1_MOUSE	*romo1*	Reactive oxygen species modulator 1	15			X
RP3A_MOUSE	*rph3a*	Rabphilin-3A	641	X		X
SAHH3_MOUSE	*ahcyl2*	Putative adenosylhomocysteinase 3	400	X		X
SC6A5_MOUSE	*slc6a5*	Sodium- and chloride-dependent glycine transporter 2	333	X		X
SNAB_MOUSE	*napb*	Beta-soluble NSF attachment protein	66			X
SPRL1_MOUSE	*sparcl1*	SPARC-like protein 1	501			X
STIP1_MOUSE	*stip1*	Stress-induced-phosphoprotein 1	26			X
STXB1_MOUSE	*stxbp1*	Syntaxin-binding protein 1	180	X		X
SUCA_MOUSE	*suclg1*	Succinyl-CoA ligase [ADP/GDP-forming] subunit alpha,	172	X		X
SUCA_MOUSE	*suclg1*	Succinyl-CoA ligase [ADP/GDP-forming] subunit alpha,	181	X		X
SUCB1_MOUSE	*sucla2*	Succinyl-CoA ligase [ADP-forming] subunit beta,	152	X		
SUCB1_MOUSE	*sucla2*	Succinyl-CoA ligase [ADP-forming] subunit beta,	158	X		
SUCB1_MOUSE	*sucla2*	Succinyl-CoA ligase [ADP-forming] subunit beta,	430	X		
SUSD2_MOUSE	*susd2*	Sushi domain-containing protein 2	748			X
SUSD2_MOUSE	*susd2*	Sushi domain-containing protein 2	762			X
SYPH_MOUSE	*syp*	Synaptophysin	87	X	X	X
TBA1A_MOUSE	*tuba1a*	Tubulin alpha-1A chain	347	X		X
TBA1B_MOUSE	*tuba1b*	Tubulin alpha-1B chain	347	X	X	X
TBA1C_MOUSE	*tuba1c*	Tubulin alpha-1C chain	347	X	X	X
TBA4A_MOUSE	*tuba4a*	Tubulin alpha-4A chain	347	X	X	X
TBA4A_MOUSE	*tuba4a*	Tubulin alpha-4A chain	54	X		X
TBB2A_MOUSE	*tubb2a*	Tubulin beta-2A chain	12	X		X
TBB2A_MOUSE	*tubb2a*	Tubulin beta-2A chain	354	X		X
TBB2C_MOUSE	*tubb2c*	Tubulin beta-2C chain	12			X

Protein ID	Gene Name	Protein Name	Cysteine #	SNI	SNI + L-NAME	Control
TBB2C_MOUSE	*tubb2c*	Tubulin beta-2C chain	354			X
TBB3_MOUSE	*tubb3*	Tubulin beta-3 chain	12	X	X	X
TBB3_MOUSE	*tubb3*	Tubulin beta-3 chain	354	X		X
TBB4_MOUSE	*tubb4*	Tubulin beta-4 chain	12	X	X	X
TBB5_MOUSE	*tubb5*	Tubulin beta-5 chain	12	X	X	X
TBB5_MOUSE	*tubb5*	Tubulin beta-5 chain	354			X
TERA_MOUSE	*vcp*	Transitional endoplasmic reticulum ATPase	535	X		X
THIL_MOUSE	*acat1*	Acetyl-CoA acetyltransferase, mitochondrial	116	X		X
THY1_MOUSE	*thy1*	Thy-1 membrane glycoprotein	28	X		X
TPIS_MOUSE	*tpi1*	Triosephosphate isomerase	127	X		X
TPIS_MOUSE	*tpi1*	Triosephosphate isomerase	218	X		X
UCHL1_MOUSE	*uchl1*	Ubiquitin carboxyl-terminal hydrolase isozyme L1	152	X	X	X
UCHL1_MOUSE	*uchl1*	Ubiquitin carboxyl-terminal hydrolase isozyme L1	220	X		X
VATB2_MOUSE	*atp6v1b2*	V-type proton ATPase subunit B, brain isoform	289	X		X
VDAC1_MOUSE	*vdac1*	Voltage-dependent anion-selective channel protein 1	245	X		X
VDAC2_MOUSE	*vdac2*	Voltage-dependent anion-selective channel protein 2	77	X		X
VISL1_MOUSE	*vsnl1*	Visinin-like protein 1	187	X		X
VPP1_MOUSE	*atp6v0a1*	V-type proton ATPase 116 kDa subunit a isoform 1	254			X

9.7 Appendix VII - Full list of proteins identified with the SILAC method

Protein ID	Protein name	WT+R / WT	NOS / WT	NOS+R / NOS	NOS+R / WT	Ttest (WT:WT+R)	TTest (WT:NOS)	TTest (NOS:NOS+R)	TTest (NOS+R:WT)
CH10_HUMAN	10 kDa heat shock protein, mitochondrial	0,79	0,68	1,33	0,90	0,003	0,014	0,052	0,229
U5S1_HUMAN	116 kDa U5 small nuclear ribonucleoprotein component	0,96	0,97	1,33	1,29	0,403	0,434	0,036	0,104
1433E_HUMAN	14-3-3 protein epsilon	0,01	0,26	0,04	0,01	0,183	0,251	0,184	0,250
1433G_HUMAN	14-3-3 protein gamma	0,98	0,85	1,07	0,90	0,453	0,280	0,373	0,167
1433T_HUMAN	14-3-3 protein theta	0,77	0,86	1,17	1,01	0,224	0,305	0,265	0,492
1433Z_HUMAN	14-3-3 protein zeta/delta	1,16	0,90	0,81	0,73	0,373	0,357	0,116	0,141
PLCE_HUMAN	1-acyl-sn-glycerol-3-phosphate acyltransferase epsilon	1,07	0,96	1,00	0,96	0,155	0,399	0,499	0,450
PSMD1_HUMAN	26S proteasome non-ATPase regulatory subunit 1	0,74	1,92	0,64	1,22	0,143	0,297	0,312	0,353
PSD12_HUMAN	26S proteasome non-ATPase regulatory subunit 12	0,72	0,77	0,90	0,69	0,015	0,011	0,170	0,011
PSMD3_HUMAN	26S proteasome non-ATPase regulatory subunit 3	1,01	1,68	0,70	1,17			0,270	
PSMD6_HUMAN	26S proteasome non-ATPase regulatory subunit 6	0,81	0,73	1,06	0,77	0,073	0,031	0,305	0,040
RM12_HUMAN	39S ribosomal protein L12, mitochondrial	0,80	0,77	1,59	1,23	0,033	0,041	0,095	0,286
HCD2_HUMAN	3-hydroxyacyl-CoA dehydrogenase type-2	0,60	0,76	1,23	0,93	0,003	0,088	0,089	0,088
THIM_HUMAN	3-ketoacyl-CoA thiolase, mitochondrial	0,79	1,14	1,17	1,33			0,085	
RS10_HUMAN	40S ribosomal protein S10	0,63	0,91	0,65	0,59			0,004	
RS12_HUMAN	40S ribosomal protein S12								
RS13_HUMAN	40S ribosomal protein S13	1,03	0,91	1,33	1,22			0,142	
RS14_HUMAN	40S ribosomal protein S14	1,24	1,28	1,13	1,44	0,302	0,272	0,278	0,253
RS16_HUMAN	40S ribosomal protein S16	0,78	0,84	1,09	0,92	0,083	0,038	0,153	0,222
RS17L_HUMAN	40S ribosomal protein S17-like	0,83	0,90	0,69	0,63			0,103	
RS18_HUMAN	40S ribosomal protein S18			0,86				0,361	
RS19_HUMAN	40S ribosomal protein S19	0,39	0,47	0,83	0,38	0,159	0,192	0,286	0,208
RS20_HUMAN	40S ribosomal protein S20	0,97	0,84	1,22	1,02	0,429	0,167	0,092	0,449
RS23_HUMAN	40S ribosomal protein S23	0,83	0,72	1,56	1,12	0,226	0,088	0,135	0,427
RS24_HUMAN	40S ribosomal protein S24	1,52	1,38	1,37	1,90			0,040	
RS25_HUMAN	40S ribosomal protein S25	0,86	0,86	1,10	0,94	0,265	0,287	0,340	0,187
RS3_HUMAN	40S ribosomal protein S3	1,47	1,22	1,21	1,47	0,185	0,308	0,015	0,155
RS3A_HUMAN	40S ribosomal protein S3a	0,83	0,72	1,16	0,84	0,108	0,029	0,099	0,086
RS4X_HUMAN	40S ribosomal protein S4, X isoform	1,27	1,36	0,57	0,77			0,002	
RS6_HUMAN	40S ribosomal protein S6	0,84	0,73	1,19	0,87	0,183	0,056	0,106	0,120
RS8_HUMAN	40S ribosomal protein S8	0,89	0,92	0,97	0,89	0,233	0,334	0,402	0,132
RSSA_HUMAN	40S ribosomal protein SA	0,80	0,91	1,05	0,95	0,022	0,168	0,329	0,270
CH60_HUMAN	60 kDa heat shock protein, mitochondrial	0,99	0,98	0,98	0,96	0,450	0,450	0,437	0,253
RLA0_HUMAN	60S acidic ribosomal protein P0	1,09	0,89	1,05	0,94	0,334	0,263	0,393	0,289
RLA1_HUMAN	60S acidic ribosomal protein P1	1,18	0,73	1,26	0,93			0,273	
RLA2_HUMAN	60S acidic ribosomal protein P2	0,66	0,73	1,42	1,03	0,028	0,011	0,126	0,463
RL10_HUMAN	60S ribosomal protein L10	0,69	0,70	1,36	0,95	0,087	0,052	0,044	0,390
RL10A_HUMAN	60S ribosomal protein L10a	1,42	0,76	1,90	1,44	0,286	0,365	0,054	0,350
RL11_HUMAN	60S ribosomal protein L11	0,88	0,86	1,25	1,08	0,061	0,166	0,110	0,362
RL12_HUMAN	60S ribosomal protein L12	1,08	0,99	1,12	1,11	0,302	0,455	0,222	0,257
RL13_HUMAN	60S ribosomal protein L13	0,79	0,83	0,92	0,76	0,193	0,165	0,246	0,138

Protein ID	Protein name	WT+R / WT	NOS / WT	NOS+R / NOS	NOS+R / WT	Ttest (WT:WT+R)	TTest (WT:NOS)	TTest (NOS:NOS+R)	TTest (NOS+R:WT)
RL17_HUMAN	60S ribosomal protein L17	0,99	0,94	1,17	1,10	0,482	0,339	0,090	0,438
RL18_HUMAN	60S ribosomal protein L18	0,92	0,67	1,31	0,88	0,221	0,102	0,120	0,145
RL19_HUMAN	60S ribosomal protein L19	0,98	0,99	0,98	0,97	0,154	0,334	0,313	0,238
RL22_HUMAN	60S ribosomal protein L22	0,93	0,92	1,07	0,98	0,135	0,319	0,328	0,235
RL23_HUMAN	60S ribosomal protein L23	0,85	0,67	0,57	0,38		0,067		
RL23A_HUMAN	60S ribosomal protein L23a	0,97	0,95	1,01	0,96	0,402	0,413	0,484	0,268
RL26_HUMAN	60S ribosomal protein L26	0,86	0,61	1,63	0,99			0,200	
RL27A_HUMAN	60S ribosomal protein L27a	0,84	0,81	1,03	0,84	0,054	0,135	0,433	0,075
RL29_HUMAN	60S ribosomal protein L29	1,00	1,14	0,85	0,96		0,329	0,324	
RL30_HUMAN	60S ribosomal protein L30	1,49	0,81	46,78	37,92	0,152			0,189
RL37A_HUMAN	60S ribosomal protein L37a	1,02	0,97	1,16	1,12			0,187	
RL4_HUMAN	60S ribosomal protein L4	1,13	1,49	1,02	1,53	0,274	0,024	0,443	0,038
RL5_HUMAN	60S ribosomal protein L5	1,14	1,14	0,84	0,95	0,222	0,244	0,099	0,270
RL7_HUMAN	60S ribosomal protein L7	0,72	0,80	1,36	1,09	0,114	0,206	0,169	0,148
RL7A_HUMAN	60S ribosomal protein L7a	1,03	1,08	0,97	1,05	0,415	0,290	0,402	0,314
RL8_HUMAN	60S ribosomal protein L8	1,08	1,10	0,85	0,93	0,208	0,159	0,036	0,296
RL9_HUMAN	60S ribosomal protein L9	1,38	1,47	0,97	1,42	0,021	0,044	0,438	0,095
GRP78_HUMAN	78 kDa glucose-regulated protein	1,27	1,20	1,06	1,27	0,107	0,182	0,157	0,177
ACTB_HUMAN	Actin, cytoplasmic 1	1,43	1,32	1,00	1,33	0,176	0,239	0,486	0,238
TCP4_HUMAN	Activated RNA polymerase II transcriptional coactivator p15	0,97	1,10	0,72	0,79	0,311	0,210	0,012	0,007
ADNP_HUMAN	Activity-dependent neuroprotector homeobox protein	1,08	0,92	1,13	1,05		0,371		
SAHH_HUMAN	Adenosylhomocysteinase	1,00	0,90	0,79	0,71	0,494			0,161
KAD2_HUMAN	Adenylate kinase 2, mitochondrial	0,84	0,52	2,58	1,35	0,242	0,071	0,143	0,485
APMAP_HUMAN	Adipocyte plasma membrane-associated protein	0,85	0,74	1,52	1,13			0,046	
ADT2_HUMAN	ADP/ATP translocase 2	1,28	1,23	1,12	1,37	0,272	0,312	0,078	0,287
ADT3_HUMAN	ADP/ATP translocase 3	0,88	0,93	1,28	1,20	0,294	0,286	0,006	0,071
AKAP8_HUMAN	A-kinase anchor protein 8	0,85	0,89	1,33	1,19	0,224	0,269	0,034	0,103
ADAS_HUMAN	Alkyldihydroxyacetonephosphate synthase, peroxisomal	1,01	1,36	1,24	1,69	0,412	0,068	0,072	0,010
ACTN1_HUMAN	Alpha-actinin-1	1,07	1,33	0,86	1,14	0,353	0,022	0,144	0,186
ACTN4_HUMAN	Alpha-actinin-4	0,81	0,93	0,99	0,92	0,267	0,410	0,479	0,096
ENOA_HUMAN	Alpha-enolase	0,32	0,37	0,58	0,21	0,180	0,201	0,205	0,206
AINX_HUMAN	Alpha-internexin	1,09	1,19	1,18	1,40	0,268	0,007	0,184	0,116
AIMP1_HUMAN	Aminoacyl tRNA synthase complex-interacting multifunctional protein 1	0,94	0,83	0,49	0,41	0,396			0,074
SYRC_HUMAN	Arginine--tRNA ligase, cytoplasmic	0,85	0,77	0,62	0,47	0,374	0,290	0,078	0,155
SYDC_HUMAN	Aspartate--tRNA ligase, cytoplasmic	1,01	0,93	0,99	0,92	0,444			0,413
ATPA_HUMAN	ATP synthase subunit alpha, mitochondrial	0,94	0,87	1,12	0,98	0,129	0,098	0,181	0,339
AT5F1_HUMAN	ATP synthase subunit b, mitochondrial			1,24				0,157	
ATPB_HUMAN	ATP synthase subunit beta, mitochondrial	1,26	1,21	1,11	1,35	0,293	0,328	0,058	0,280
ATP5H_HUMAN	ATP synthase subunit d, mitochondrial	0,52	0,42	1,96	0,83	0,045	0,037	0,008	0,138
ATP5L_HUMAN	ATP synthase subunit g, mitochondrial	0,59	0,68	1,12	0,76			0,238	
ATPG_HUMAN	ATP synthase subunit gamma, mitochondrial	0,71	0,53	1,96	1,05		0,059		
ATPO_HUMAN	ATP synthase subunit O, mitochondrial	0,74	0,75	1,06	0,80	0,026	0,020	0,263	0,010
ABCD3_HUMAN	ATP-binding cassette sub-family D member 3	1,02	0,86	1,06	0,91			0,343	

Protein ID	Protein name	WT+R / WT	NOS / WT	NOS+R / NOS	NOS+R / WT	Ttest (WT:WT+R)	TTest (WT:NOS)	TTest (NOS:NOS+R)	TTest (NOS+R:WT)
ABCF1_HUMAN	ATP-binding cassette sub-family F member 1	1,46	1,13	0,47	0,53	0,114	0,320	0,041	0,066
DHX9_HUMAN	ATP-dependent RNA helicase A	0,81	0,91	1,27	1,15	0,211	0,134	0,104	0,346
ARI1A_HUMAN	AT-rich interactive domain-containing protein 1A	1,37	1,67	1,31	2,19	0,058	0,032	0,342	0,190
BCLF1_HUMAN	Bcl-2-associated transcription factor 1	0,92	1,02	1,68	1,72	0,264	0,439	0,006	0,014
SYEP_HUMAN	Bifunctional glutamate/proline--tRNA ligase	0,89	0,88	0,92	0,81	0,330	0,318	0,284	0,219
BASP1_HUMAN	Brain acid soluble protein 1	0,60	0,90	3,19	2,86	0,001	0,385	0,064	0,068
FACE1_HUMAN	CAAX prenyl protease 1 homolog	0,89	0,78	1,33	1,04	0,158	0,065	0,047	0,314
CMC2_HUMAN	Calcium-binding mitochondrial carrier protein Aralar2	0,78	0,75	1,24	0,93	0,163	0,155	0,223	0,332
CALD1_HUMAN	Caldesmon	2,43	2,38	0,81	1,93			0,163	
CALM_HUMAN	Calmodulin	0,70	1,12	2,00	2,25	0,024	0,310	0,144	0,182
CALX_HUMAN	Calnexin	0,92	0,85	1,00	0,86	0,066	0,030	0,498	0,042
CALR_HUMAN	Calreticulin	0,96	0,94	1,34	1,25	0,385	0,345	0,010	0,042
CALU_HUMAN	Calumenin	0,81	0,93	1,30	1,21	0,209	0,328	0,085	0,379
CAPR1_HUMAN	Caprin-1	1,11	0,92	0,85	0,78	0,297	0,089	0,020	0,003
CPT2_HUMAN	Carnitine O-palmitoyltransferase 2, mitochondrial			0,88				0,347	
CTNA1_HUMAN	Catenin alpha-1	0,74	0,85	1,15	0,97	0,027	0,202	0,132	0,385
CD166_HUMAN	CD166 antigen	1,34	1,57	1,41	2,21	0,251	0,153	0,011	0,031
CDC5L_HUMAN	Cell division cycle 5-like protein	0,91	1,04	1,10	1,15	0,308	0,114	0,244	0,304
ZW10_HUMAN	Centromere/kinetochore protein zw10 homolog	0,41	0,36	1,13	0,41			0,330	
CBX3_HUMAN	Chromobox protein homolog 3	0,73	0,75	1,38	1,03	0,037	0,053	0,029	0,396
CBX5_HUMAN	Chromobox protein homolog 5	0,83	1,23	0,94	1,15	0,389	0,360	0,370	0,370
CHD4_HUMAN	Chromodomain-helicase-DNA-binding protein 4	0,68	0,70	1,06	0,75	0,298	0,348	0,438	0,400
CHD7_HUMAN	Chromodomain-helicase-DNA-binding protein 7	1,02	0,91	1,31	1,19	0,405			
CMGA_HUMAN	Chromogranin-A	0,84	1,14	1,66	1,90	0,162	0,325	0,046	0,046
CISY_HUMAN	Citrate synthase, mitochondrial	1,01	0,91	1,14	1,04	0,453	0,160	0,161	0,484
CLH1_HUMAN	Clathrin heavy chain 1	1,11	0,77	1,13	0,87	0,290	0,272	0,365	0,188
CPSF7_HUMAN	Cleavage and polyadenylation specificity factor subunit 7	1,08			0,76	0,469			
COF1_HUMAN	Cofilin-1	0,98	0,96	0,80	0,77	0,440	0,351	0,035	0,056
CHCH3_HUMAN	Coiled-coil-helix-coiled-coil-helix domain-containing protein 3, mitochondrial	0,88	0,89	1,14	1,02	0,124	0,234	0,157	0,376
C1QBP_HUMAN	Complement component 1 Q subcomponent-binding protein, mitochondrial	0,93	0,90	1,22	1,09	0,239	0,037	0,020	0,164
CNTN1_HUMAN	Contactin-1	0,85	0,66	1,60	1,05			0,049	
H2AY_HUMAN	Core histone macro-H2A.1	0,75	0,86	1,39	1,20	0,152	0,017	0,005	0,057
H2AW_HUMAN	Core histone macro-H2A.2	0,74	0,79	1,57	1,23	0,054	0,076	0,029	0,153
CELF1_HUMAN	CUGBP Elav-like family member 1	0,94	0,93	1,59	1,47			0,007	
QCR2_HUMAN	Cytochrome b-c1 complex subunit 2, mitochondrial	1,04	1,14	1,04	1,19	0,408	0,197	0,340	0,211
UCRI_HUMAN	Cytochrome b-c1 complex subunit Rieske, mitochondrial	0,87	0,87	1,13	0,99	0,244	0,308	0,260	0,279
COX2_HUMAN	Cytochrome c oxidase subunit 2	0,89	1,02	1,00	1,03	0,286	0,456	0,492	0,273
COX41_HUMAN	Cytochrome c oxidase subunit 4 isoform 1, mitochondrial	0,71	0,95	1,03	0,97	0,172	0,162	0,345	0,494
COX5B_HUMAN	Cytochrome c oxidase subunit 5B, mitochondrial	0,62	0,82	1,25	1,02	0,071	0,062	0,011	0,430
DYHC1_HUMAN	Cytoplasmic dynein 1 heavy chain 1	0,51	0,41	1,21	0,49	0,210	0,229	0,101	0,264
DC1I2_HUMAN	Cytoplasmic dynein 1 intermediate chain 2	0,86	0,83	1,09	0,91		0,017	0,155	0,166
CKAP4_HUMAN	Cytoskeleton-associated protein 4	0,83	1,13	1,04	1,17	0,143	0,350	0,436	0,186
SERA_HUMAN	D-3-phosphoglycerate dehydrogenase	1,07	1,35	0,83	1,12	0,163	0,181	0,211	0,357

Protein ID	Protein name	WT+R / WT	NOS / WT	NOS+R / NOS	NOS+R / WT	Ttest (WT:WT+R)	TTest (WT:NOS)	TTest (NOS:NOS+R)	TTest (NOS+R:WT)
DCA13_HUMAN	DDB1- and CUL4-associated factor 13	1,08	1,32	1,26	1,66	0,250			0,084
DPYL3_HUMAN	Dihydropyrimidinase-related protein 3	0,83	4,08	0,46	1,86			0,287	
DDB1_HUMAN	DNA damage-binding protein 1	1,11	1,06	1,17	1,23	0,152	0,348	0,248	
TOP1_HUMAN	DNA topoisomerase 1	1,13	1,34	1,25	1,67	0,407	0,143	0,202	0,056
TOP2B_HUMAN	DNA topoisomerase 2-beta	0,05	0,04	1,82	0,08	0,184	0,183	0,149	0,189
APEX1_HUMAN	DNA-(apurinic or apyrimidinic site) lyase	2,68	0,88	0,54	0,48	0,262	0,422	0,146	0,408
PRKDC_HUMAN	DNA-dependent protein kinase catalytic subunit	0,98	1,01	0,90	0,92	0,461	0,471	0,073	0,468
RPB1_HUMAN	DNA-directed RNA polymerase II subunit RPB1	1,22	1,23	0,92	1,12		0,001	0,365	0,341
DJB11_HUMAN	DnaJ homolog subfamily B member 11	0,67	0,67	1,58	1,06	0,127	0,022	0,069	0,419
DPM1_HUMAN	Dolichol-phosphate mannosyltransferase	0,83	0,78	1,36	1,07	0,210	0,164	0,066	0,316
OST48_HUMAN	Dolichyl-diphosphooligosaccharide--protein glycosyltransferase 48 kDa subunit	0,76	0,69	1,31	0,91			0,019	
RPN1_HUMAN	Dolichyl-diphosphooligosaccharide--protein glycosyltransferase subunit 1	1,11	1,00	1,17	1,17	0,002	0,494	0,030	0,005
RPN2_HUMAN	Dolichyl-diphosphooligosaccharide--protein glycosyltransferase subunit 2	1,11	0,99	1,56	1,55	0,335	0,493	0,069	0,298
DOPO_HUMAN	Dopamine beta-hydroxylase	0,77	0,84	1,14	0,96	0,176	0,141	0,202	0,441
DSRAD_HUMAN	Double-stranded RNA-specific adenosine deaminase	2,11	1,73	1,03	1,78	0,080	0,165	0,464	0,043
DREB_HUMAN	Drebrin	0,83	1,09	1,20	1,31	0,101	0,380	0,165	0,016
DYL1_HUMAN	Dynein light chain 1, cytoplasmic	1,16	1,28	1,24	1,59		0,110	0,031	0,005
RBP2_HUMAN	E3 SUMO-protein ligase RanBP2	3,92	2,14	0,94	2,02			0,458	
UBR4_HUMAN	E3 ubiquitin-protein ligase UBR4	0,85	0,82	1,04	0,85	0,168	0,116	0,390	
ELAV1_HUMAN	ELAV-like protein 1	0,87	0,88	1,06	0,94	0,383	0,390	0,435	0,353
ELAV3_HUMAN	ELAV-like protein 3	1,70	1,88	0,63	1,18	0,074			
ELMD2_HUMAN	ELMO domain-containing protein 2	1,57	1,73			0,064			
EF1A1_HUMAN	Elongation factor 1-alpha 1	0,92	0,92	0,85	0,79	0,384	0,317	0,147	0,007
EF1B_HUMAN	Elongation factor 1-beta	0,76	0,90	1,20	1,07	0,064	0,309	0,117	0,292
EF1D_HUMAN	Elongation factor 1-delta	1,00	1,03	1,00	1,03	0,476	0,439	0,490	0,360
EF2_HUMAN	Elongation factor 2	1,37	1,38	0,42	0,57	0,239	0,177	0,007	0,153
EFTU_HUMAN	Elongation factor Tu, mitochondrial	0,83	0,65	1,19	0,77	0,182	0,112	0,250	0,081
ERP29_HUMAN	Endoplasmic reticulum resident protein 29	0,84	0,83	1,52	1,26	0,245	0,267	0,050	0,121
ENPL_HUMAN	Endoplasmin	1,38	1,44	1,02	1,47	0,230	0,202	0,359	0,206
ERH_HUMAN	Enhancer of rudimentary homolog	0,75	0,77	1,65	1,28			0,133	
ERLN1_HUMAN	Erlin-1	0,93	0,96	1,26	1,22	0,265	0,253	0,004	0,039
DHB12_HUMAN	Estradiol 17-beta-dehydrogenase 12	0,71	0,75	1,05	0,78	0,076	0,069	0,271	0,084
IF4A1_HUMAN	Eukaryotic initiation factor 4A-I	0,73	0,78	0,98	0,77		0,185	0,448	0,195
IF4A3_HUMAN	Eukaryotic initiation factor 4A-III	0,97	1,26	1,29	1,63	0,457	0,256	0,096	0,058
IF2G_HUMAN	Eukaryotic translation initiation factor 2 subunit 3	0,93	1,31	1,06	1,39		0,251	0,452	0,272
IF4E_HUMAN	Eukaryotic translation initiation factor 4E	1,30	1,03	0,51	0,52		0,464		
IF6_HUMAN	Eukaryotic translation initiation factor 6			0,97				0,473	
SP16H_HUMAN	FACT complex subunit SPT16	1,21	1,49	0,62	0,92	0,347	0,247	0,165	0,287
SSRP1_HUMAN	FACT complex subunit SSRP1	0,97	0,97	0,83	0,81	0,375	0,394	0,287	0,262
CAZA1_HUMAN	F-actin-capping protein subunit alpha-1	1,59	1,04	0,88	0,91	0,236	0,465	0,342	0,395
FUBP1_HUMAN	Far upstream element-binding protein 1	0,98	0,98	1,17	1,15	0,483	0,487	0,274	0,391
FUBP2_HUMAN	Far upstream element-binding protein 2	1,10	1,04	1,74	1,80	0,236	0,388	0,153	0,244
FUBP3_HUMAN	Far upstream element-binding protein 3	1,19	0,28	1,96	0,54	0,431			0,165

Protein ID	Protein name	WT+R / WT	NOS / WT	NOS+R / NOS	NOS+R / WT	Ttest (WT:WT+R)	TTest (WT:NOS)	TTest (NOS:NOS+R)	TTest (NOS+R:WT)
FLNA_HUMAN	Filamin-A	0,04	0,04	0,88	0,04	0,187	0,188	0,234	0,189
FLOT2_HUMAN	Flotillin-2	0,78				0,122			
FIZ1_HUMAN	Flt3-interacting zinc finger protein 1			1,29				0,092	
FXR1_HUMAN	Fragile X mental retardation syndrome-related protein 1	1,07	1,38	0,80	1,10	0,402	0,260	0,272	0,154
FXR2_HUMAN	Fragile X mental retardation syndrome-related protein 2	0,87	0,80	1,19	0,95	0,217	0,081	0,105	0,263
FUMH_HUMAN	Fumarate hydratase, mitochondrial			1,66				0,051	
LEG1_HUMAN	Galectin-1	0,94	0,97	1,17	1,13	0,338	0,431	0,202	0,403
GDAP1_HUMAN	Ganglioside-induced differentiation-associated protein 1	0,68	0,63	1,07	0,68			0,414	
TF3C3_HUMAN	General transcription factor 3C polypeptide 3	0,85	1,12	1,33	1,49			0,063	
GTF2I_HUMAN	General transcription factor II-I	0,74	1,02	0,89	0,91	0,240	0,445	0,218	0,453
G6PD_HUMAN	Glucose-6-phosphate 1-dehydrogenase	0,45	0,52	0,87	0,45	0,073	0,041	0,165	0,028
G6PI_HUMAN	Glucose-6-phosphate isomerase	0,85	0,54	0,39	0,21	0,370	0,109	0,096	0,030
GLU2B_HUMAN	Glucosidase 2 subunit beta	0,84	0,94	1,14	1,07	0,279	0,366	0,174	0,460
DHE3_HUMAN	Glutamate dehydrogenase 1, mitochondrial			0,81				0,149	
SYQ_HUMAN	Glutamine--tRNA ligase	1,75	1,74	0,82	1,42	0,076	0,124	0,260	0,124
G3P_HUMAN	Glyceraldehyde-3-phosphate dehydrogenase	1,06	1,00	0,97	0,97	0,427	0,488	0,396	0,493
GPAT4_HUMAN	Glycerol-3-phosphate acyltransferase 4	0,96	1,00	0,99	0,99			0,481	
NMT1_HUMAN	Glycylpeptide N-tetradecanoyltransferase 1	0,75	0,65	1,23	0,80	0,236	0,097	0,198	0,097
RAN_HUMAN	GTP-binding nuclear protein Ran	0,87	0,77	1,03	0,79	0,143	0,035	0,361	0,015
GBB1_HUMAN	Guanine nucleotide-binding protein G(I)/G(S)/G(T) subunit beta-1	1,46	2,33	0,29	0,67	0,200	0,089	0,049	0,248
GNAI3_HUMAN	Guanine nucleotide-binding protein G(k) subunit alpha	1,31	1,72	1,15	1,98	0,222	0,142	0,230	0,029
GNAS2_HUMAN	Guanine nucleotide-binding protein G(s) subunit alpha isoforms short	1,00	1,11			0,498			
GNAS1_HUMAN	Guanine nucleotide-binding protein G(s) subunit alpha isoforms XLas			0,99				0,482	
NHP2_HUMAN	H/ACA ribonucleoprotein complex subunit 2	1,97	1,57	0,05	0,08	0,255	0,390	0,215	
HSP71_HUMAN	Heat shock 70 kDa protein 1A/1B	1,10	1,03	1,01	1,04	0,384	0,468	0,466	0,452
HSP74_HUMAN	Heat shock 70 kDa protein 4	0,26	0,22	0,76	0,17	0,195	0,186	0,105	0,169
HSP7C_HUMAN	Heat shock cognate 71 kDa protein	0,94	0,90	0,99	0,89	0,123	0,056	0,432	0,040
HS105_HUMAN	Heat shock protein 105 kDa	0,35	0,30	1,14	0,34	0,232			0,241
HSPB1_HUMAN	Heat shock protein beta-1	1,07	0,82	1,06	0,88	0,384	0,154	0,388	0,219
HS90A_HUMAN	Heat shock protein HSP 90-alpha	0,90	0,91	0,88	0,80	0,267	0,225	0,069	0,076
HS90B_HUMAN	Heat shock protein HSP 90-beta	1,52	1,43	0,91	1,30	0,135	0,144	0,146	0,187
HDGR2_HUMAN	Hepatoma-derived growth factor-related protein 2	1,02	1,06	0,89	0,94	0,245	0,002	0,050	0,246
HP1B3_HUMAN	Heterochromatin protein 1-binding protein 3	1,14	1,26	0,78	0,98	0,212	0,059	0,088	
ROA1_HUMAN	Heterogeneous nuclear ribonucleoprotein A1	0,82	0,85	1,45	1,23	0,056	0,025	0,003	0,036
ROA3_HUMAN	Heterogeneous nuclear ribonucleoprotein A3	1,07	1,10	0,96	1,06	0,313	0,270	0,377	0,400
HNRPD_HUMAN	Heterogeneous nuclear ribonucleoprotein D0	0,96	1,03	0,97	1,00	0,330	0,356	0,357	0,385
HNRDL_HUMAN	Heterogeneous nuclear ribonucleoprotein D-like	0,77	0,86	1,18	1,01	0,032	0,011	0,003	0,361
HNRPF_HUMAN	Heterogeneous nuclear ribonucleoprotein F	0,61	0,68	1,14	0,78	0,007	0,087	0,225	0,038
HNRH1_HUMAN	Heterogeneous nuclear ribonucleoprotein H	0,84	0,93	1,08	1,01	0,199	0,370	0,397	0,367
HNRH3_HUMAN	Heterogeneous nuclear ribonucleoprotein H3	0,61	0,64	1,62	1,04	0,096	0,078	0,059	0,335
HNRPK_HUMAN	Heterogeneous nuclear ribonucleoprotein K	0,82	0,88	1,08	0,95	0,105	0,168	0,248	0,190
HNRPL_HUMAN	Heterogeneous nuclear ribonucleoprotein L	0,50	0,51	1,57	0,80	0,116	0,115	0,001	0,299
HNRPM_HUMAN	Heterogeneous nuclear ribonucleoprotein M	0,75	0,82	1,31	1,08	0,042	0,074	0,093	0,359

Protein ID	Protein name	WT+R / WT	NOS / WT	NOS+R / NOS	NOS+R / WT	Ttest (WT:WT+R)	TTest (WT:NOS)	TTest (NOS:NOS+R)	TTest (NOS+R:WT)
HNRPQ_HUMAN	Heterogeneous nuclear ribonucleoprotein Q	1,61	0,97	1,15	1,11	0,113	0,471	0,292	0,315
HNRPR_HUMAN	Heterogeneous nuclear ribonucleoprotein R	0,68	0,70	1,57	1,10	0,009	0,004	0,000	0,052
HNRPU_HUMAN	Heterogeneous nuclear ribonucleoprotein U	0,10	0,10	1,26	0,13	0,180	0,182	0,023	0,189
HNRL2_HUMAN	Heterogeneous nuclear ribonucleoprotein U-like protein 2	0,82	0,78	1,70	1,32	0,146	0,164	0,019	0,058
ROA2_HUMAN	Heterogeneous nuclear ribonucleoproteins A2/B1	1,35	1,39	1,11	1,55	0,259	0,239	0,230	0,230
HNRPC_HUMAN	Heterogeneous nuclear ribonucleoproteins C1/C2	0,74	0,76	1,49	1,13	0,009	0,020	0,014	0,188
HXK1_HUMAN	Hexokinase-1	1,25	1,20	1,17	1,40	0,288	0,362	0,096	0,220
HMGB1_HUMAN	High mobility group protein B1	0,64	0,67	1,16	0,78	0,016	0,075	0,238	0,049
HMGB2_HUMAN	High mobility group protein B2	0,63	0,99	1,43	1,42	0,160	0,489	0,235	0,215
HMGA1_HUMAN	High mobility group protein HMG-I/HMG-Y	1,00	1,00	1,59	1,59	0,495	0,497	0,052	0,268
SYHC_HUMAN	Histidine--tRNA ligase, cytoplasmic	0,94	0,63	1,26	0,80	0,467			
HDAC2_HUMAN	Histone deacetylase 2	0,98	1,13	1,31	1,48	0,460	0,222	0,088	0,162
H10_HUMAN	Histone H1.0	0,57	0,70	1,08	0,76			0,316	
H12_HUMAN	Histone H1.2	0,68	0,92	1,14	1,05			0,183	
H15_HUMAN	Histone H1.5	1,29	1,43	1,35	1,92	0,287	0,207	0,030	0,067
H1X_HUMAN	Histone H1x	0,75	0,95	1,09	1,04	0,004	0,323	0,229	0,363
H2A1H_HUMAN	Histone H2A type 1-H	1,13	1,22	1,37	1,67	0,392	0,326	0,013	0,103
H2B1K_HUMAN	Histone H2B type 1-K	0,95	1,05	1,02	1,07	0,410	0,387	0,325	0,343
H31_HUMAN	Histone H3.1	0,93	0,92	1,47	1,36	0,309	0,232	0,010	0,031
H4_HUMAN	Histone H4	1,13	1,31	1,35	1,76	0,403	0,279	0,050	0,104
RBBP4_HUMAN	Histone-binding protein RBBP4	0,91	0,79	1,07	0,84			0,429	
HYOU1_HUMAN	Hypoxia up-regulated protein 1	0,99	1,07	1,29	1,38	0,486	0,318	0,028	0,007
IMA2_HUMAN	Importin subunit alpha-2	1,18	0,90	0,82	0,74	0,117	0,243	0,123	0,036
IMA4_HUMAN	Importin subunit alpha-4	1,48	1,62	0,53	0,86	0,154	0,150	0,051	
IMB1_HUMAN	Importin subunit beta-1	0,96	0,90	1,16	1,05	0,408	0,312	0,187	0,430
IPYR_HUMAN	Inorganic pyrophosphatase	2,74	2,31	0,69	1,59	0,005	0,001	0,153	0,202
ITB1_HUMAN	Integrin beta-1	0,67	0,96	1,20	1,15	0,070	0,457	0,335	0,268
ILF2_HUMAN	Interleukin enhancer-binding factor 2	0,76	0,79	1,52	1,20	0,011	0,033	0,012	0,112
ILF3_HUMAN	Interleukin enhancer-binding factor 3	1,11	1,11	1,31	1,45	0,316	0,311	0,010	0,055
IDHP_HUMAN	Isocitrate dehydrogenase [NADP, mitochondrial	1,76	0,88	3,09	2,72			0,050	
NADAP_HUMAN	Kanadaptin	0,82	1,16	0,85	0,99		0,370	0,335	
KTN1_HUMAN	Kinectin	1,02	0,95	1,16	1,11	0,430	0,315	0,077	0,368
LAP2B_HUMAN	Lamina-associated polypeptide 2, isoforms beta/gamma	0,80	0,57	1,94	1,10	0,044	0,129	0,041	0,018
LMNB1_HUMAN	Lamin-B1	1,04	1,16	1,30	1,52	0,428	0,262	0,041	0,047
LMNB2_HUMAN	Lamin-B2	0,12	0,12	1,59	0,20	0,169	0,170	0,012	0,189
LAMB1_HUMAN	Laminin subunit beta-1	0,69	0,86	1,14	0,98	0,068	0,035	0,200	0,428
LAMC1_HUMAN	Laminin subunit gamma-1	0,95	1,12	0,86	0,97	0,428	0,284	0,207	0,327
LARP7_HUMAN	La-related protein 7	1,07	1,14	1,02	1,16			0,010	
LETM1_HUMAN	LETM1 and EF-hand domain-containing protein 1, mitochondrial	1,20	1,22	0,83	1,01	0,208	0,260	0,228	0,226
LPPRC_HUMAN	Leucine-rich PPR motif-containing protein, mitochondrial	1,08	1,14	1,24	1,42	0,184	0,072	0,044	0,035
LRC59_HUMAN	Leucine-rich repeat-containing protein 59	0,81	0,84	1,10	0,93	0,068	0,113	0,179	0,142
LMF2_HUMAN	Lipase maturation factor 2			1,33				0,086	
LDHA_HUMAN	L-lactate dehydrogenase A chain	1,60	5,11	0,12	0,59	0,290	0,263	0,184	0,266

Protein ID	Protein name	WT+R / WT	NOS / WT	NOS+R / NOS	NOS+R / WT	Ttest (WT:WT+R)	TTest (WT:NOS)	TTest (NOS:NOS+R)	TTest (NOS+R:WT)
LDHB_HUMAN	L-lactate dehydrogenase B chain	0,82	2,73	0,27	0,73	0,285	0,222	0,190	0,222
S27A3_HUMAN	Long-chain fatty acid transport protein 3	0,90	1,04	1,25	1,30	0,277			0,035
ACSL3_HUMAN	Long-chain-fatty-acid--CoA ligase 3	1,23	1,37	1,42	1,94	0,053	0,038	0,098	0,045
MDHM_HUMAN	Malate dehydrogenase, mitochondrial	0,88	1,05	1,05	1,10	0,328	0,435	0,427	0,070
MLEC_HUMAN	Malectin			0,87				0,263	
MRP_HUMAN	MARCKS-related protein	1,71	1,59	1,01	1,61	0,006	0,030	0,475	0,042
MATR3_HUMAN	Matrin-3	0,95	0,97	1,31	1,28	0,294	0,378	0,013	0,054
PGRC1_HUMAN	Membrane-associated progesterone receptor component 1	0,75	0,57	1,74	1,00	0,216	0,087	0,083	0,425
MAP1B_HUMAN	Microtubule-associated protein 1B	1,13	1,20	1,08	1,29	0,209	0,146	0,258	0,073
MAP4_HUMAN	Microtubule-associated protein 4	2,10	1,24	0,76	0,94	0,131	0,201	0,100	0,335
MTCH2_HUMAN	Mitochondrial carrier homolog 2	0,87	0,82	1,54	1,26	0,064	0,021	0,001	0,015
TOM70_HUMAN	Mitochondrial import receptor subunit TOM70	0,99	0,97	1,90	1,83		0,471	0,029	0,128
IMMT_HUMAN	Mitochondrial inner membrane protein	0,92	0,82	1,35	1,11	0,267	0,220	0,071	0,347
BUB3_HUMAN	Mitotic checkpoint protein BUB3	1,20	1,19	1,27	1,52			0,041	
MOT1_HUMAN	Monocarboxylate transporter 1	0,70	0,74	2,50	1,84	0,042			0,006
MDR1_HUMAN	Multidrug resistance protein 1	1,16	0,88	1,72	1,52		0,362	0,081	
MRP1_HUMAN	Multidrug resistance-associated protein 1	1,78	1,36				0,244		
PUR6_HUMAN	Multifunctional protein ADE2	0,91	0,75	1,09	0,81	0,327	0,063	0,265	0,118
MBB1A_HUMAN	Myb-binding protein 1A	0,74	1,01	1,68	1,71	0,280	0,482	0,140	0,257
MYEF2_HUMAN	Myelin expression factor 2	1,03			2,16	0,487			0,225
MYADM_HUMAN	Myeloid-associated differentiation marker	0,80	1,21	0,97	1,17	0,252	0,300	0,424	0,221
ML12A_HUMAN	Myosin regulatory light chain 12A	1,80	1,25	0,60	0,75	0,193			0,086
MYH10_HUMAN	Myosin-10	0,88	0,91	0,83	0,75	0,270	0,407	0,297	0,085
MYH9_HUMAN	Myosin-9	1,61	1,33	1,07	1,42	0,057	0,286	0,415	0,388
MARCS_HUMAN	Myristoylated alanine-rich C-kinase substrate	1,13	1,18	1,56	1,84	0,369	0,329	0,002	0,048
NNTM_HUMAN	NAD(P) transhydrogenase, mitochondrial	0,98	0,92	1,06	0,97	0,474	0,374	0,387	0,238
NDUA7_HUMAN	NADH dehydrogenase [ubiquinone 1 alpha subcomplex subunit 7	0,74	0,82	1,43	1,17	0,032	0,000	0,005	0,034
NDUS3_HUMAN	NADH dehydrogenase [ubiquinone iron-sulfur protein 3, mitochondrial	0,70	0,82	1,16	0,95			0,015	
NDUS1_HUMAN	NADH-ubiquinone oxidoreductase 75 kDa subunit, mitochondrial	1,23	0,71	3,48	2,47	0,395	0,027	0,013	0,022
NACA_HUMAN	Nascent polypeptide-associated complex subunit alpha	0,91	0,91	0,82	0,75	0,199	0,089	0,103	0,060
NEST_HUMAN	Nestin	1,86	1,27	1,24	1,58	0,071	0,326	0,269	0,232
NCAM1_HUMAN	Neural cell adhesion molecule 1	0,89	1,83	1,62	2,96	0,222	0,239	0,175	0,144
VGF_HUMAN	Neurosecretory protein VGF	1,18	1,78	1,21	2,16	0,162	0,049	0,236	0,058
GANAB_HUMAN	Neutral alpha-glucosidase AB	0,90	0,90	1,08	0,97	0,288	0,275	0,237	0,327
AAAT_HUMAN	Neutral amino acid transporter B(0)			2,19				0,009	
NH2L1_HUMAN	NHP2-like protein 1	1,89	1,71	1,21	2,07	0,037	0,092	0,299	0,063
HMGN1_HUMAN	Non-histone chromosomal protein HMG-14	0,45	0,63	2,18	1,37	0,029	0,037	0,002	0,019
NONO_HUMAN	Non-POU domain-containing octamer-binding protein	1,08	1,17	1,25	1,47	0,316	0,119	0,050	0,031
NLTP_HUMAN	Non-specific lipid-transfer protein	0,70	0,93	0,96	0,90	0,082	0,339	0,406	0,446
NASP_HUMAN	Nuclear autoantigenic sperm protein	0,09	0,10	0,98	0,10	0,184	0,185	0,398	0,186
NUMA1_HUMAN	Nuclear mitotic apparatus protein 1	0,82	1,39	0,66	0,92	0,357	0,330	0,271	0,261
NU107_HUMAN	Nuclear pore complex protein Nup107	1,13	1,10	1,75	1,92			0,062	
NU205_HUMAN	Nuclear pore complex protein Nup205	1,26	1,54	1,10	1,69	0,246	0,007	0,323	0,052

Protein ID	Protein name	WT+R / WT	NOS / WT	NOS+R / NOS	NOS+R / WT	Ttest (WT:WT+R)	TTest (WT:NOS)	TTest (NOS:NOS+R)	TTest (NOS+R:WT)
NUP50_HUMAN	Nuclear pore complex protein Nup50	1,07	0,97	1,59	1,54	0,311			0,030
NUP88_HUMAN	Nuclear pore complex protein Nup88			1,28				0,218	
NUP93_HUMAN	Nuclear pore complex protein Nup93	0,98	0,89	1,41	1,25	0,456	0,218	0,018	0,066
NUP62_HUMAN	Nuclear pore glycoprotein p62			2,54				0,190	
YBOX1_HUMAN	Nuclease-sensitive element-binding protein 1	0,58	0,75	1,34	1,00	0,006	0,085	0,267	0,497
NOC3L_HUMAN	Nucleolar complex protein 3 homolog	1,40	1,34	0,90	1,20			0,344	
NOP56_HUMAN	Nucleolar protein 56	1,30	1,44	0,85	1,22	0,264	0,284	0,390	0,258
NOP58_HUMAN	Nucleolar protein 58	1,30	1,24	1,36	1,68	0,026	0,254	0,124	0,003
DDX21_HUMAN	Nucleolar RNA helicase 2	0,61	0,72	1,74	1,26	0,024	0,063	0,003	0,050
NUCL_HUMAN	Nucleolin	0,97	1,01	1,01	1,02	0,275	0,459	0,461	0,306
NPM_HUMAN	Nucleophosmin	1,01	0,98	1,29	1,26	0,477	0,457	0,055	0,302
TPR_HUMAN	Nucleoprotein TPR	0,75	0,76	1,45	1,10	0,105	0,025	0,011	0,179
NDKA_HUMAN	Nucleoside diphosphate kinase A	0,83	0,93	1,00	0,93	0,026	0,204	0,493	0,101
BPTF_HUMAN	Nucleosome-remodeling factor subunit BPTF	0,64	0,82	1,20	0,99	0,055	0,239	0,130	0,400
PALM_HUMAN	Paralemmin-1	0,78	0,99	1,37	1,36	0,112	0,484	0,053	0,250
PSIP1_HUMAN	PC4 and SFRS1-interacting protein	1,20	1,23	1,36	1,66	0,212	0,192	0,045	0,032
PPIA_HUMAN	Peptidyl-prolyl cis-trans isomerase A	0,70	0,70	0,50	0,35	0,334	0,320	0,073	0,178
PPIB_HUMAN	Peptidyl-prolyl cis-trans isomerase B	0,75	0,87	1,35	1,17	0,078	0,123	0,035	0,194
FKBP8_HUMAN	Peptidyl-prolyl cis-trans isomerase FKBP8	0,52	0,47	2,21	1,05		0,004	0,052	0,431
PRDX1_HUMAN	Peroxiredoxin-1	0,99	0,85	1,06	0,90	0,472	0,091	0,269	0,052
PRDX5_HUMAN	Peroxiredoxin-5, mitochondrial	0,55	0,49	1,16	0,57	0,317	0,246	0,283	0,227
DHB4_HUMAN	Peroxisomal multifunctional enzyme type 2	1,19	1,05	0,75	0,79	0,179	0,360	0,014	0,090
PHF6_HUMAN	PHD finger protein 6	0,65	0,77	1,10	0,85			0,379	
MPCP_HUMAN	Phosphate carrier protein, mitochondrial	0,80	0,87	1,15	1,00	0,070	0,156	0,236	0,420
PGAM1_HUMAN	Phosphoglycerate mutase 1	0,09	0,21	0,47	0,10	0,145	0,248	0,292	0,243
PININ_HUMAN	Pinin	0,98	0,96	1,40	1,35	0,419	0,410	0,080	0,413
PLEC_HUMAN	Plectin	1,11	1,16	1,26	1,46		0,188	0,057	0,221
POGZ_HUMAN	Pogo transposable element with ZNF domain	0,89	0,94	1,44	1,36	0,082	0,293	0,011	0,012
PARP1_HUMAN	Poly [ADP-ribose polymerase 1	1,03	0,99	0,96	0,96	0,421	0,476	0,380	0,460
PCBP1_HUMAN	Poly(rC)-binding protein 1	0,59	0,67	0,86	0,58	0,150	0,177	0,251	0,176
PUF60_HUMAN	Poly(U)-binding-splicing factor PUF60	0,56	0,03	1,40	0,04	0,354	0,246	0,234	0,249
PABP1_HUMAN	Polyadenylate-binding protein 1	1,15	1,06	1,11	1,18	0,335	0,414	0,218	0,176
PABP2_HUMAN	Polyadenylate-binding protein 2		1,29	0,86	1,11		0,405	0,422	0,373
PTBP1_HUMAN	Polypyrimidine tract-binding protein 1	1,00	0,85	1,42	1,20	0,496	0,284	0,063	0,462
UBC_HUMAN	Polyubiquitin-C	0,56	0,68	1,15	0,78			0,045	
LMNA_HUMAN	Prelamin-A/C	0,89	0,98	1,31	1,29	0,049	0,421	0,027	0,053
PRP19_HUMAN	Pre-mRNA-processing factor 19	1,16	1,27	0,90	1,15	0,131	0,004	0,121	0,127
PRP6_HUMAN	Pre-mRNA-processing factor 6		0,84	1,47	1,24			0,098	
PRP8_HUMAN	Pre-mRNA-processing-splicing factor 8	0,97	0,98	1,33	1,30	0,345	0,444	0,038	0,052
DDX17_HUMAN	Probable ATP-dependent RNA helicase DDX17	0,72	0,73	1,03	0,76	0,046	0,151	0,463	0,108
DDX5_HUMAN	Probable ATP-dependent RNA helicase DDX5	0,76	0,92	1,42	1,30	0,221	0,229	0,016	0,046
AT131_HUMAN	Probable cation-transporting ATPase 13A1	1,06	0,69	1,45	1,00	0,420	0,077	0,008	0,494
PROF1_HUMAN	Profilin-1	0,45	0,52	0,51	0,26	0,195	0,230	0,087	0,131

Protein ID	Protein name	WT+R / WT	NOS / WT	NOS+R / NOS	NOS+R / WT	Ttest (WT:WT+R)	TTest (WT:NOS)	TTest (NOS:NOS+R)	TTest (NOS+R:WT)
PHB_HUMAN	Prohibitin	0,80	0,86	1,13	0,98	0,172	0,214	0,245	0,256
PHB2_HUMAN	Prohibitin-2	0,95	0,92	0,96	0,88	0,394	0,366	0,422	0,247
PA2G4_HUMAN	Proliferation-associated protein 2G4	1,27	1,33	1,00	1,33			0,483	
P4HA1_HUMAN	Prolyl 4-hydroxylase subunit alpha-1	1,07	0,98	0,91	0,89	0,317	0,475	0,343	0,225
PSME1_HUMAN	Proteasome activator complex subunit 1	0,76	1,08	0,45	0,49	0,336	0,433	0,103	0,416
PSA1_HUMAN	Proteasome subunit alpha type-1	0,85	0,90	0,81	0,72	0,062	0,029	0,129	0,055
PSA5_HUMAN	Proteasome subunit alpha type-5	1,11	1,11	0,88	0,98	0,265	0,272	0,186	0,446
PSA7_HUMAN	Proteasome subunit alpha type-7	0,79	0,75	1,05	0,79			0,280	
ANM1_HUMAN	Protein arginine N-methyltransferase 1	2,90	2,01	0,32	0,65	0,077	0,004	0,004	0,107
CNPY2_HUMAN	Protein canopy homolog 2	0,72	0,77	1,33	1,02	0,120	0,042	0,055	0,413
DEK_HUMAN	Protein DEK	1,89	1,77	1,28	2,26			0,356	
PDIA1_HUMAN	Protein disulfide-isomerase	1,20	1,15	1,43	1,63	0,089	0,057	0,002	0,005
PDIA3_HUMAN	Protein disulfide-isomerase A3	1,02	1,08	1,17	1,27	0,476	0,393	0,021	0,202
PDIA4_HUMAN	Protein disulfide-isomerase A4	0,65	0,54	1,34	0,73	0,143	0,092	0,020	0,195
PDIA6_HUMAN	Protein disulfide-isomerase A6	0,38	0,47	1,39	0,66	0,172	0,208	0,017	0,294
TMX3_HUMAN	Protein disulfide-isomerase TMX3	0,63	0,83	1,36	1,13	0,038	0,207	0,048	0,161
LMAN1_HUMAN	Protein ERGIC-53		1,46	1,01	1,46			0,491	
K1967_HUMAN	Protein KIAA1967	0,88	0,94	1,43	1,35	0,186	0,335	0,077	0,305
LYRIC_HUMAN	Protein LYRIC	0,95	0,64	1,23	0,79	0,220	0,187	0,307	0,133
SCAFB_HUMAN	Protein SCAF11		0,66	0,97	0,64		0,014		
SON_HUMAN	Protein SON	1,86	2,12	1,40	2,96			0,027	
DHX15_HUMAN	Putative pre-mRNA-splicing factor ATP-dependent RNA helicase DHX15	1,04	0,84	1,37	1,15	0,350	0,237	0,077	0,337
RAB1C_HUMAN	Putative Ras-related protein Rab-1C	1,03	0,84	1,76	1,47			0,024	
NOP2_HUMAN	Putative ribosomal RNA methyltransferase NOP2	0,72	0,63	1,77	1,11	0,049	0,060	0,038	0,330
LC7L2_HUMAN	Putative RNA-binding protein Luc7-like 2	1,31	0,81	0,76	0,61			0,361	
RRMJ3_HUMAN	Putative rRNA methyltransferase 3	1,02	0,97	1,21	1,17	0,424	0,453	0,182	0,469
P5CR2_HUMAN	Pyrroline-5-carboxylate reductase 2			1,37				0,084	
ODPB_HUMAN	Pyruvate dehydrogenase E1 component subunit beta, mitochondrial	0,87	0,80	1,10	0,88	0,116	0,061	0,367	0,247
KPYM_HUMAN	Pyruvate kinase isozymes M1/M2	0,60	1,25	0,71	0,89	0,123	0,356	0,293	0,315
GDIB_HUMAN	Rab GDP dissociation inhibitor beta	0,45	1,15	0,24	0,28		0,427	0,179	0,133
RANB3_HUMAN	Ran-binding protein 3	0,56	0,14			0,207			
RAB14_HUMAN	Ras-related protein Rab-14	0,96	0,60	1,48	0,89	0,412	0,103	0,112	0,360
RAB1A_HUMAN	Ras-related protein Rab-1A	0,34	0,59	1,72	1,02			0,229	
RAB2A_HUMAN	Ras-related protein Rab-2A	8,53	1,34	0,77	1,03	0,246	0,291	0,261	0,241
RAB2B_HUMAN	Ras-related protein Rab-2B	1,16	1,16	0,92	1,06	0,030	0,238	0,285	0,168
RAB3A_HUMAN	Ras-related protein Rab-3A	1,00	1,14	1,08	1,23	0,488	0,136	0,233	0,061
RAB5C_HUMAN	Ras-related protein Rab-5C	1,24	1,12	1,01	1,13	0,019	0,131	0,477	0,263
RAB7A_HUMAN	Ras-related protein Rab-7a	0,80	0,99	0,90	0,88	0,114	0,473	0,312	0,447
F213A_HUMAN	Redox-regulatory protein FAM213A	0,91	0,99	1,38	1,36			0,057	
RSF1_HUMAN	Remodeling and spacing factor 1	0,83	0,91	1,12	1,03	0,173	0,146	0,092	0,457
RTN4_HUMAN	Reticulon-4	4,35	2,35	1,87	4,39		0,286	0,271	0,227
RTL1_HUMAN	Retrotransposon-like protein 1	0,90	0,73	0,96	0,70	0,347	0,116	0,425	0,193
RHOG_HUMAN	Rho-related GTP-binding protein RhoG	1,49	1,57	0,88	1,39	0,181	0,192	0,252	

Protein ID	Protein name	WT+R / WT	NOS / WT	NOS+R / NOS	NOS+R / WT	Ttest (WT:WT+R)	TTest (WT:NOS)	TTest (NOS:NOS+R)	TTest (NOS+R:WT)
RL1D1_HUMAN	Ribosomal L1 domain-containing protein 1	1,27	1,21	1,11	1,33	0,280	0,245	0,353	0,090
BOP1_HUMAN	Ribosome biogenesis protein BOP1	0,87	0,84	1,90	1,60			0,020	
RRBP1_HUMAN	Ribosome-binding protein 1			0,75				0,151	
RCL1_HUMAN	RNA 3'-terminal phosphate cyclase-like protein			1,21				0,071	
RBMX_HUMAN	RNA-binding motif protein, X chromosome	0,81	0,88	1,19	1,06	0,075			0,474
RBM14_HUMAN	RNA-binding protein 14	0,87	0,95	1,08	1,03	0,127	0,260	0,340	0,398
RBM25_HUMAN	RNA-binding protein 25	1,02	1,01	1,21	1,22	0,418	0,465	0,189	0,319
RBM39_HUMAN	RNA-binding protein 39	0,78	0,84	1,61	1,36			0,012	
RBM4_HUMAN	RNA-binding protein 4	0,74	0,77	1,20	0,93	0,011			0,268
RBM8A_HUMAN	RNA-binding protein 8A	0,77	0,87	1,10	0,96	0,129	0,182	0,341	0,424
FUS_HUMAN	RNA-binding protein FUS	0,67	0,79	1,16	0,92	0,000	0,045	0,080	0,074
RALY_HUMAN	RNA-binding protein Raly	0,92	0,74	1,65	1,23	0,392	0,233	0,070	0,456
FBRL_HUMAN	rRNA 2'-O-methyltransferase fibrillarin	0,27	0,29	1,22	0,36	0,220	0,225	0,048	0,169
RUVB1_HUMAN	RuvB-like 1	0,09	0,12	0,51	0,06	0,233	0,239	0,070	0,164
RUVB2_HUMAN	RuvB-like 2	1,07	0,72	0,87	0,62	0,412			
SARNP_HUMAN	SAP domain-containing ribonucleoprotein	0,78	1,03	0,90	0,92	0,058	0,457	0,298	0,199
AT2A2_HUMAN	Sarcoplasmic/endoplasmic reticulum calcium ATPase 2	1,30	1,03	1,24	1,28	0,210	0,454	0,028	0,156
SAFB1_HUMAN	Scaffold attachment factor B1	0,77	0,58	1,71	1,00	0,077	0,004	0,058	0,495
SCFD1_HUMAN	Sec1 family domain-containing protein 1			1,20				0,174	
SCAM1_HUMAN	Secretory carrier-associated membrane protein 1			0,87				0,216	
SCAM3_HUMAN	Secretory carrier-associated membrane protein 3	1,57	1,40	0,81	1,13	0,055	0,102	0,267	0,140
SEPT2_HUMAN	Septin-2	0,69	0,76	1,28	0,97	0,138	0,210	0,059	0,453
SEPT6_HUMAN	Septin-6	0,93	1,05	0,94	0,99	0,432	0,451	0,410	0,437
SEPT7_HUMAN	Septin-7	0,95	0,94	1,03	0,97	0,298	0,260	0,467	0,353
SEPT9_HUMAN	Septin-9	1,15	0,85	1,03	0,88	0,141	0,220	0,422	0,070
SRRM1_HUMAN	Serine/arginine repetitive matrix protein 1	0,98	1,17	1,14	1,33			0,296	
SRRM2_HUMAN	Serine/arginine repetitive matrix protein 2	0,88	0,95	0,86	0,82	0,117	0,297	0,182	0,110
SRSF1_HUMAN	Serine/arginine-rich splicing factor 1	0,99	1,13	0,86	0,98	0,479	0,336	0,215	0,462
SRSF7_HUMAN	Serine/arginine-rich splicing factor 7	1,54	1,30	1,13	1,47	0,258			
2AAA_HUMAN	Serine/threonine-protein phosphatase 2A 65 kDa regulatory subunit A alpha isoform	0,44	0,67	1,54	1,03	0,032	0,185	0,096	0,432
PP1A_HUMAN	Serine/threonine-protein phosphatase PP1-alpha catalytic subunit	1,19	1,14	1,33	1,52	0,428	0,448	0,270	0,333
STRAP_HUMAN	Serine-threonine kinase receptor-associated protein	3,16	2,74	0,96	2,64			0,467	
SERPH_HUMAN	Serpin H1	0,75	0,82	1,22	0,99	0,068	0,163	0,229	0,369
SRRT_HUMAN	Serrate RNA effector molecule homolog	0,75			1,17	0,101			0,441
SFXN1_HUMAN	Sideroflexin-1	1,11	0,93	1,23	1,14	0,288	0,274	0,148	0,301
SPCS3_HUMAN	Signal peptidase complex subunit 3	0,86	1,01	1,19	1,20	0,331	0,489	0,117	
SRP14_HUMAN	Signal recognition particle 14 kDa protein	3,25	3,35	1,58	5,27	0,024	0,017	0,201	0,049
SRP09_HUMAN	Signal recognition particle 9 kDa protein	1,34	0,98	0,88	0,86	0,323	0,366	0,302	0,325
SRPRB_HUMAN	Signal recognition particle receptor subunit beta	1,02	0,97	1,17	1,14	0,415	0,405	0,175	0,322
SSBP_HUMAN	Single-stranded DNA-binding protein, mitochondrial	0,81	0,75	1,09	0,82	0,104	0,159	0,369	0,144
PDS5A_HUMAN	Sister chromatid cohesion protein PDS5 homolog A	0,62	0,71	0,86	0,61	0,135			0,142
PDS5B_HUMAN	Sister chromatid cohesion protein PDS5 homolog B	0,20	0,51	1,46	0,75			0,281	

Protein ID	Protein name	WT+R / WT	NOS / WT	NOS+R / NOS	NOS+R / WT	Ttest (WT:WT+R)	TTest (WT:NOS)	TTest (NOS:NOS+R)	TTest (NOS+R:WT)
SMD1_HUMAN	Small nuclear ribonucleoprotein Sm D1	0,33	0,47	1,12	0,53	0,198	0,242	0,102	0,180
SMD2_HUMAN	Small nuclear ribonucleoprotein Sm D2	0,60	0,96	0,75	0,72	0,137	0,418	0,190	0,385
SMD3_HUMAN	Small nuclear ribonucleoprotein Sm D3	0,78	0,85	1,31	1,11	0,147	0,188	0,257	0,461
SUMO2_HUMAN	Small ubiquitin-related modifier 2		0,70	1,32	0,93			0,078	
AT1A1_HUMAN	Sodium/potassium-transporting ATPase subunit alpha-1	0,79	0,83	1,30	1,07	0,017	0,156	0,057	0,175
SPTA2_HUMAN	Spectrin alpha chain, brain	0,68	0,76	1,48	1,12	0,146	0,214	0,012	0,337
SPTB2_HUMAN	Spectrin beta chain, brain 1	0,98	1,08	1,49	1,62	0,395	0,322	0,012	0,006
SKP1_HUMAN	S-phase kinase-associated protein 1	0,79	0,93	1,19	1,10			0,105	
SGPL1_HUMAN	Sphingosine-1-phosphate lyase 1	0,91	0,92	0,98	0,91	0,068	0,066	0,356	
SF3A1_HUMAN	Splicing factor 3A subunit 1	0,75	0,76	1,30	0,99	0,138	0,082	0,105	0,353
SF3B1_HUMAN	Splicing factor 3B subunit 1	0,73	0,59	1,73	1,02	0,173	0,145	0,049	0,473
SF3B2_HUMAN	Splicing factor 3B subunit 2	0,79	0,77	1,41	1,08	0,129	0,105	0,057	0,433
SF3B3_HUMAN	Splicing factor 3B subunit 3	1,36	0,96	1,06	1,01	0,231	0,382	0,373	0,471
SF3B5_HUMAN	Splicing factor 3B subunit 5	0,71	0,87	1,45	1,26	0,097	0,325	0,193	0,136
U2AF2_HUMAN	Splicing factor U2AF 65 kDa subunit	0,70	0,79	1,15	0,91	0,094	0,083	0,200	0,280
SFPQ_HUMAN	Splicing factor, proline- and glutamine-rich	1,20	1,21	1,19	1,45	0,346	0,334	0,050	0,269
SRC8_HUMAN	Src substrate cortactin	0,98	1,05	1,23	1,29		0,296		
SND1_HUMAN	Staphylococcal nuclease domain-containing protein 1	0,86	0,84	0,95	0,80	0,001	0,016	0,317	0,070
STMN1_HUMAN	Stathmin	0,40	0,46	1,64	0,76	0,002			0,035
STML2_HUMAN	Stomatin-like protein 2	1,16	1,01	1,08	1,09	0,212	0,477	0,351	0,446
GRP75_HUMAN	Stress-70 protein, mitochondrial	0,96	0,92	1,32	1,22	0,270	0,186	0,019	0,094
STIP1_HUMAN	Stress-induced-phosphoprotein 1	5,99	3,53	0,36	1,27		0,206	0,157	0,361
SMC1A_HUMAN	Structural maintenance of chromosomes protein 1A	1,12	1,16	0,93	1,08	0,168			
SMRC1_HUMAN	SWI/SNF complex subunit SMARCC1	0,79	0,89	1,32	1,18		0,239	0,136	0,373
SMRC2_HUMAN	SWI/SNF complex subunit SMARCC2	1,14	0,90	1,81	1,62			0,075	
SMCE1_HUMAN	SWI/SNF-related matrix-associated actin-dependent regulator of chromatin subfamily E member 1	0,81	0,87	1,56	1,35	0,115	0,120	0,033	0,116
SMRD1_HUMAN	SWI/SNF-related matrix-associated actin-dependent regulator of chromatin subfamily D member 1	0,74	0,81	1,30	1,06	0,065	0,118	0,049	0,257
SMCA5_HUMAN	SWI/SNF-related matrix-associated actin-dependent regulator of chromatin subfamily A member 5	1,02	0,97	1,37	1,33	0,477	0,463	0,092	0,394
VAT1_HUMAN	Synaptic vesicle membrane protein VAT-1 homolog	1,40	1,04	1,11	1,15	0,339	0,479	0,306	0,434
SYNP2_HUMAN	Synaptopodin-2	1,09	1,13	0,91	1,03	0,322	0,297	0,321	0,119
TADBP_HUMAN	TAR DNA-binding protein 43	1,01	1,03	1,17	1,20	0,473	0,438	0,189	0,351
TCPA_HUMAN	T-complex protein 1 subunit alpha	1,06	1,61	0,60	0,97	0,453	0,107	0,079	0,290
TCPB_HUMAN	T-complex protein 1 subunit beta	1,16	0,78	1,01	0,79	0,310	0,026	0,459	0,022
TCPD_HUMAN	T-complex protein 1 subunit delta	0,53	0,39	0,64	0,25	0,307	0,255	0,182	0,218
TCPZ_HUMAN	T-complex protein 1 subunit zeta	0,92	1,11	0,34	0,37	0,428	0,432	0,069	0,378
THIO_HUMAN	Thioredoxin	1,33	1,20	0,51	0,62	0,314	0,352	0,164	
TXD12_HUMAN	Thioredoxin domain-containing protein 12	0,52	0,46	1,86	0,85	0,051	0,077	0,043	0,141
TXND5_HUMAN	Thioredoxin domain-containing protein 5	1,10	0,78	1,65	1,28			0,097	
PRDX3_HUMAN	Thioredoxin-dependent peroxide reductase, mitochondrial	0,85	0,86	1,20	1,03	0,038	0,033	0,139	0,427
TMX1_HUMAN	Thioredoxin-related transmembrane protein 1			0,96				0,438	
TMX2_HUMAN	Thioredoxin-related transmembrane protein 2	0,80	0,77	1,46	1,12	0,011			0,010

Protein ID	Protein name	WT+R / WT	NOS / WT	NOS+R / NOS	NOS+R / WT	Ttest (WT:WT+R)	TTest (WT:NOS)	TTest (NOS:NOS+R)	TTest (NOS+R:WT)
THOC2_HUMAN	THO complex subunit 2	0,98	0,99	1,15	1,14	0,410	0,462	0,139	0,183
THOC4_HUMAN	THO complex subunit 4	0,83	0,86	1,19	1,02	0,107	0,242	0,228	0,397
TR150_HUMAN	Thyroid hormone receptor-associated protein 3	0,96	1,16	1,11	1,29	0,389	0,102	0,102	0,029
TOIP1_HUMAN	Torsin-1A-interacting protein 1	0,92	1,02	1,40	1,43	0,332	0,474	0,043	0,077
TIF1B_HUMAN	Transcription intermediary factor 1-beta	0,43	0,71	0,74	0,53	0,001	0,162	0,221	0,025
ATRX_HUMAN	Transcriptional regulator ATRX	0,91	0,68	1,15	0,79	0,352			
TFR1_HUMAN	Transferrin receptor protein 1	1,12	1,11	1,01	1,13	0,273	0,355	0,473	0,481
TRA2B_HUMAN	Transformer-2 protein homolog beta	1,56			0,98	0,275			0,369
TERA_HUMAN	Transitional endoplasmic reticulum ATPase	13,31	1,56	0,59	0,92	0,237	0,031	0,007	0,094
TMED9_HUMAN	Transmembrane emp24 domain-containing protein 9	0,70	0,80	1,25	1,00	0,052	0,153	0,087	0,211
TCOF_HUMAN	Treacle protein	0,81	0,87	1,04	0,91		0,210	0,423	0,276
ECHA_HUMAN	Trifunctional enzyme subunit alpha, mitochondrial	1,15	1,36	1,30	1,78	0,110	0,054	0,058	0,062
ECHB_HUMAN	Trifunctional enzyme subunit beta, mitochondrial	0,99	1,47	1,22	1,80	0,411	0,134	0,168	0,008
TPIS_HUMAN	Triosephosphate isomerase	3,04	1,52	0,10	0,15	0,200	0,325	0,081	0,474
TPM3_HUMAN	Tropomyosin alpha-3 chain	0,85	0,93	0,89	0,82	0,169			
TPM4_HUMAN	Tropomyosin alpha-4 chain	0,98	22,10	0,05	1,12		0,211	0,137	0,247
TBA1B_HUMAN	Tubulin alpha-1B chain		1,27	0,81	1,03			0,040	
TBB5_HUMAN	Tubulin beta chain	0,71	0,71	1,08	0,77	0,096	0,147	0,363	0,151
TBB2B_HUMAN	Tubulin beta-2B chain	1,04	1,53	0,91	1,38	0,452	0,189	0,404	0,160
TBB3_HUMAN	Tubulin beta-3 chain	0,77	1,03	0,69	0,72			0,163	
TPD54_HUMAN	Tumor protein D54	0,73	0,76	0,92	0,69	0,131	0,123	0,326	0,121
TP53B_HUMAN	Tumor suppressor p53-binding protein 1			0,83				0,145	
BAZ1B_HUMAN	Tyrosine-protein kinase BAZ1B	1,04	1,20	0,85	1,02	0,165	0,148	0,211	
RU2A_HUMAN	U2 small nuclear ribonucleoprotein A'	0,96	1,22	0,83	1,02	0,437	0,148	0,208	0,400
SR140_HUMAN	U2 snRNP-associated SURP motif-containing protein	0,54	0,61	1,97	1,20	0,107			
U520_HUMAN	U5 small nuclear ribonucleoprotein 200 kDa helicase	0,84	0,86	1,10	0,94	0,088	0,118	0,273	0,331
LSM2_HUMAN	U6 snRNA-associated Sm-like protein LSm2			1,24				0,011	
COQ6_HUMAN	Ubiquinone biosynthesis monooxygenase COQ6	0,74	0,79	0,91	0,72	0,142	0,167	0,176	
UCHL1_HUMAN	Ubiquitin carboxyl-terminal hydrolase isozyme L1	1,24	1,55	0,33	0,51	0,339	0,083	0,002	0,031
MYO1B_HUMAN	Unconventional myosin-Ib	0,98	1,15	1,47	1,70	0,374	0,230	0,029	0,008
USMG5_HUMAN	Up-regulated during skeletal muscle growth protein 5	0,78	0,85	1,07	0,91			0,405	
SYVC_HUMAN	Valine--tRNA ligase			0,67				0,309	
VAPB_HUMAN	Vesicle-associated membrane protein-associated protein B/C	0,79	1,29	0,94	1,21	0,156	0,343	0,443	0,141
SC22B_HUMAN	Vesicle-trafficking protein SEC22b	1,31	1,42	0,96	1,36	0,121			0,058
VIME_HUMAN	Vimentin	1,21	1,01	1,06	1,08	0,171	0,479	0,371	0,457
VDAC1_HUMAN	Voltage-dependent anion-selective channel protein 1	0,79	0,78	1,28	1,00	0,008	0,013	0,007	0,488
VDAC2_HUMAN	Voltage-dependent anion-selective channel protein 2	0,79	0,81	1,24	1,00	0,087	0,077	0,071	0,296
VDAC3_HUMAN	Voltage-dependent anion-selective channel protein 3	0,94	0,61	3,04	1,87	0,376	0,070	0,150	0,144
CA2D1_HUMAN	Voltage-dependent calcium channel subunit alpha-2/delta-1	1,44	1,06	1,44	1,54	0,128	0,439	0,118	0,347
XRCC5_HUMAN	X-ray repair cross-complementing protein 5	1,50	1,69	0,84	1,43	0,141	0,087	0,083	0,171
XRCC6_HUMAN	X-ray repair cross-complementing protein 6	0,98	1,14	0,89	1,01	0,469	0,283	0,264	0,367
YLPM1_HUMAN	YLP motif-containing protein 1	0,67	0,61	2,01	1,23		0,012		
ZCH18_HUMAN	Zinc finger CCCH domain-containing protein 18	0,86	0,76	1,68	1,27	0,153			0,203

Protein ID	Protein name	WT+R / WT	NOS / WT	NOS+R / NOS	NOS+R / WT	Ttest (WT:WT+R)	TTest (WT:NOS)	TTest (NOS:NOS+R)	TTest (NOS+R:WT)
ZN384_HUMAN	Zinc finger protein 384	0,84	0,90	1,02	0,92	0,296	0,219	0,406	0,179
ZRAB2_HUMAN	Zinc finger Ran-binding domain-containing protein 2	0,88	0,86	1,09	0,94	0,274	0,301	0,079	0,410